The role of *Lin28a* in thymic epithelial cell development and function

Inauguraldissertation

zur
Erlangung der Würde eines Doktors der Philosophie
vorgelegt der
Philosophisch-Naturwissenschaftlichen Fakultät
der Universität Basel

von

Veysel Kaya

Basel, 2021

Genehmigt von der Philosophisch-Naturwissenschaftlichen Fakultät

auf Antrag von

Prof. Dr. Georg Andreas Holländer

Prof. Dr. Primo Leo Schär

Prof. Dr. Graham Anderson

Basel, den 22. Juni 2021

Prof. Dr. Marcel Mayor
Dekan

“Yolunda yürüyen bir yolcunun, yalnız ufku görmesi kâfi değildir. Muhakkak ufkun ötesini de görmesi ve bilmesi lazımdır.

-

“The traveler not only has to see the path but also the horizon behind it.”

Mustafa Kemal Atatürk

Table of Contents

ABSTRACT ..... **i**

ACKNOWLEDGEMENTS ..... **iv**

ABBREVIATIONS ..... **vi**

1. INTRODUCTION **1**

1.1 THE HISTORY OF THE THYMUS 1

1.2 ANATOMY OF THE THYMUS 2

1.3 THYMUS ORGANOGENESIS 3

1.4 THYMIC EPITHELIAL CELL DEVELOPMENT AND HETEROGENEITY 6

1.5 T CELL DEVELOPMENT 9

1.6 THYMIC EPITHELIAL CELL FUNCTION 15

1.7 THE ROLE OF MICRORNAS AND THEIR IMPORTANCE IN TEC BIOLOGY 17

1.8 THE LET-7 FAMILY OF MIRNAS 18

1.9 THE RNA BINDING PROTEIN LIN28 19

1.10 ISOFORMS AND STRUCTURE OF LIN28 20

1.11 LIN28 RBPS REGULATE GENE EXPRESSION VIA TWO DISTINCT BIOLOGICAL PATHWAYS 21

1.11.1 LET-7 DEPENDENT FUNCTIONS OF LIN28 21

1.11.2 LET-7 INDEPENDENT FUNCTIONS OF LIN28 21

1.12 ROLES OF LIN28 IN HUMAN DISEASES 23

2. HYPOTHESIS AND AIMS **24**

3. MATERIALS AND METHODS **25**

3.1 GENERATION OF LIN28 TRANSGENIC MOUSE MODELS 25

3.2 MOUSE GENOTYPING 25

3.3 FLOW CYTOMETRY ANALYSIS REAGENTS 26

3.4 CELL ISOLATION AND ANALYSIS WITH FLOW CYTOMETRY 28

3.5 REAL TIME QUANTITATIVE PCR ANALYSIS 30

3.6 LET-7 ISOFORM QUANTITATIVE PCR ANALYSIS 30

3.7 IMMUNOFLUORESCENCE 31

3.8 CELL PROLIFERATION ANALYSIS USING BRDU 31

3.9 FETAL THYMIC ORGAN CULTURES 31

3.10 REAGGREGATE THYMIC ORGAN CULTURES 32

3.11 SCENITH 32

3.12 MITOTRACKER STAINING 33

3.13 TNF-A TREATMENT 33

3.14 STATISTICAL ANALYSIS 34

3.15 PROTEOMIC ANALYSES 34

3.16 TRANSCRIPTOMIC ANALYSES 35

4. RESULTS 36

4.1 ENDOGENOUS *LIN28* AMOUNTS IN TEC DECREASE DURING THYMUS ONTOGENY AND CORRELATES WITH THE EXPRESSION OF MATURE LET-7 ISOMIRS 36

4.2 TRANSGENIC *LIN28A* AND *LIN28B* EXPRESSION IN TEC INHIBITS LET-7 MATURATION 38

4.3 TEC PHENOTYPE OF YOUNG ADULT *LIN28* MUTANT ANIMALS 40

4.3.1 *LIN28A* AND *LIN28B* TG DIFFERENTIALLY AFFECT THYMUS AND TEC CELLULARITY 40

4.3.2 ECTOPIC EXPRESSION OF *LIN28A* TG INCREASES TEC PROLIFERATION AND APOPTOSIS 44

4.4 THYMOCYTE DEVELOPMENT IN YOUNG ADULT *LIN28* TRANSGENIC MICE 46

4.4.1 THYMUS SETTLING IS DIFFERENTIALLY AFFECTED BY *LIN28A* AND *LIN28B* 46

4.4.2 INITIAL STAGES OF THYMOCYTE MATURATION ARE UNAFFECTED IN *LIN28* MUTANT MICE 48

4.4.3 THYMOCYTE POSITIVE SELECTION IS COMPROMISED IN LIN28A^{TEC} AND LIN28AXB^{TEC} MICE 49

4.4.4 LATE STAGES OF SP THYMOCYTE MATURATION ARE ALTERED BY *LIN28A* TG 52

4.4.5 *LIN28A* TG CTEC ARE LIMITED IN THEIR CAPACITY TO INDUCE THYMOCYTE NEGATIVE SELECTION 54

4.5 THYMUS PHENOTYPE OF JUVENILE LIN28A^{TEC} ANIMALS 56

4.5.1 JUVENILE LIN28A^{TEC} MICE HAVE A REGULAR CTEC BUT ALTERED MTEC SUBSET COMPOSITION 56

4.5.2 CORTICAL SELECTION PROCEEDS NORMALLY WHILE MEDULLARY THYMOCYTE MATURATION IS COMPROMISED IN JUVENILE LIN28A^{TEC} ANIMALS 58

4.6 CTEC^{LO} AND CTEC^{HI} POSSESS DISTINCT POSITIVE SELECTION POTENTIALS 61

4.7 TRANSCRIPTOMIC ANALYSES OF CTEC^{LO} AND CTEC^{HI} FROM JUVENILE AND YOUNG ADULT LIN28A^{TEC} MICE 64

4.7.1 *LIN28A* OVER-EXPRESSION CHANGES THE TEC SUBTYPE COMPOSITION AT JUVENILE AND ADULT AGE 64

4.7.2 THE IMPACT OF *LIN28A* TG ON THE TRANSCRIPTOME OF CTEC INCREASES WITH AGE 66

4.7.3 EPITHELIAL TO MESENCHYMAL TRANSITION IS INCREASED IN CTEC THAT EXPRESS *LIN28A* TG AT 7 WEEKS OF AGE 69

4.7.4 WNT SIGNALING IS DOWN-REGULATED IN *LIN28A* TG CTEC FROM 2 TO 7 WEEKS OF AGE 71

4.8 MOLECULAR CONSEQUENCES OF *LIN28A* ECTOPIC EXPRESSION IN TEC 74

4.8.1 *LIN28A* TG RE-PROGRAMS METABOLISM OF CTEC^{HI} FROM OXIDATIVE PHOSPHORYLATION TO GLYCOLYSIS 74

4.8.2 ECTOPIC *LIN28A* INCREASES THE ACTIVATION OF MAPK IN CTEC^{LO} AND MTEC 78

4.8.3 *LIN28A* TG TEC SHOW HIGHER *FOXO3A* EXPRESSION AND INCREASED ACTIVATION OF JNK 81

4.8.4 TNF-R1 EXPRESSION IS HIGHER IN *LIN28A* TG TEC AND TNF-A INCREASES TEC APOPTOSIS UPON NF-KB INHIBITION 83
5. SUMMARY OF FINDINGS 85
6. DISCUSSION 89
7. REFERENCES 101

ABSTRACT

The thymus provides the stromal microenvironment crucial for the development of T cells. Thymic epithelial cells (TEC) constitute the most abundant cellular component of the thymic stroma and are indispensable for T cell generation, selection and maturation. TEC are classified into cortical (c) and medullary (m) epithelia based on their distinct anatomical locations, molecular phenotypes and functional features. MicroRNAs (miRNAs) are post-transcriptional regulators of gene expression that play crucial roles in numerous biological processes including cell fate determination, self-renewal, differentiation, proliferation and apoptosis. The importance of miRNA for TEC biology is reflected in the observation that miRNA-deficient TEC display defects in committing hematopoietic precursors to a T cell fate, mediating thymocyte positive selection and effecting normal promiscuous gene expression required for central tolerance induction. Lethal-7 (Let-7) miRNAs are the most abundant miRNAs in the genome, constitute a family of 10 conserved isomiRs encoded on different chromosomes and are critically involved in cell differentiation. Let-7 miRNAs are negatively regulated by the RNA binding proteins (RBPs) Lin28A and Lin28B. Both paralogues inhibit the generation of mature Let-7 transcripts and in addition regulate gene expression via direct mRNA target-binding, thus controlling multiple cellular processes such as development, cell-cycle control, differentiation, apoptosis and metabolism. However, the role of the Lin28/Let-7 axis is unknown for TEC development, function and maintenance. To investigate the importance of this axis, I expressed either Lin28A, Lin28B or both gene products in TEC using tissue-directed transgenesis. Lin28A and Lin28B differentially regulated thymic organ size, TEC maturation and function under the experimental condition doses. Thymic hypoplasia and hyperplasia were prominent findings in Lin28A and Lin28B transgenic mice, respectively. Their corresponding thymic size correlated with the number of early thymic progenitors (ETP)

detected thus reflecting opposing roles for Lin28A and Lin28B. Both RBPs mediated changes in the mTEC subset composition whereas the cTEC compartment was only altered in Lin28A mutant animals. The changes in the composition of cTEC imposed by Lin28A impaired the positive and cortical negative selection of thymocytes. In adult mice, Lin28A mediated the persistence of phenotypically immature cTEC, that are more stringent in regulating thymocyte positive selection than cTEC with a mature phenotype. Finally, I show that Lin28A enhances glucose metabolism of cTEC and induces TEC apoptosis through tumor necrosis factor receptor 1 (TNF-R1) signaling. Taken together, this work demonstrates that Lin28A and Lin28B expression differentially affect both thymus development and function despite their comparable ability to target Let-7 transcripts thus identifying previously unrecognized roles for Lin28 in thymus biology.

ACKNOWLEDGEMENTS

This dissertation would not have been possible without the help, support and guidance of my mentors, lab mates, friends and family.

To start, I want to thank Professor Georg A. Holländer for his guidance and great mentorship during the past four years. Right from day one, Georg has been teaching me to always keep an eye on the bigger picture and to constantly “keep the foot on the accelerator”. From my days of playing around with ideas of which direction to take this project, to the thrilling time of revealing the mechanisms behind the Lin28 imposed effects on TEC biology, to the painful months of grooming and fine-tuning the paper – Georg has always supported me with his wisdom and helped me to get through these times even when I could not see the light at the end of the tunnel. Your great leadership, your superhuman energy and your passion for science has been very inspiring and encouraging. It has been a privilege to join your lab and to grow under your leadership.

I also want to express my deep gratitude to Doctor Thomas Barthlott who shaped the second half of my PhD studies. If I think about where I started four years ago and where I am standing right now, I can truly say that Thomas' insightful feedbacks and critical questions pushed me to sharpen my mind and brought my skills to a higher level. I could not have imagined having a better advisor for my PhD studies.

I would also like to acknowledge my PhD committee members, Professor Primo Schär and Professor Tudor Fulga for their valuable guidance throughout my doctoral studies.

Of course, my thanks also go to my lab-mates Lucas Musette and Anja Kusch for their camaraderie and for always lending a helping hand. I will miss the fun discussions we had during our lunch breaks. To Katrin Hafen and Elli Christen, thank you for the technical and mental support you gave me during my PhD. I was lucky to have such great lab-mums. To Saulius Zuklys and Irene Calvo, thank you for the stimulating discussions, sound advice and encouragement. I am also thankful for the time spent with past members of the Paediatric Immunology Lab: Hong Ying Teh, Carlos Mayer and Sanjay Gawade.

My special gratitude goes to my close circle of friends, Christian Soldo, Güney Boz, Nemanja Stanic, Mladen Mitrovic and Mikel Tran. Thank you for listening, offering advice and giving me the necessary distraction outside of the lab to rest my mind.

A very special word of thanks goes to my girlfriend, Léa Drai who has been by my side throughout my PhD studies and who has been a major source of support whenever things would get difficult. Thank you for always being there for me.

Finally, I want to dedicate my doctoral thesis to my family for their endless support, love and encouragement. To my mother Döndü and my father Mehmet who made countless sacrifices to offer their children the best future possible and for giving my sister and me the strength to chase our dreams. To my sister, Duygu for being such an important person in my life.

ABBREVIATIONS

AIRE	Autoimmune regulator
APC	Antigen presenting cell
BrdU	Bromodeoxyuridine
C. elegans	Caenorhabditis elegans
CCL#	CC-chemokine ligand#
CCHC	Cysteine cysteine histidine cysteine zinc knuckle domain
CD#	Cluster of differentiation#
CK#	Cytokeratin #
CLP	Common lymphoid progenitor
CSD	Cold shock domain
cTEC	Cortical thymic epithelial cell
CTL	Cytotoxic T cell
Ctsl	Cathepsin L
DAMP	Danger-associated molecular pattern
DAPI	4’,6-diamidino-2-phenylindole
DLL4	Delta-like ligand 4
DN	Double negative
DP	Double positive
EDTA	Ethylenediaminetetraacetic acid
ETP	Early thymic progenitor
FACS	Fluorescence-activated cell sorting
GFP	Green fluorescent protein
gMFI	geometric mean fluorescence intensity
IL	Interleukin
IRES	Internal ribosomal entry site
ISP	Immature single positive
Let-7	Lethal-7
MHC	Major histocompatibility complex
MSI1	Musashi 1
mTEC	Medullary thymic epithelial cell
n.d.	Not detectable
PCR	Polymerase chain reaction
PD-1	Programmed cell death protein 1
qPCR	quantitative PCR
RAG	Recombination activating gene
S1P1	Sphingosine-1-phosphate 1
SD	Standard deviation
SP	Single positive
TEC	Thymic epithelial cell
TNF	Tumor necrosis factor
TNF-R1	Tumor necrosis factor receptor 1
TRA	Tissue restricted antigen

FCS	Fetal calf serum
fl or floxed	Flanked by loxP sites
FoxP3	Forkhead-Box-Protein 3
Treg	Regulatory T cell
TSSP	Thymus specific serine protease
WPRE	Woodchuck hepatitis virus post-transcriptional regulatory element

1. INTRODUCTION

1.1 The history of the Thymus

The immune system plays a crucial role in protecting the body against a vast number of harmful challenges, including microbial pathogens and other diseases, a function which is dependent on the ability to discriminate between vital "self" and injurious "non-self". This competence is acquired by T lymphocytes in the thymus, the last organ in our body that revealed its essential role in health and disease. The first direct references to the thymus as an organ were noted by the Greek physicians Rufus of Ephesus and Galen of Pergamum circa 100-200 AD. They believed the thymus to be the "Seat of the soul" because of its close vicinity to the heart as well as its aura of mystery that surrounded it [1]. In the Middle Ages, the thymus gland was largely ignored, though some believed the organ to be a protective cushion for the vasculature of the chest cavity. The crucial milestone in disentangling the thymus physiology was marked in the 17th century with the invention of the first microscope, when the surgeons William Hewson and Arthur Hill Hassall identified the lymphatic nature of the thymus through histological analyses. By the late 1950s, the thymus' importance in the immune system was well recognized [2]. It would, however, take the efforts of the immunologist Jacques Miller in 1961 to ultimately understand the importance of the thymus in regulating the immune response. In a series of experiments, Miller observed that the surgical removal of the thymus in neonatal mice resulted in a deficiency of a lymphocyte population, later named as T cells [3]. In the subsequent years, the combined work of several scientists has revealed critical roles of the thymus in processes such as positive selection [4], negative selection of auto-reactive T cells [5] as well as the generation of regulatory T cells (T_{reg}) [6]. The detailed understanding of thymus physiology has therefore resulted from several decades of research. However, the rapid

development of novel technologies, like single cell RNA sequencing, has enabled discoveries of so far unknown mechanisms regulating thymic organogenesis and function.

1.2 Anatomy of the Thymus

The thymus is a primary lymphoid organ of jawed vertebrates which is located in the upper anterior thorax adjacent to the heart and consists of two separate lobes that are connected to each other via an isthmus. The thymus consists to 99% of developing T cells, known as thymocytes, whereas only 1% of cells make up the stromal compartment. Within the thymus stroma thymic epithelial cells (TEC) play a crucial role in supporting T cell development by producing soluble and cell-bound factors which are needed to navigate thymocytes through the different stages of T cell development. The thymus stroma, however, also consists of non-epithelial cells, such as mesenchymal cells, B cells, dendritic cells (DCs), macrophages, vascular and peri-vascular cells that collectively contribute to T cell development [7, 8].

The thymus microarchitecture includes two spatially and functionally distinct regions, namely an outer cortex and an inner medulla, which are separated by the cortico-medullary junction (CMJ) [9]. The majority of the thymocytes, are situated in the outer cortical region rendering this compartment heavily packed with developing T lymphocytes. The cortex is marked by a scaffold of thymic epithelial cells that create a mesh-like organization providing a large cell surface area allowing the simultaneous interaction of an individual cortical (c) TEC with several thymocytes. One of the key roles of cTEC is to provide survival signals to useful thymocytes (i.e. express a T cell receptor (TCR) that weakly interacts with peptide/self-MHC molecule complexes). In parallel, cTEC are capable to instruct the elimination of possibly dangerous cells (i.e. cells with a TCR able to strongly interact with peptide/self-MHC complexes) [10]. Other cell types present within the cortex are macrophages responsible for clearing apoptotic thymocytes, mesenchymal cells necessary for the functional development of

TEC and endothelial cells providing the portal for the entry of hematopoietic progenitor cells into the thymus and the exit of naïve T cells into the periphery [11, 12, 13]. In contrast to the cortex, the medulla is less densely populated as only a small number of thymocytes access this compartment consequent to the selection in the cortex which removes the majority of thymocytes. Medullary (m) TEC have a less sponge-like structure than cTEC and present a nearly complete repertoire of self-antigens in order to eliminate auto-reactive thymocytes [14, 15]. The medulla contains additional antigen presenting cells, such as B cells and dendritic cells, which are able to acquire autoantigens and present them to developing thymocytes and hence contribute to the depletion of self-reactive cells [16, 17, 18]. Taken together, the thymic stroma provides a specialized microenvironment that fosters the development and selection of functionally competent T cells.

1.3 Thymus Organogenesis

Organogenesis of the thymus is a well-organized sequence developmental steps that are closely tied to the formation of the parathyroid glands (Figure 1). Both organs arise bilaterally at around embryonic day 10.5 (E10.5) from the endodermal lining of the ventral aspect of the third pharyngeal pouch (3^{rd}pp) which is surrounded by neural crests cells (NCCs) that support the outgrowth of the primordium [7] (Figure 1). Parallel to the extension of this early structure, the expression of the transcription factor Forkhead box protein N1 (Foxn1) starts in the dorsoventral region of the primordium at around E11.25 [19]. Simultaneously, the expression of the transcription factor Glial cells missing 2 (Gcm2) is initiated in the adjacent part of the primordium. The expression of these two transcription factors delineates the separate areas of the primordium with distinct developmental fates: Foxn1 controls the construction of the thymic epithelial scaffold while Gcm2 regulates parathyroid differentiation. Although Foxn1 is indispensable for the proliferation, maturation and function of TEC, it is not responsible for

their fate determination (i.e. lineage commitment). Thus, once epithelia from the 3rdpp have committed to the TEC fate, Foxn1 drives the cells' further development and function. In addition, Foxn1 is crucial for the maintenance of the thymic organ and its decline in expression contributes to thymic involution. It is to be noted that Foxn1 is also expressed in the skin where it is responsible for the robustness of hair shafts [20, 21]. Reflecting the functional role of Foxn1, mice deficient for this transcription factor (*Foxn1* gene is located at the nude locus, hence these animals were designated as nude; "nu/nu" mice as they have little to no hair) still make a rudimentary and cystic thymus anlage that lacks the ability to attract blood-borne lymphoid progenitors to foster the cells development to T cells [21]. At E12.5, the common anlage has given rise to a separate thymic lobe and a parathyroid gland in each side of the neck. In the subsequent development of the thymus, the interaction of multiple cell types is essential, including the neural crest cells, mesenchymal cells, endothelial cells, TEC and hematopoietic cells, especially maturing thymocytes. Neural crest cells hereby support the development of the thymic capsule and the trabeculae while mesenchymal cells are required for epithelial cell proliferation though the production of fibroblast growth factors (Fgf)-7 and -10 as well as retinoic acid (RA) and insulin-like growth factor (Igf)-1 and -2 [22, 23, 24]. Endothelial cells play an important role in the seeding of the thymus with blood-borne lymphoid progenitors as the cells expressing lymphotoxin beta receptor (LTβR), the adhesion molecules P-selectin, VCAM-1 and ICAM-1 whereas their corresponding ligands are expressed on early thymic progenitors (ETP) [12, 25, 26]. ETP enter at E12.5 the still avascular thymus anlage via migration through the capsule of the developing organ [27, 28, 29]. Between embryonic days 12 and 14, a next wave of precursor cells seeds the thymus and fosters TEC development by signaling through several tumor necrosis factor receptor superfamily (TNFRSF) members, such as LTβR, receptor activator of nuclear factor-κB (RANK) and CD40 [22, 23, 24, 25, 29].

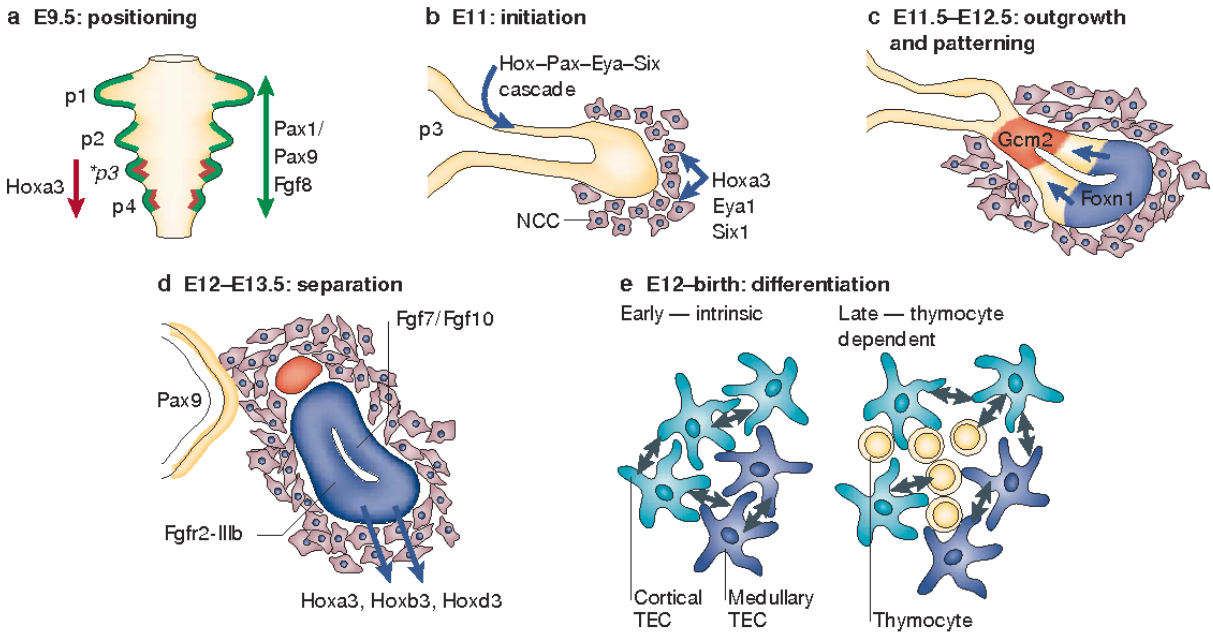

Figure 1: Current model of the thymus organogenesis

(**a**) At embryonic day 9.5 (E9.5), the thymus starts to develop from the outgrowth of the third pharyngeal pouch together with the parathyroid. The paired box genes (Pax) 1 and 9 as well as fibroblast growth factor (Fgf) 8 are hereby necessary for pharyngeal pouch formation while the expression of homeobox A3 (Hoxa3) is required for specifying organ identity within the 3rd pharyngeal pouch. (**b**) At E11, the outgrowing of the rudiment begins. The Hox-Pax-Eya-Six cascade is required the development of the endodermal cells (in yellow) whereas Hoxa3a, Eya1 and Six1 are also expressed in neural crest cells and thus might be important for proper thymus development (NCC). (**c**) At E11.5-12.5, the fate of the endodermal cells into thymic or parathyroid cells is decided by the mutually exclusive expression of Foxn1 and Gcm2, respectively. Thymic cells express Foxn1 (displayed in blue) while Gcm2 (shown in red) is expressed in parathyroid cells. (**d**) During E12-13.5, Pax9 drives the detachment of the thymic rudiment and parathyroid structure from the pharynx. In addition, Hoxa3, Hoxb3 and Hox3d initiate the separation and migration of the thymus primordium from the parathyroid. (**e**) From E12-birth the development of a functional thymus is also dependent on the interaction of the thymus organ primordia with different factors from surrounding cells and the developing thymocytes. *(Image stems from [7]).*

1.4 Thymic epithelial cell development and heterogeneity

TEC differentiation is a dynamic process that is initiated during embryonic development and continues after birth (Figure 2) [34]. Despite the anatomical and functional differences between cTEC and mTEC, both develop from a common thymic epithelial progenitor cell (TEPC) [35]. The existence of these progenitors was first suggested by the identification of cells which are located at the cortico-medullary junction in postnatal mice and that stained positively for cytokeratins 8 (CK8; a classical cortical marker) and 5 (CK5; a characteristic marker for medullary epithelia), respectively [36, 37]. Further evidences for the presence of TEPC came from experiments showing that the microinjection of single enhanced yellow fluorescent protein (eYFP)-tagged E12.5 TEC into embryonic wild-type thymi gave rise to both cTEC and mTEC lineages [38].

The developmental connection between the seemingly distinct cTEC and mTEC lineages was further corroborated by in vivo cell lineage tracing experiments using a fluorescent reporter gene triggered by a doxycycline-inducible Cre recombinase under the transcriptional control of the *Psmb11* promoter. *Psmb11* is a gene which encodes the cortical TEC-specific β5t catalytic subunit of the thymoproteasome [39]. Hence, this fate-mapping system was used to mark TEC that have expressed β5t at any time subsequently to constitutively express an enhanced green fluorescent protein (eGFP). The work by Ohigashi and others inferred that TEPC express β5t and that these progenitor cells first acquire characteristics of cTEC (i.e. expressing CD205, β5t and IL-7) before committing to the mTEC differentiation pathway [40]. Because eGFP was detected in the vast majority of mTEC in young mice but these cells lack β5t expression, this finding implied that most mTEC at this age are derived from β5t positive progenitors. Additional studies localized these mTEC precursors to the cortico-medullary junction [40, 41].

After lineage divergence into cTEC or mTEC, immature TEC to up-regulate the expression of MHCII. Cortical and medullary TEC can hereby be distinguished using a set of well-defined markers, namely Ly51, CD205, CK8 and β5t for identifying cTEC and CK5, CD86, Autoimmune regulator (Aire) and reactivity for Ulex Europaeus Agglutinin 1 (UEA1) for delineating mTEC. Experimental evidence further suggests that the differentiation into the mTEC lineage requires the activation of the nuclear factor-kB (NF-kB) signaling pathway which is initiated by interactions of mTEC progenitors with hematopoietic cells. Specifically, CD4 single positive thymocytes influence mTEC differentiation via signals including CD40L, Lymphotoxin-beta (LTβ) and Receptor Activator of NF-kB Ligand (RANKL) [42, 43, 44, 45,]. Parallel to MHCII up-regulation, developing mTEC increase their surface levels of co-stimulatory molecules including CD80 and CD86 and attain a phenotype defined to as mature mTEC once they express Aire [45].

This historical view of TEC development and heterogeneity has, however, recently been challenged by single cell RNA sequencing (scRNA-seq) studies. These analyses have identified at least 9 distinct cTEC and mTEC subtypes whose frequencies dynamically change over the life course [46, 47, 48, 49]. In addition, biocomputational approaches allowed to establish developmental trajectories between individual TEC subtypes that can be analysed under different experimental conditions to probe not only changes in the heterogeneity of the TEC stromal compartment but to also interrogate precursor::progeny relationships.

These transcriptomic studies have provided evidence that the classical segregation of TEC into cTEC and mTEC constitutes a simplification based on available cell surface markers used in flow cytometry. In effect, these two TEC subsets are highly heterogenous and are likely comprised of various cell subtypes with possibly very different functional competences.

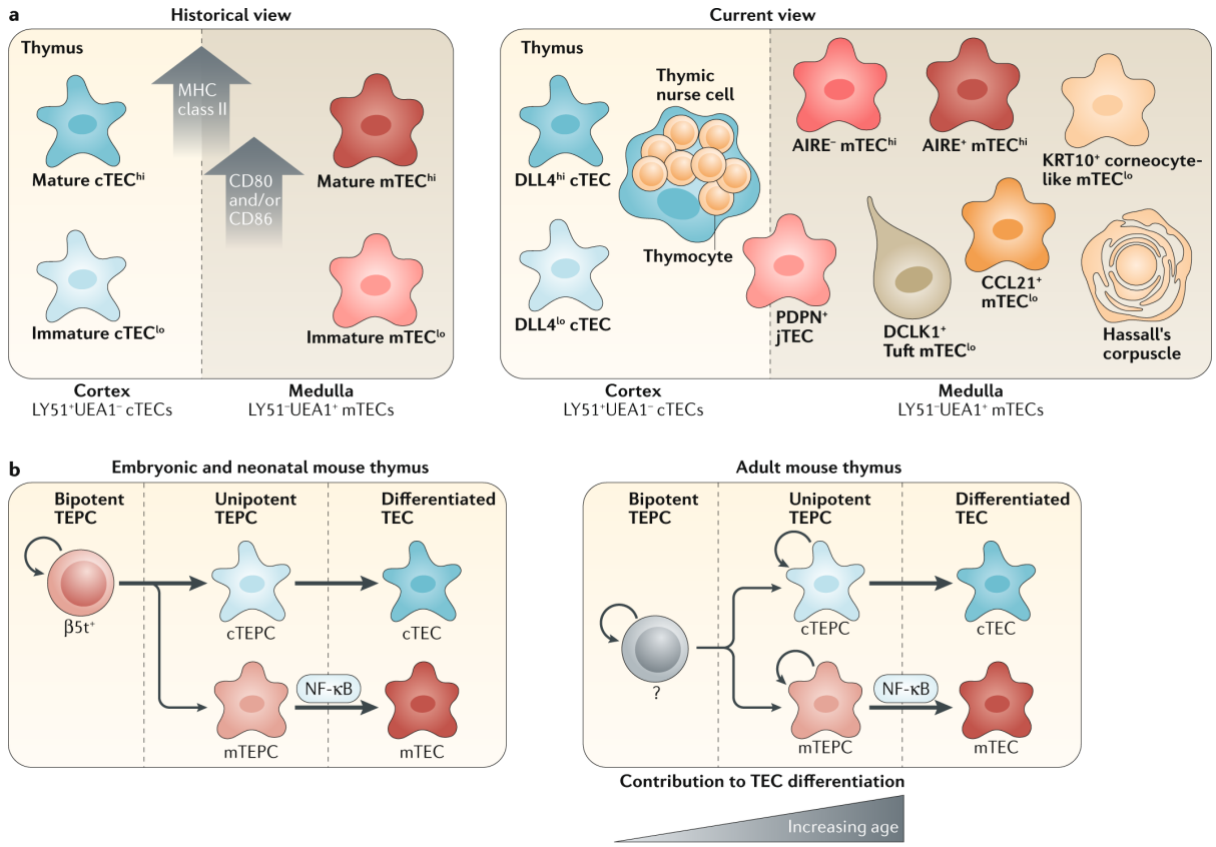

Figure 2: Thymic epithelial cell development and heterogeneity

(**a**) Historically, the two main TEC subpopulations were differentiated using a set of surface markers, such as UEA-1 (for mTEC) and Ly51 (for cTEC) and MHCII, CD80 and CD86 (for the separation of immature from more mature TEC developmental states). However, recent single cell genomic technologies have been used to show that TEC are highly heterogenous and comprise multiple subpopulations. (**b**) In the embryonic and neonatal thymus, a common β5t-expressing TEC progenitor can give rise to cTEC and mTEC. While the commitment into the cTEC lineage occurs by default, the differentiation into the mTEC lineage requires nuclear factor- kB (NF-kB) signaling. In adult mice, however, the existence of a bipotent TEC is still under debate. Abbreviations: AIRE, autoimmune regulator; CCL21, CC-chemokine ligand 21; cTEPC, cTEC progenitor; DLL4, delta-like ligand 4; jTEC, junctional TEC; KRT10, keratin type I cytoskeletal 10; mTEPC, mTEC progenitor; PDPN, podoplanin. *(Image stems from [35]).*

1.5 T cell development

The thymus is the site for T cell formation and selection. T cell development comprises a series of maturational processes within the thymic microenvironment and is initiated with the recruitment of T lymphoid progenitors from the blood, also known as thymus seeding. These blood-borne progenitors enter the thymus as early as E12.5 in a vasculature-independent manner and in post-natal mice via the well-developed vasculature at the cortico-medullary junction of the thymus [50, 51]. The seeding of the thymus is orchestrated by the expression of CC-chemokine ligand 25 (CCL25), CXC-motif-chemokine 12 (CXCL12) which are mainly expressed by cTEC and CC-chemokine ligand 21 (CCL21), CC-chemokine ligand 19 (CCL19) which are produced by mTEC [52]. Moreover, thymus settling of these hematopoietic precursors is also regulated by the interplay of platelet (P)-selectin glycoprotein ligand 1 (PSGL1) expressed on T lymphoid progenitors with P-selectin present on the thymic endothelium [25]. However, the entry of progenitors into the thymus is not a continuous process but rather happens in two successive waves, one between E11-E14 and the second at E18 [53]. The mechanisms behind this intermittent process are, however, yet unknown.

Upon thymus entry, these blood-borne progenitors give rise to ETP which start their maturation as CD4 and CD8 double negative (DN) cells. DN maturation can be phenotypically followed using the cell surface expression of CD25, the IL-2 receptor α-chain, CD71, a transferrin receptor essential for iron uptake and CD44, a glycoprotein involved in cell-cell interactions, adhesion and migration. The maturational trajectory of DN development starts with cells that express CD44 but lack CD25 and CD71 expression (designated as DN1) and is followed by a stage that expresses CD44 and CD25 but is CD71 negative (designated DN2). Subsequently, these thymocytes gives rise to cells that only express CD25 (DN3a) which is followed by a stage that is CD25 and CD71 positive (DN3b). The development of DN1 to DN3 is supported by interactions with cTEC. DN1 and DN2 cells express the stem cell factor (SCF)

receptor c-kit, a transmembrane tyrosine kinase which upon interaction with SCF expressed by cTEC promotes the proliferation of these immature thymocytes [54, 55]. Moreover, cTEC also express Delta like ligand 4 (Dll4), which commits ETP to the T cell lineage engaging Notch signaling in DN1 and DN2 cells [56]. These initial maturational steps of DN1 to DN3 also depend on survival signals provided by cTEC in the form of interleukin-7 (IL-7) [57, 58]. Parallel to their development, DN thymocytes also migrate from the CMJ to the sub-capsular zone, a process controlled by numerous chemokine receptors including C-X-C chemokine receptor type 4 (CXCR4, recognizing CXCL12), C-C chemokine receptor 7 (CCR7, recognizing CCL19 and CCL21) and CCR9 (recognizing CCL25) [59, 60, 61]. As part of this interaction, DN1, DN2 and DN3 thymocytes also regulate cTEC differentiation although the exact signals provided for this phenomenon remain yet elusive [37].

Concomitant to the relocation towards the subcapsular region, DN cells start to rearrange their TCRß-locus. During this process of somatic gene recombination, individual gene segments of variable (V), diversity (D) and joining (J) region within the TCRß-locus are recombined by a machinery of nuclear enzymes, including the recombination-activating genes (RAG) 1 and 2. The successful and productive (i.e. in-frame) recombination results in the generation of a locus that encodes a complete TCRß-chain with unique antigen specificity [62]. DN3 and DN4 cells are then characterized by the surface expression of a pre-TCR composed of a complete ß-chain that associates with an invariant pre-TCRα chain. Only those DN3 cells which have successfully rearranged ß-chain and thus express a functional pre-TCR will receive survival signals in a process known as ß-selection and are enabled to differentiate further [63]. Cells passing the ß-selection checkpoint also undergo a proliferative burst and continue their maturation by down-regulating CD25 to attain a DN4 stage. Subsequently, these cells start to express CD8 to become CD8 immature single positives (CD8 ISP) before up-regulating CD4 to develop into $CD4^+CD8^+$ double positive (DP) cells.

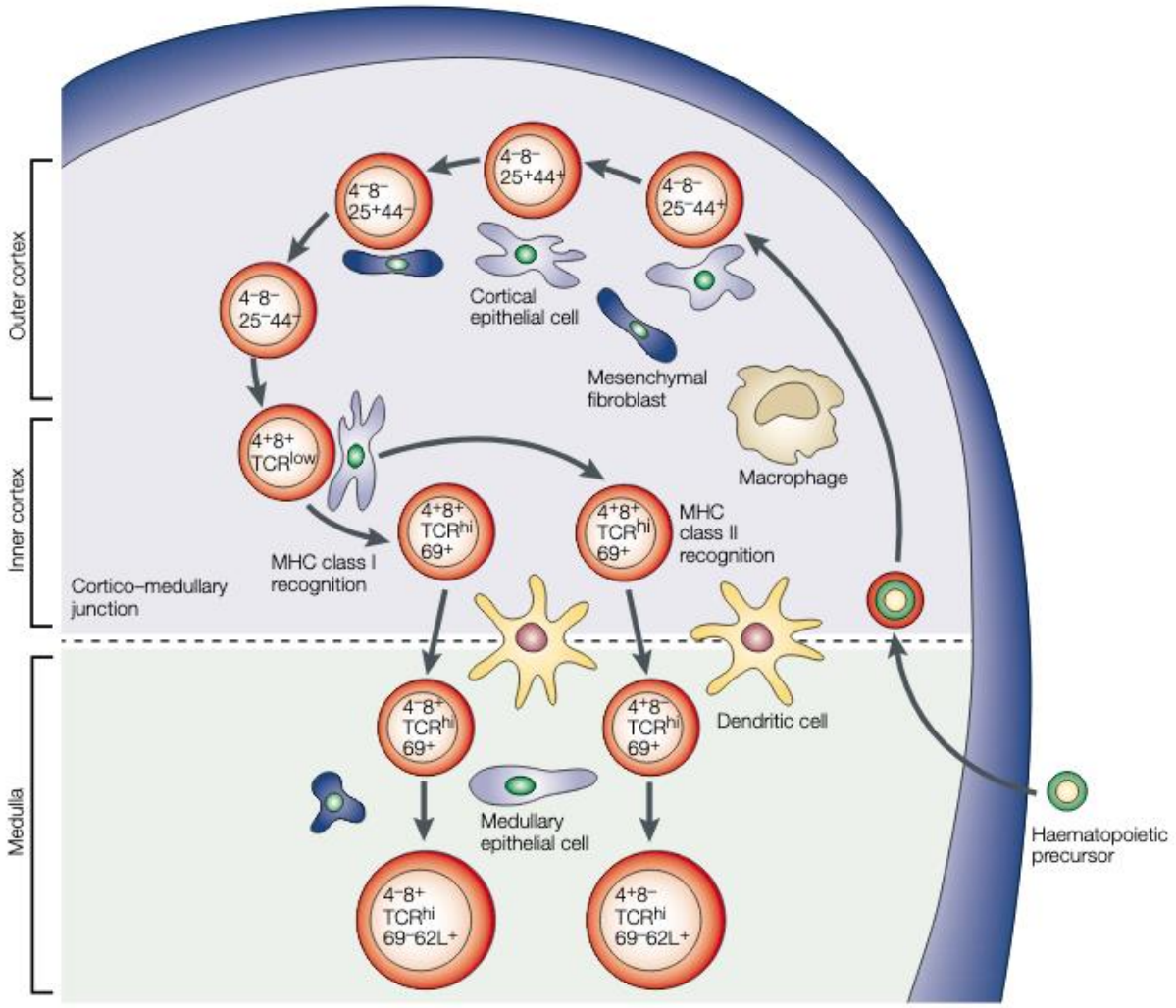

Figure 3: Schematic representation of T-cell development and selection

Hematopoietic precursors are recruited to the thymus via blood vessels near the cortico-medullary junction. Guided by chemokines from the thymic stroma, these progenitors relocate to the cortex, commit to a T cell fate and start to rearrange their TCRß-locus. The initial stages of T cell maturation lack the expression of the co-receptors CD4 and CD8 expression (termed as double negatives, i.e. DN) and can be phenotypically followed using the cell surface expression of CD25 and CD44 (termed as DN1 to DN4). Upon successful TCRß rearrangement and subsequent expression of a functional pre-TCR, developing T cells receive survival signals and up-regulate CD4 and CD8 to attain a double positive (termed DP) stage. DP cells that have a TCR with strong affinity to self-antigens are removed from the T cell repertoire in a process called negative selection. Thymocytes that generated a TCR with intermediate affinity to self-peptide/MHC experience a positive selection signal and can develop further while the rest dies by neglect. Subsequently, thymocytes down-modulate one of the co-receptors to enter the SP stage in the medulla. The remaining self-reactive thymocytes undergo further negative selection by mTEC. Finally, thymocytes that completed all the selections steps enter the periphery as self-MHC restricted and non-autoreactive naïve T cells. *(Image stems from* [174]*).*

The newly generated DP rearrange their TCRα-locus to express heterodimeric TCRα/TCRβ chains together with the CD3 complex on the cells' surface. At this developmental stage, thymocytes are probed for the functionality of their TCR specificity when binding peptide/MHC-complexes expressed on the surface of cTECs [64]. This stage marks the second checkpoint of thymocyte development, whereby the strength of TCR binding to peptide/MHC-complexes determines the fate of these DP cells. Collectively, a number of studies have resulted in the so called affinity model of T cell selection that explains the outcome of this important process as a function of the receptors affinity to its cognate ligand (Figure 4) [15]. The majority of DP thymocytes express a TCR with low or no affinity to peptide/MHC-complex. Consequently, the necessary survival signals are not received by these thymocytes and a cell-intrinsic process of programmed cell death is not prevented. As a consequence, these thymocytes will undergo apoptosis in a process known as "death by neglect". On the other hand, cells having a TCR that mediates the interaction to self-MHC plus peptide complexes with intermediate affinity will survive. This quality check is referred to as positive selection and ensures the further maturation of cells. Thymocytes with high TCR affinity are removed from the repertoire in a process called "negative selection" which is mediated by the up-regulation of the pro-apoptotic molecule Bim through protein kinase C [15]. Other thymocytes display TCR affinity which confers sufficient binding strength to escape negative selection but that is nonetheless higher to what is required for the escape of programmed cell death by conventional effector cells. This alternative selection process has been termed "agonist selection" [65], and generates regulatory T cells (T_{reg}) [66].

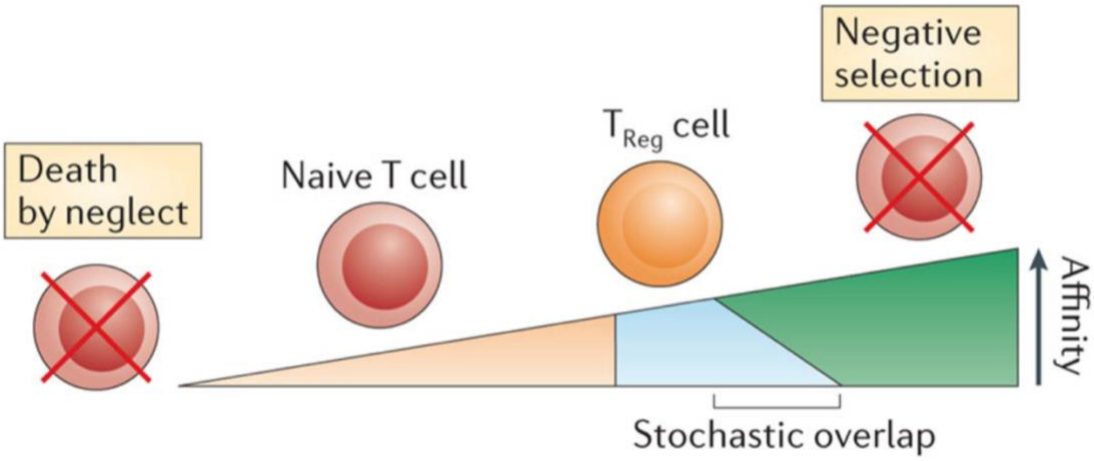

Figure 4: The affinity model of T cell selection

Newly generated TCR are being tested for their affinity to self-peptide/MHC-complexes. The majority of thymocytes do not recognize peptide/MHC-complexes and "die by neglect". Cells baring a TCR with intermediate affinity are positively selected and continue their maturation while thymocytes with high binding strengths are negatively selected and removed from the repertoire. As there is no sharp affinity threshold for positive and negative selection of cells there is a range at which some thymocytes are stochastically selected and usually develop into the T_{reg} lineage. *(Image stems from [15]).*

Positively selected thymocytes transiently express the early activation marker CD69 and down-module the expression of the co-receptors CD4 and CD8, also known as "dulling" [67]. Thereafter, these thymocytes will commit to the separate CD4 or CD8 lineages, depending on the class of MHC recognized. While DP cells that bind MHC II down-regulate CD8 surface expression to become CD4 single positive (SP), MHC I recognition promotes CD4 down-modulation and subsequent maturation into CD8 SP [68, 69]. However, the generation of CD4 and CD8 SP is an sequential process where CD4 SP arise before CD8 SP [68]. Although it was suggested that the co-receptors have different transcriptional activities, the exact molecular mechanisms behind the asynchrony of CD4 and CD8 differentiation are yet unknown. The earliest CD4 SP subset (designated SM, semi-mature) is CD24 positive and still localized in the cortex due to lack of a cell surface expression of the CC-chemokine receptor 7 (CCR7) [70]. CCR7 binds to the two chemokine ligands 19 (CCL19) and 21

(CCL21), that in the thymus are predominantly produced by mTEC, and control the access of the cells from the cortex to the medulla [60]. Once in the medulla CD4 SP thymocytes up-regulate the expression of CD69 (achieving a developmental stage designated mature 1, M1). Subsequently, these cells down-modulate CD69 and CD24 expression and attain a fully mature phenotype (designated mature 2, M2) equipped to produce cytokines and to proliferate upon activation. Mature CD8 SP thymocytes are exclusively detected in the medulla where they first adopt a $CD69^{+}CD24^{+}$ stage (M1) before down-regulating both of these markers to develop a mature (M2) phenotype.

Thymocytes that express a TCR with high affinity to tissue restricted antigens (a.k.a. "self-peptides") receive an apoptotic signal and undergo negative selection. This process promotes central tolerance and is important to remove potentially auto-reactive cells from the repertoire [71]. The first negative selection event occurs in the cortex (designated wave 1) and is followed by a second negative selection which occurs in the medulla (known as wave 2) [72]. Thymocytes subjected to wave 1 are identified by the co-expression of the transcription factor Helios and the programmed cell death protein 1 (PD-1) whereas those of wave 2 are phenotypically recognized by Helios [72].

In the medulla, thymocytes spend approximately 12 days before they are sufficiently mature to exit the thymus [73, 74]. During this sojourn, SP cells are also being tested for both ubiquitous and tissue restricted antigens (TRA) presented by mTEC to remove the remaining auto-reactive cells. The expression of a variety of peripheral tissue self-antigens is mediated by a subpopulation of mature mTEC and involves the expression of the transcription factor Autoimmune Regulator (Aire). Another group of medullary cells, namely dendritic cells (DCs), also contribute to the process of negative selection by cross-presenting mTEC derived TRAs [75]. Moreover, medullary thymic B cells purge negative selection by presenting self-antigens with their BCR [18].

Once having successfully survived all selection steps and completed all maturational stages, thymocytes exit to the periphery as mature and functionally competent naïve T cells. The egress of these mature cells happens via the perivascular space and is controlled by G-protein coupled sphingosine-1-phosphate receptor 1 (S1P1) [51]. Thymic emigrants join the pool of peripheral T cells capable to mount an immune response to foreign antigens whilst tolerant to self-antigens.

1.6 Thymic epithelial cell function

cTEC are responsible for the attraction of hematopoietic precursors to the thymus, their commitment to the T cell lineage, their subsequent survival, expansion and early maturation including the decisive steps of positive and first wave of negative selection. One characteristic that distinguishes cTEC from other antigen presenting cells (APC) is the possession of a specific molecular machinery by which peptides are processed and presented in the context of MHC class I and class II molecules. For example, cTEC express a unique proteasome known as thymoproteasome as its β5 subunit is replaced by a tissue-specific variant designated β5t. The expression of β5t in cTEC catalyzes a unique set of MHC-I associated peptides that are important for the positive selection of CD8 SP thymocytes [76]. Moreover, cTEC express proteases such as Cathepsin L (Ctsl) and thymus specific serine proteases (TSSP) which are involved in the processing of antigens to peptides that are presented in the context of MHC-II molecules (Figure 5). Both peptide producing pathways influence the efficacy by which CD4 SP thymocytes are generated as their deficiency impairs positive selection [77, 78].

One of the major roles of mTEC is to guarantee a comprehensive negative selection of thymocytes with a high affinity receptor for TRA. Crucial to this function of mTEC is the unique ability to promiscuously express and present a largely comprehensive array of peptides

derived from TRA. The promiscuous expression of TRAs is achieved by the transcriptional facilitator Aire, which in the thymus is exclusively expressed in a subset of mature mTEC (MHCII^{hi} Sca-1^{int}) [79]. The transcription factor Forebrain Embryonic Zinc Finger-like 2 (Fezf2), has also been implicated in TRA expression by mTEC [80]. In addition to expressing a large number of self-peptides, mTEC also express co-stimulatory molecules CD80 and CD86, which complement the peptide/MHC derived signals and contribute to the signaling in thymocytes that upon sufficient strength induce apoptosis [81].

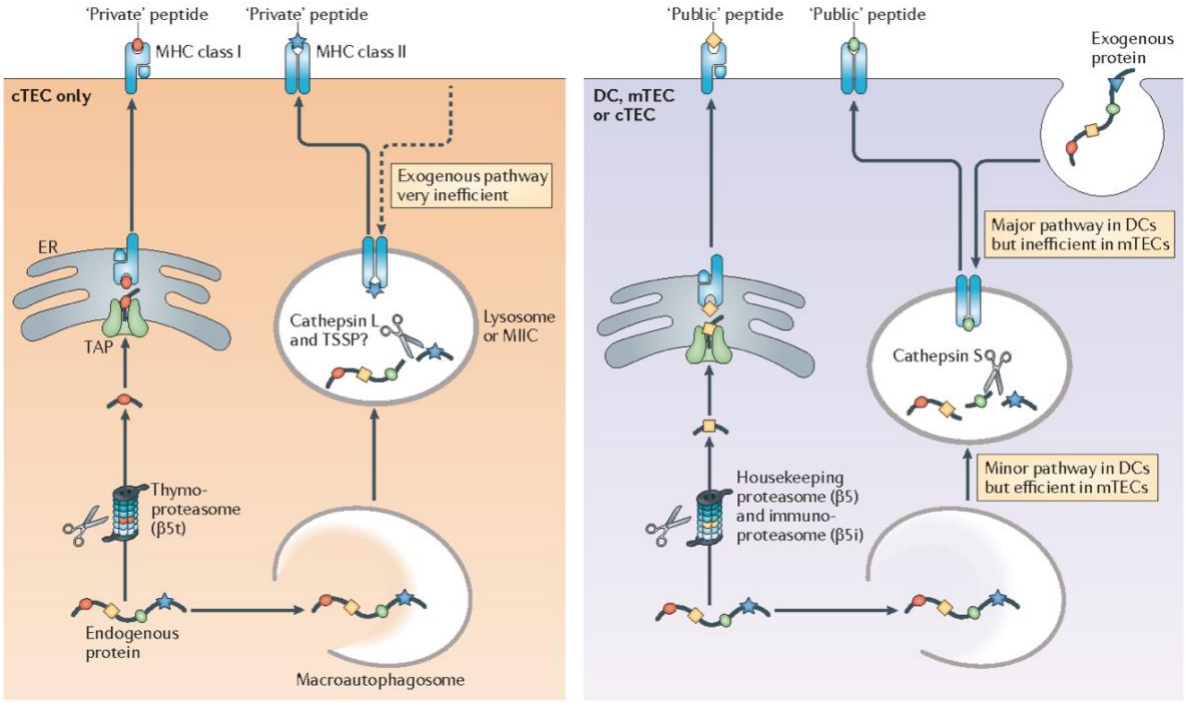

Figure 5: Antigen presentation in TEC requires unique proteolytic machineries
Endogenous proteins are degraded by proteasomes and the resulting peptides are transported into the ER and loaded on MHC class I molecules. The peptide/MHC complex is then transported to the cell surface where it can be detected by thymocytes. The proteasomes can contain different subunits in different cell types. MHC class II molecules acquire their peptides mostly through macroautophagy derived lysosomes in TEC. Various lysosomal proteases process proteins derived from macroautophagosomes or endosomes, depending on the cell type. *(Image stems from [15]).*

1.7 The role of microRNAs and their importance in TEC biology

MicroRNAs (miRNAs) are a class of small (19-25 nucleotides), single stranded, non-coding RNAs that function as post-transcriptional gene regulators and have been implicated in many different biological processes, including cell development, self-renewal, proliferation, metabolism and apoptosis [82]. The biogenesis of mature miRNA involves a series of catalytic processes steps, including the cleavage of primary (pri) and precursor (pre) miRNA molecules by endoribonucleases Drosha and Dicer, respectively [82]. Mature miRNAs, together with Argonaute proteins, form a multiprotein complex, known as RNA-induced silencing complex (RISC). Guided by the miRNA via base-pairing, the miRNA-RISC complex binds to the 3' untranslated region (3'UTR) of target messenger RNAs (mRNAs) and enforces a translational repression or the cleavage and degradation of the mRNA (Figure 6) [82].

The collective importance of miRNA for TEC biology was shown for example, in TEC deficient for the RNA-processing enzyme Dicer. TEC devoid of miRNAs fail to maintain a normal thymic architecture, are unable to commit hematopoietic precursors to a T cell fate and display defects in thymocyte positive and negative selection [83]. The impact of single miRNAs on TEC biology was also revealed using transfections of miR-181a into mTEC which resulted in a higher proliferation rate of these cells [84]. Furthermore, the development of mature mTEC (i.e. $MHCII^{hi}$) is impaired in mice where the activity of miR-449a is inhibited [85]. Finally, a TEC-restricted ablation of miR-155 impairs the development and function of mTEC in fostering T_{reg} maturation [86]. Although these studies provided evidence for the importance of miRNAs in TEC biology, the exact functional roles of the majority of the approximately 2000 individual mouse miRNAs for TEC development and function remain unknown.

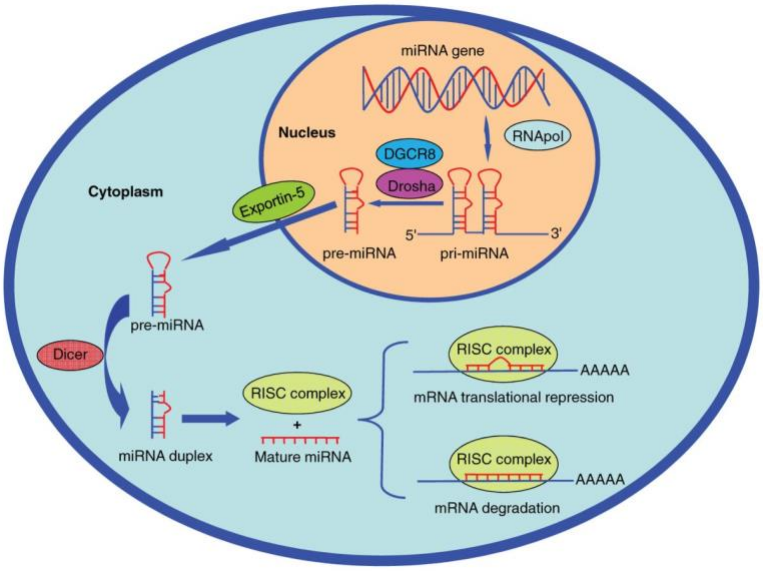

Figure 6: Schematic representation of miRNAs biogenesis and function
Primary miRNA (pri-miRNA) molecules are produced by RNA polymerase before being processed by the microprocessor-complex Drosha-DGCR8 in the nucleus. The resulting precursor miRNA (pre-miRNA) is then translocated into the cytoplasm via Exportin-5 and further processed by the ribonuclease Dicer to generate mature miRNA. The functional strand of the mature miRNA is then associated with the silencing complex (RISC), where it guides RISC to silence target mRNA molecules through translational repression or RNA degradation. *(Image stems from [175]).*

1.8 The Let-7 family of miRNAs

The most abundant miRNA family is Lethal-7 (Let-7), which was discovered in the nematode *Caenorhabditis elegans* (*C. elegans*) and is highly conserved across animal species. Unlike *C. elegans*, higher animals have multiple (10-14) Let-7 isoforms whereby each isoform is encoded on different chromosomes. All of these isoforms share the same consensus sequence, called the "seed sequence", which is crucial for the binding to target mRNAs [87]. The expression of the Let-7 family has been shown to be indispensable for terminal cell differentiation. Undetectable in progenitor cells, Let-7 isoforms accumulate during cellular differentiation and target transcripts of several stemness factors for degradation thus inhibiting self-renewal and promoting cell differentiation [88]. Besides its involvement in stem cell regulation, Let-7 has also been shown to suppress cancer development and progression by negatively regulating the expression of proteins with oncogenic potentials, such as Rat sarcoma

(RAS), high-mobility group AT-hook 2 (HMGA2), c-Myc and cyclin-D2 [89]. Moreover, Let-7 is also involved in the regulation of glucose metabolism in multiple organs and its disruption results in insulin resistance and impaired glucose tolerance [90].

1.9 The RNA binding protein Lin28

The Let-7 family of miRNAs is negatively regulated by the RNA binding protein (RBP) Lin28. Lin28, like Let-7, was first discovered in *C. elegans* and described as a promoter of pluripotency critical during embryonic development. Differing to Let-7, Lin28 is highly expressed early during cell development and declines in response to signals driving cellular differentiation (Figure 7). Thus, Lin28 promotes an uncommitted, undifferentiated cell fate whilst acting in parallel as a gatekeeper of the transition from a pluripotent stage to a committed cell lineage. In addition, and independently of an effect on Let-7 biogenesis, Lin28 also directly binds to numerous mRNAs coding for molecules involved in diverse cellular functions, including proliferation and metabolism. Let-7 itself also binds to the 3' UTR of *Lin28* mRNA and block its translation, thus forming a negative feedback loop [91].

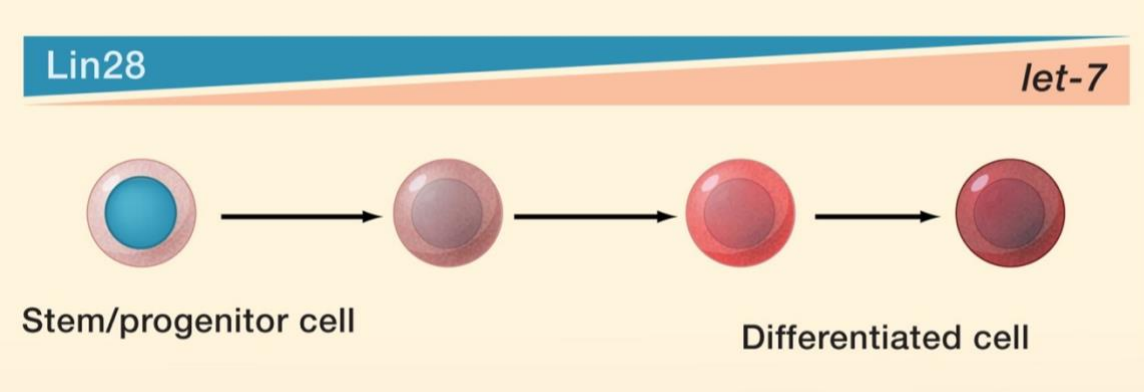

Figure 7: The Lin28/Let-7 feedback axis in cell development
During cell development, Lin28 is highly expressed in progenitor cells and blocks the biogenesis of mature Let-7 miRNAs, hence maintaining the expression of genes that induce self-renewal and proliferation. Concomitant to cellular differentiation, Lin28 expression decreases, allowing the production of mature Let-7 molecules. Subsequently, Let-7 represses the expression of genes involved in self-renewal, resulting in lineage commitment and terminal cell differentiation. *(Image stems from [176]).*

1.10 Isoforms and structure of Lin28

There are two paralogues of Lin28, namely Lin28A and Lin28B, which share an amino acid sequence identity of 77%. Both regulate protein expression by controlling Let-7 family miRNA biogenesis and by binding to target mRNAs consequently altering their translation. Both Lin28 RBPs are highly conserved across many species and harbor a unique combination of distinct RNA-binding motifs, a cold-shock domain (CSD) and two cysteine cysteine histidine cysteine (CCHC) zinc finger domains (ZFD) (Figure 8) [91]. The CSD domain is crucial for initial pri- and pre-Let-7 binding as it induces conformational changes and allows the binding of the zinc finger domains to pri- and pre-Let-7, respectively. The binding of Lin28 to mRNA strongly depends on the interaction of ZFD with a conserved "GGAG"-like motif present on hairpin loops of target mRNAs [92, 93, 94]. In contrast to Lin28A, Lin28B contains an extended tail region at its C-terminus and has additional nuclear and nucleolar localization sequence (NLS and NoLS, respectively). Hence, Lin28A is predominantly located in the cytoplasm while Lin28B is enriched in the nucleus, which has functional ramifications as detailed below [95].

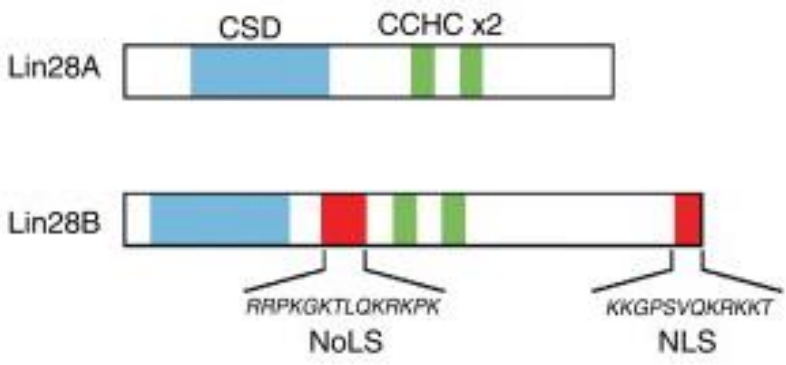

Figure 8: Lin28A and Lin28B protein structures

Lin28A and Lin28B have high sequence identity and comprise multiple common domains, namely a cold shock domain (CSD, displayed in blue) and two cysteine cysteine histidine cysteine (CCHC, shown in green) zink finger domains. Lin28B has, in addition, a nuclear localization signal (NLS) and a nucleolar localization signal (NoLS). *(Image stems from [177]).*

1.11 Lin28 RBPs regulate gene expression via two distinct biological pathways

1.11.1 Let-7 dependent functions of Lin28

The inhibition of Let-7 biogenesis is currently the best described mechanism of Lin28 mediated epigenetic regulation. Lin28 RBPs associate with the bulging "GGAG"-motif in the terminal loop of pri- and pre-Let-7 molecules and block their further processing. However, due to their distinct subcellular localization, Lin28A and Lin28B differ in their mechanism of inhibiting Let-7 processing. In the nucleus, Lin28B binds to pri-Let-7 and blocks its processing by the microprocessor complex Drosha:DGCR8. In contrast, Lin28A, which is primarily located in the cytoplasm, associates with pre-Let-7 and block its further cleavage by the ribonuclease Dicer. This interaction also mediates the terminal oligo-uridylation of pre-Let-7 molecules which induces their degradation (Figure 9) [87]. Although Lin28A is mainly localized in the cytoplasm, and Lin28B predominantly found in the nucleus, they can both shuttle between those two subcellular compartments and target pri- and pre-Let-7, respectively [88, 89].

1.11.2 Let-7 independent functions of Lin28

In addition to the negative regulation of Let-7 biogenesis, both Lin28A and Lin28B are able to directly bind to target mRNAs and modulate their translation by recruitment of RNA helicase A to polysomes and/or control mRNA stability through their RNA-binding domains (Figure 9) [91, 96, 97]. As an example, the increased expression of Lin28A enhances the ability of muscle cells to use glucose as an energy source through up-regulation of multiple components of the Insulin-PI3K-mTOR pathway, including Insulin receptor (Insr), Insulin-like growth factor 1 receptor (Igf1r) and Insulin receptor substrate 2 (Irs2). In contrast, a loss of Lin28A expression results in insulin resistance and impaired glucose tolerance in these cells [90, 91, 98]. Loss- and gain-of-function assays in myoblasts have furthermore shown that

Lin28A controls the differentiation of skeletal muscle cells through directly enhancing the expression IGF-2, an important growth and maturation factor in these cells [99]. Finally, two studies found that Lin28A promotes the proliferation of embryonic stem cells in part by binding to and increasing the expression of cell cycle related genes, such as cyclin A and B and cyclin dependent kinase 4 (CDK4) [99, 100]. On the other hand, Lin28B inhibits apoptosis in ovarian cancer cells by directly decreasing the expression of the pro-apoptotic B-cell lymphoma 2 (Bcl-2) family protein Bim [102]. Although it is still unclear how Lin28 confers specificity when targeting mRNAs, it seems that it primarily associates with hairpin structures in its targets, similar to its interaction with Let-7. Specifically, it was shown that Lin28 recognizes "AAGNNG" (N=A, C, G or U), "AAGNG" and less frequently "UGUG", that are localized in the terminal loop of small hairpin structures and thus suppresses the translation of mRNAs destined for the endoplasmic reticulum (ER) [103]. In sharp contrast to this mechanism, Lin28:mRNA interactions were also demonstrated to promote protein synthesis through recruitment of RNA helicase-A and translation initiation factor elF3-beta to polysomes [104]. The molecular basis behind this differential regulation of mRNA targets remain largely elusive.

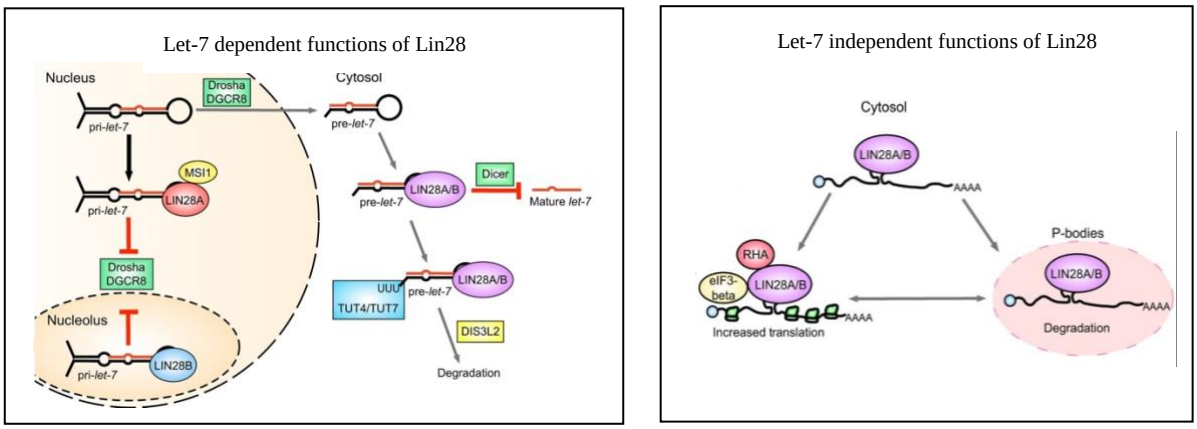

Figure 9: Lin28 RBPs regulate gene expression via two distinct biological pathways

Lin28 binds to both pri- and pre-Let-7 and blocks their further processing (Left). In the nucleus, Lin28 associates with pri-Let-7 and inhibits its processing by the Drosha-DGCR8 complex. In the cytoplasm, Lin28 binds to pre-Let-7 to blocks its processing by Dicer and instead induces oligo-uridylation and subsequent degradation of pre-Let-7. Lin28 also regulates gene expression by directly binding to and altering mRNA translation (Right). However, it remains unclear how Lin28 mediates these distinct functions. For example, Lin28 was shown to increase translation by recruitment of RNA

helicase-A and translation initiation factor elF3-beta to polysomes. In addition, Lin28 is known to accompany bound mRNA to P-bodies for their degradation. *(Image stems from [91]).*

1.12 Roles of Lin28 in human diseases

Consistent with the functions of Lin28 in controlling cell development, proliferation and metabolism, Lin28 activity was identified as a modulator of various human diseases, suggesting that Lin28:mRNA interactions are effective drug targets. For example, Lin28A was shown to be of therapeutic importance for patients with sickle cell anemia, as the over-expression of Lin28A in cultured, sickle-cell shaped erythrocytes significantly reduced their pathogenic morphology [105]. Moreover, the forced expression of Lin28A in mouse adult tissues, enhanced their repair capacities by fostering a metabolic state characteristic of embryonic stem cells [106]. Here, the over-expression of Lin28A resulted in an enhanced digit repair, epidermal hair regrowth and pinnal tissue repair, implying to use Lin28A for repairing damaged and degenerated tissues. Also, a recent study showed that a loss-of-function variant of Lin28A contributes to Parkinson's disease pathogenesis which can be rescued by re-expression of a functional Lin28A, suggesting that future personalized therapies may target this variant in Parkinson's patients [107]. Lastly, the de-regulation of Lin28 expression in some tumors promotes enhanced invasiveness, tumor growth, and thus worsens their prognosis [106, 107, 108, 109, 110, 111]. Key to these effects seems to be the Lin28-mediated control of cell proliferation, leading to more aggressive tumors. Indeed, the enforced expression of Lin28A promotes breast cancer cell growth via post-transcriptional stimulation of human epidermal growth factor receptor 2 (HER2) which in turn mediates cell proliferation [108]. Likewise, high expression of Lin28B in oesophageal cancer cells promotes tumor aggressiveness which is mediated through increased cell division rates as knock-down of Lin28B in these cells reduced their proliferative activity [109].

2. HYPOTHESIS AND AIMS

The Lin28/Let-7 regulatory feedback loop controls cell differentiation, developmental timing, growth, tissue homeostasis and energy utilization, thus regulating the transition from undifferentiated to differentiated cell states. In addition to the modulation of miRNA biogenesis, Lin28 regulates translation via direct mRNA binding and/or the control of RNA stability.

The hypothesis underpinning the experimental work presented in this study assumes that the Lin28/Let-7 feedback axis is essential for TEC biology and its disruption impairs the cells' maturation, metabolism and function.

This experimental work presented here addresses the objective to identify the roles and underlying molecular mechanisms of Let-7 miRNA and Lin28 in TEC biology.

Mice were generated that over-express Lin28A, Lin28B or both RBPs in a TEC-restricted fashion to ablate Let-7 function in thymic epithelia. Although this approach does not allow to dissect the function of individual Let-7 isomiRs, it enables me to study the general roles of the Let-7 family of miRNAs and to investigate Let-7 independent pathways affected by Lin28 RBPs in TEC biology.

3. MATERIALS AND METHODS

3.1 Generation of Lin28 transgenic mouse models

Rosa26 knock-in mice containing the CAG-loxP-stop-loxP-Lin28a/Lin28b sequences (designated $Lin28a^{Ctrl}$ and $Lin28b^{Ctrl}$, respectively) have been designed by Saule Zhanybekova, Johannes Schulte, Leonid Pobezinsky and Alfred Singer comparably to previously described Cre-dependent mouse lines [114]. These two mouse lines were crossed to animals expressing Cre recombinase under the transcriptional control of Foxn1 regulatory elements to obtain heterozygous mice ectopically expressing either *Lin28a* or *Lin28b* specifically in TEC (designated $Lin28a^{TEC}$ and $Lin28b^{TEC}$). To obtain mice that express both *Lin28a* and *Lin28b*, $Lin28a^{TEC}$ and $Lin28b^{TEC}$ mice were crossed to create triple transgenic animals ($Lin28axb^{TEC}$). All animals were kept under specific pathogen-free conditions and experiments were carried out in accordance with local and national regulations and permissions.

3.2 Mouse Genotyping

Toes of 1 - 2 week old mice were clipped and placed into 500 µl lysis buffer (0.1 M Tris adjusted to pH 8.5 (Sigma-Aldrich), 5 mM EDTA (Sigma-Aldrich), 0.2 M NaCl (Sigma-Aldrich), 0.4% SDS (Sigma-Aldrich), 100 µg/ml Proteinase K (Amresco). Samples were subsequently incubated for at least 2 hours at 56°C in a thermal shaker at 750 rpm and diluted with ddH_2O (1:2). To define the mouse genotype a 1X PCR reaction mixture was prepared:

Lin28a

10x PCR buffer	2.5 µl
dNTPs	0.5 µl
Primers forward and reverse	0.5 µl
RNase, DNase free H2O	19.9 µl
Taq polymerase	0.1 µl
DNA	1 µl

Lin28b & Foxn1Cre

10x PCR buffer	2.5 µl
dNTPs	0.5 µl
Primers forward and reverse	0.5 µl
RNase, DNase free H2O	20.4 µl
Taq polymerase	0.1 µl
DNA	0.5 µl

The reactions were then placed into a Mastercycler (Eppendorf) with the appropriate PCR program:

Lin28a

94°C	5 min.	
94 °C	30 sec.	34 X
59 °C	45 sec.	
72 °C	60 sec.	
72 °C	10 min.	

Lin28b & Foxn1Cre

94°C	4 min.	
94 °C	30 sec.	34 X
59 °C	40 sec.	
72 °C	60 sec.	
72 °C	10 min.	

The resulting PCR products were mixed 5:1 with 6x DNA loading Dye and run in a 1.5% agarose TAE gel at 80V for 30min. The separated DNA products were visualized with GelDoc (BIO-RAD).

Gene	Forward Primer	Reverse Primer
Lin28a	CAGACGAGCCGCAGCTGCTGCACG	GCATTCCTTGGCATGATGGTCTAG
Lin28b	GTGACATTGACATCCACTTTGC	CCCAAGGCACACAAAAAACC
Foxn1Cre	TCTGATGAAGTCAGGAAGAACC	GAGATGTCCTTCACTCTGATTC

Table 1: *Primers used for PCR genotyping in 5'-3' orientation*

3.3 Flow cytometry analysis reagents

Antibodies were conjugated with allophycocyanin (APC), Alexa Fluor 488 / fluorescein isothiocyanate (FITC), Alexa Fluor 647 (A647), Alexa Fluor 700 (A700), biotin, Brilliant Violet dyes BV421, BV510, BV605, BV650, BV786, cyanin 5 (Cy5), phycoerythrin (PE) or tandem dyes APC-Cy7, PE-Cy7, peridin chlorophyll protein (PerCP)-Cy5.5 and PE-Texas Red. Biotinylated antibodies were detected with fluorophore-conjugated streptavidin. Other fluorescent reagents that were used were 4',6-diamidino-2-phenylindole (DAPI), 2-deoxy-2-[(7-nitro-2,1,3-benzoxadiazol-4-yl)amino]-D-glucose (2-NBDG), MitoTracker DeepRed and Zombie dyes Zombie Red, Zombie Violet and Zombie Aqua.

Antigen	Conjugate	Clone	Manufacturer
EpCAM	PE-Cy7	G8.8	BioLegend
	Biotin		Self-made
FLAG	Mouse IgG	M2	Sigma
Ly51	PE	6C3	BioLegend
	PE-Cy7		
IA/IE (MHCII)	APC-Cy7	M5/114.15.2	BioLegend
	PerCP-Cy5.5		
Ly6A/E (Sca-1)	BV786	D7	BioLegend
UEA-1	Cy5	Lectin	Rectolab
	Biotin		Self-made
	Rhodamine		Vector Laboratories
CD274 (PD-L1)	PE	10F.9G2	BioLegend
Activated Caspase-3	V450	C92-605	BD
Total Caspase-3	A700	31A1067	Novusbio
BrdU	APC	PRB-1	BD
Puromycin	A647	12D10	Merck
Glut4	PE	Polyclonal	Novusbio
TNF-R1	PE	55R-170	Santa Cruz
Phospho-TAK1 (Thr184/187)	Rabbit IgG	K.846.3	Life technologies
Phospho c-Jun (pS63)	A647	KM-1	Santa Cruz
CD3	A647	KT3	Self-made
CD4	PE-eFluor610	RM4-5	eBioscience
CD5	APC-Cy7	53-7.3	eBioscience
CD8a	FITC	53-6.7	BioLegend
	A700		
CD24	PerCP-Cy5.5	M1/69	BioLegend
CD25	BV605	PC61	BioLegend
CD44	BV786	IM7	BioLegend
	APC-Cy7		
CD45	PE-TxRed	30-F11	Life technologies
	A700	M1/9.3.3.HL	Self-made
CD62L	PerCy-Cy5.5	MEL-14	BioLegend
CD69	FITC	H1.2F3	BioLegend
	PE-Cy7		
CD71	PE-Cy7	RI7217	BioLegend
CD117 (ckit)	APC	2B8	BioLegend
CD197 (CCR7)	BV421	4B12	BioLegend
CFSE	FITC	-	ThermoFisher

Foxp3	PE	FJK-16s	eBioscience
Helios	APC	22F6	eBioscience
IL-2	PE	JES6-5H4	BioLegend
CD279 (PD-1)	BV786	29F.1A12	BioLegend
TCR ß	APC	H57-597	BioLegend
	FITC		
	Biotin		
TCR γδ	PE	GL3	BioLegend
CD11b	Biotin	M1/70	BioLegend
CD11c	Biotin	N418	BioLegend
CD19	Biotin	ID3	Self-made
F4/80	Biotin	BM8	BioLegend
Gr1 (Ly6G)	Biotin	RB6-8C5	BioLegend
Ter119	Biotin	Ter119	BioLegend
MHCI	Biotin	AF6-120.1	BioLegend
Streptavidin	BV650	-	BioLegend
Anti-Mouse IgG	A555	-	Molecular probes
Anti-Rabbit IgG	A488	-	Molecular probes
	A750		
DAPI	-	-	Invitrogen
2-NBDG	-	-	ThermoFisher
MitoTracker DeepRed	-	-	ThermoFisher
Zombie	BV510	-	BioLegend
	BV421		
	PE-TxRed		

Table 2: *List of antibodies and fluorescent reagents*

3.4 Cell isolation and analysis with flow cytometry

For analyses of TEC, thymic lobes from postnatal mice were harvested and cleaned of remaining fat and connective tissues. The lobes were subsequently separated, cut into cuboids and transferred into IMDM without fetal calf serum (FCS). The cells were gently rocked at room temperature on a shaker/rocker and supernatant was removed (2 x 3 min.). The cuboids were thereafter incubated in phosphate buffer saline (PBS) containing Liberase (200 μg/ml, Roche Diagnostics), DNaseI (20 μg/ml, Roche Diagnostics) and Papain (0.5 mg/ml, Sigma)

for 45 min. at 37ºC. Cells were gently pipetted up and down every 10 min. to obtain a single cell suspension and transferred into IMDM, containing 10% FCS and 10 mM EDTA (Invitrogen). After centrifugation, cells were filtered through a nylon mesh (100micron pore size, Sefar Nitex) to remove debris and counted using a Z1 Particle Counter (Beckmann Coulter). Due to the scarcity of TEC, cells were magnetically enriched for EpCAM with biotinylated G8.8 antibody and anti-biotin microbeads using AutoMACS Pro (Miltenyi Biotec) according to the protocol of the manufacturer. The enriched fraction was subsequently counted and stained with antibodies for 20 min. on ice in PBS containing 2% FCS. For intracellular staining, cells were fixed and permeabilized using either Cytofix/Cytoperm Kit (BD Biosciences) or eBioscience transcription factor staining buffer set (Invitrogen) and labeled with antibodies for 1 hour on ice.

Single-cell suspensions of thymus, lymph nodes and spleen were obtained by transferring the organs into a petri dish containing PBS with 2% FCS and gently squeezing them in between two 100 µm nylon meshes with bent tweezers. The cell suspension was subsequently transferred into a 5 ml tube. Cells were counted and stained with conjugated antibodies on ice for 20 min. followed, if applicable, by conjugated Streptavidin staining for 20 min. on ice. For intracellular staining, cells fixed and permeabilized using eBioscience transcription factor staining buffer set (Invitrogen) and labeled with antibodies on ice for 1 hour. Cells were filtered through a 40 µm mesh before acquisition.

Flow cytometric analysis was performed using BD LSRFortessa or Cytek Aurora while cell sorting was done using FACSAria II flow cytometer. The data was analyzed using the FlowJo (Treestar) software.

3.5 Real time quantitative PCR analysis

Total RNA was isolated from sorted cells with the RNeasy plus micro Kit (Qiagen) according to the instructions provided by the manufacturer. cDNA was synthesized using SuperScriptIII (Live Technologies) according to manufacturer's protocol. Real time quantitative PCR was carried out using SensiMix SYBR kit (Bioline) on Rotor-Gene 3000A (Qiagen).

Gene	Forward Primer	Reverse Primer
Gapdh	TGAAGCAGGCATCTGAGGG	CGAAGGTGGAAGAGTGGGAG
Beta-actin	CAATAGTGATGACCTGGCCGT	AGAGGGAAATCGTGCGTGAC
Ccl19	CCTGGGTGGATCGCATCATCC	AGAGCATCAGGAGGCCTGGT
Ccl21	AGCTATGTGCAAACCCTGAGG	TTCCAGACTTAGAGGTTCCCC
Ccl25	GTTACCAGCACAGGATCAAAT	GGAAGTAGAATCTCACAGCA
Cxcl12	AAATCCTCAACACTCCAAAC	GCTTTCTCCAGGTACTCTTG
Il-7	ATTATGGGTGGTGAGAGCCG	GTTCATTATTCGGGCAATTACTATCA
Scf	AAGGAGATCTGCGGGAATCC	CGGCGACATAGTTGAGGGTTA
Glut4	GTGACTGGAACACTGGTCCTA	CCAGCCACGTTGCATTGTAG
Igf1r	GCTTCGTTATCCACGACGATG	GAATGGCGGATCTTCACGTAG
Insr	ATGGGCTTCGGGAGAGGAT	GGATGTCCATACCAGGGCAC
Irs2	AGCCAGGAGACAAGAACTCC	AGTGATGGGACAGGAAGTCG
Foxo3a	CCTACTTCAAGGATAAGGGCG	GGTTGTGCCGGATGGAGTT

Table 3: *List of primers used for quantitative PCR*

3.6 Let-7 isoform quantitative PCR analysis

RNA was extracted from sorted cells using Let7 Isoform Real-Time qPCR Assay Kit according to manufacturer's manual (BioCat). Real time PCR of miRNAs was done using manufacturer's protocol on Rotor-Gene 3000A (Rotor Gene).

3.7 Immunofluorescence

For subcellular localization of transgenic Lin28A, TEC were sorted into IMDM containing 10% fetal calf serum, washed with phosphate saline buffer and transferred into µ-Slides (ibidi). The cells were subsequently fixed and permeabilized using Cytofix/Cytoperm (BD Bioscience), washed, blocked with 2% goat serum in perm wash solution and stained with FLAG antibody at 4°C overnight. The next day samples were washed and develop using a secondary antibody for 1 hour at room temperature. Vectashield (Vectorlabs) was added to the samples and images were acquired using a Leica SP5 confocal (Leica).

For immunofluorescence analyses, thymi were isolated and immediately frozen in optimal cutting temperature compound (OCT) (Cell Path). Sections of 8 µm were prepared on a cryostat, dried and fixed with 4% paraformaldehyde (Sigma). The tissue sections were then stained with cytokeratin 8 (CK8) and cytokeratin 14 (CK14) antibodies and subsequently detected using anti-IgG antibodies conjugated to an Alexa Flour fluorochrome. The images were acquired using a Zeiss Axio Imager Z2 scanning microscope (Zeiss).

3.8 Cell proliferation analysis using BrdU

For the detection of TEC proliferation, mice were injected twice intraperitoneally with 1 mg Bromodeoxyuridine (BrdU, BD Bioscience) within 4 hours. One day later, BrdU incorporation was analysed by flow cytometry using the BrdU Flow Kit according to manufacturer's protocol (BD Bioscience).

3.9 Fetal thymic organ cultures

Thymic lobes were isolated from wild-type animals at embryonic day 14.5 (E14.5) and placed on a 0.45 micro pore sized filter (Millipore) floating on IMDM + 10% FCS medium, in the additional presence of isotype control (25 µg/ml, IgG2b, κ Isotype, BioLegend) or PD-L1

blocking monoclonal antibody (25 µg/ml, BioLegend) for 8 days at 37°C. Half of the medium (with isotype control or PD-L1 blocking antibody) was changed every two days. After 8 days of culture, the thymic lobes were digested with PBS containing Collagenase D (1 mg/ml & Roche) and 20 µg/ml DNaseI (Roche) at 37°C for 30 min. with occasional pipetting to obtain a single cell suspension (it should be noted that fetal thymi, unlike adult thymi, are not digested with Liberase). The cells were then stained with fluorophore-conjugated antibodies for flow cytometric analyses.

3.10 Reaggregate thymic organ cultures

Thymic lobes were isolated from 1 – 2 week old wild-type animals and single cell suspensions of TEC and thymocytes were obtained using the method described in **Section 3.4**. The cells were stained with fluorescence-tagged antibodies for extracellular antigens and sorted to obtain specific cell populations. $cTEC^{lo}$ and $cTEC^{hi}$ were sorted into separate 1.5 mL Eppendorf tubes containing IMDM + 10% FCS. Thereafter, $CD69^{neg}$ $CD4CD8^{pos}$ thymocytes were sorted and transferred into the Eppendorf tubes containing the different cTEC subsets in a 1:1 ratio. The cells were subsequently spun down, lids opened and the samples were kept for 48 hours at 37°C in the CO_2 incubator. After culturing, the cells were stained with fluorescence-tagged antibodies and analyzed via flow cytometry.

3.11 SCENITH

Thymic lobes were harvested from new-born animals and cleaned of remaining fat and connective tissue. The lobes were separated and placed into 48 well flat bottom plates (1 lobe / well) containing 250 µl IMDM. Different metabolic inhibitors were added to the appropriate wells (250 µl of metabolic inhibitor / well); 2-Deoxy-D-Glucose (2-DG, 400 mM, Sigma Aldrich), Oligomycin (2 µM, Sigma Aldrich) and All inhibitors (2-DG + Oligomycin + FCCP

(2 µM, Abcam)). For the non-treated wells, 250 µl of IMDM was added instead. The samples were incubated at 37°C for 40 min. Thereafter, 100 µl of Puromycin (60 µg/ml, Sigma Aldrich) was added to each well. The samples were incubated at 37°C for 20 min. The lobes were washed with PBS and incubated in 96 well plates containing 250 µl Collagenase D and DNaseI at 37°C for 20 min. with occasional pipetting to obtain a single cell suspension. The cell numbers were normalized to the lowest cell concentration and the cells stained fluorophore-conjugated surface antibodies. The samples were subsequently washed with PBS and stained with Zombie Dye in PBS. Thereafter, the cells were fixed with Cytofix/Cytoperm Kit (BD Bioscience) and intracellular stain performed using anti-puromycin antibody for 1 hour on ice before flow cytometric analyses.

3.12 MitoTracker staining

Thymic lobes were isolated from 4 – 6 week old animals, a single cell suspension of TEC prepared and TEC enriched using the method described in **Section 3.4**. The cell numbers were normalized, the cells washed with PBS and resuspended in 1 ml pre-warmed PBS. MitoTracker DeepRed was added to the samples (5 nM final concentration, ThermoFisher) and the cells were incubated at 37°C for 15 min. The samples were thereafter washed with PBS and stained with fluorophore-conjugated antibodies before analysis on the FACS Fortessa.

3.13 TNF-α treatment

Thymic lobes were isolated from new-born wild-type animals, cut into half and placed on a 0.45 micro pore sized filter (Millipore) floating on IMDM + 10% FCS medium, in the additional presence of TNF-α (100 ng/ml, R&D systems) or TNF-α plus Ammonium pyrrolidinedithiocarbamate (200 µM, Sigma Aldrich) overnight at 37°C. The following day, the thymic lobes were digested with PBS containing Collagenase D (1 mg/ml & Roche) and

20 µg/ml DNaseI (Roche) at 37°C for 30 min. with occasional pipetting to obtain a single cell suspension. The cells were then stained with fluorophore-conjugated surface antibodies. The samples were subsequently washed with PBS and stained with Zombie Dye in PBS. Thereafter, the cells were fixed with Cytofix/Cytoperm Kit (BD Bioscience) and intracellular stain performed using anti cleaved-caspase-3 antibody for 2 hours on ice before flow cytometric analyses.

3.14 Statistical analysis

Results of all experimental data are expressed as mean ± standard deviation (SD). Student's *t*-test with two tailed distribution and two-sample equal variance parameters was calculated using Excel. *P*-values are indicated in figures are classified in four categories:
* $p \leq .05$, ** $p \leq .01$, *** $p \leq .005$. $p > 0.05$ values are considered as not significant.

3.15 Proteomic analyses

7575 cTEC and $mTEC^{hi}$ were sorted from 4-7 week old $Lin28a^{TEC}$, $Lin28b^{TEC}$, $Lin28axb^{TEC}$ and control animals into 25 µl of RIPA (ThermoFisher) buffer + 4% NP-40 (ThermoFisher). The samples were sent to the Discovery Proteomics Facility in Oxford (UK) for mass spectrometric analyses using the Liquid chromatography-mass spec/mass spec (LC-MS/MS) platform. The results were analysed on Perseus Software as previously described [115]. Briefly, potential contaminants were first removed before the data set was log-transformed. Thereafter, annotations were added and missing values replaced from a normal distribution. The biological replicates were grouped and the proteins averaged by the median in each group. Lastly, scatter plots were generated comparing the different cell types to each other. For statistical tests, Student's *t*-test with two tailed distribution and two-sample equal variance parameters was used.

3.16 Transcriptomic analyses

22000 cTEC^{hi} and 5500 cTEC^{lo} were sorted from 2 and 7 week old Lin28a^{TEC} and Lin28a^{Ctrl} animals. Total RNA was isolated from sorted cells with the RNeasy plus micro Kit (Qiagen) according to the instructions provided by the manufacturer. RNA quality control was performed with the 5200 fragment analyzer (Agilent) using the high-sensitivity Kit (Agilent). The samples were subsequently shipped to GENEWIZ for ultra low input bulk RNA sequencing. RNA-seq libraries were generated from total RNA isolated from either cTEC^{hi} or cTEC^{lo} from mice at 2 or 7 weeks of age. RNA libraries were generated using the PE 2x150 Nexterra mRNA library prep kit (ID) and were sequenced on the Illumina S4 flow cell (2 × 150). Reads were aligned to the mouse genome (mm10) using STAR aligner (v2.5.1b) [116], and transcript abundance was quantified using Salmon (v0.8.2) [117]. Finally, differentially expressed genes were identified using DEseq2 (v1.28.1) [118]. RNA deconvolution was performed using CIBERSORT [119] with a custom marker gene signature file derived from single cell RNA-seq of TEC from ageing mice [47]. Gene set enrichment was performed using the clusterProfiler package [120].

4. Results

4.1 Endogenous *Lin28* amounts in TEC decrease during thymus ontogeny and correlates with the expression of mature Let-7 isomiRs

To assess the post-transcriptional regulation of thymic epithelial cell (TEC) differentiation, maintenance and function by the Let-7/Lin28 axis, I first analysed the expression of *Lin28a* and *Lin28b* in wild-type mice during thymus ontogeny. Low numbers of *Lin28a* transcripts were detected in TEC at embryonic day (E) 12.5 but not at later time points (Figure 10A, 10B). In contrast, *Lin28b* transcripts were consistently found at all time points tested, albeit most prominent at E12.5 and after birth more abundantly in medullary (m) TEC than cortical (c) TEC (Figure 10B). Of the Let-7 family members, transcripts of the isomiRs 7a, 7b, 7c, 7g and miR-98 but not 7d, 7e, 7f, 7l and miR-202 were detected in TEC of 2 week old control mice (Figure 10C). The higher expression of *Lin28b* in mTEC hereby correlated with lower amounts of Let-7 isomiRs in these cells when compared to cTEC (Figure 10B, 10C).

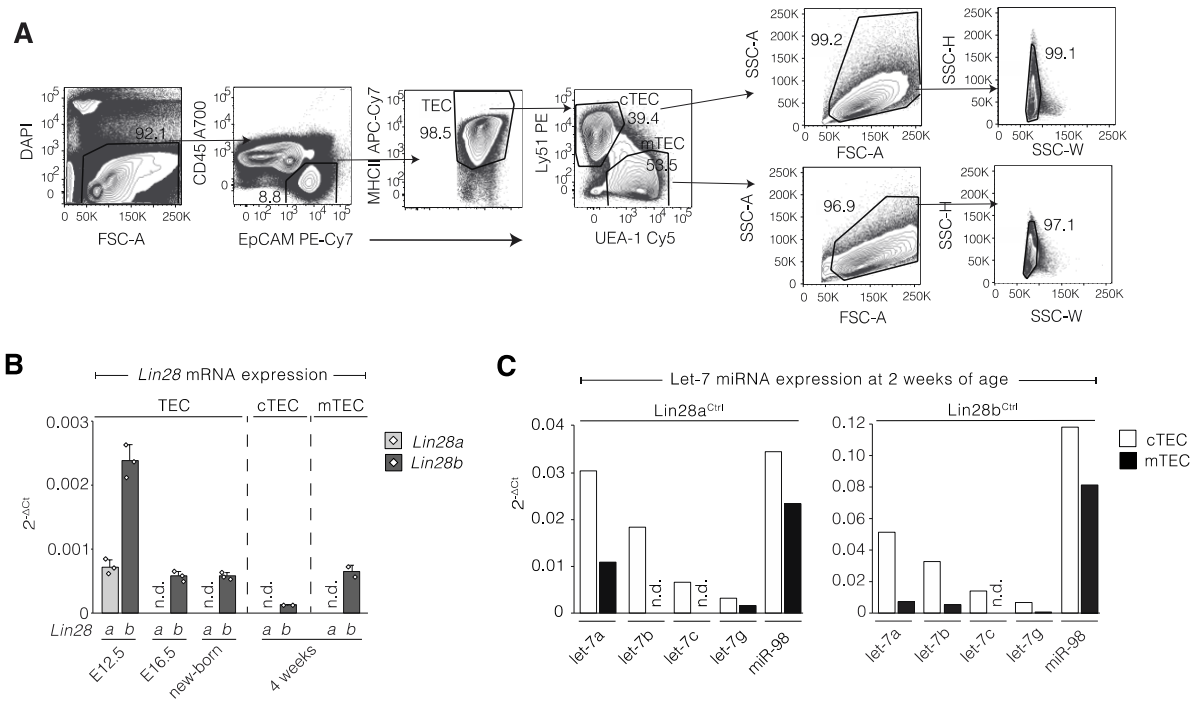

Figure 10: Endogenous *Lin28* and Let-7 expression in TEC of control mice

(**A**) TEC gating strategy. Dead cells were excluded with DAPI and forward scatter (FSC-A). TEC were identified as CD45 negative but EpCAM and MHCII positive. TEC subsets were phenotyped as cTEC ($Ly51^{+}UEA\text{-}1^{-}$) and mTEC ($Ly51^{-}UEA1^{+}$). Cellular debris was thereafter removed using forward scatter (FSC-A) and side scatter (SSC-A) signals which was followed by doublet exclusion using SSC height (SSC-H) and width (SSC-W) parameters. (**B**) Expression of endogenous *Lin28a* and *Lin28b* in sorted TEC at different time points. Representative data from at least two independent experiments analyzing TEC from wild-type animals at embryonic day 12.5 (E12.5), E16.5, new-born and 4 weeks of age. qPCR is normalized to *Gapdh* expression. n.d. = not detectable. (**C**) Quantification of mature Let-7 miRNA expression in sorted TEC subsets. Representative data from two independent experiments analyzing control (n = 5) female and male mice at 1-2 weeks of age (Let-7d, e, f, i and miR-202 were undetectable in cTEC and mTEC). qPCR normalized to u6 expression.

4.2 Transgenic *Lin28a* and *Lin28b* expression in TEC inhibits Let-7 maturation

To investigate the role of Lin28-dependent epigenetic regulation in TEC biology, I generated mice with an ectopic expression of either *Lin28a* or *Lin28b* targeted to TEC (Figure 11A). The *Lin28* transgenic constructs consisted of a CAG-promoter, a floxed stop codon, a *Lin28a* or *Lin28b* transgene and were placed into the Rosa26 locus (Figure 11A). The *Lin28a* transgenic construct consisted the *Lin28a* coding sequence fused to a FLAG-tag, followed by an internal ribosomal entry site (IRES), a sequence encoding green fluorescence protein (GFP) and woodchuck hepatitis virus post-transcriptional regulatory elements (WPRE) (Figure 11A). Mice harboring a *Lin28a* or *Lin28b* transgenic construct were crossed to animals expressing Cre under the transcriptional control of the TEC specific *Foxn1* gene (Figure 11A) [121]. Lin28a^{TEC} and Lin28b^{TEC} mice were heterozygous for both *Cre* and *Lin28a* or *Lin28b*, respectively, and were compared to Lin28a^{Ctrl} and Lin28b^{Ctrl} animals which were heterozygous for *Lin28* transgenes but lacked *Cre* expression (Figure 11A, 11B, 11C).

I first analysed the subcellular localization of transgenic Lin28A and Lin28B in Lin28a^{TEC} and Lin28b^{TEC}, respectively. Transgenic Lin28A protein was mainly localized to the cytoplasm (Figure 11E) whereas transgenic Lin28B protein could not be detected using various available detection reagents. Despite the technical difficulties to detect transgenic Lin28B protein, both mouse lines and demonstrated a significant and largely comparable reduction or complete absence of individual Let-7 isomiRs in both cTEC and mTEC, hence indicating the presence of active transgenic Lin28B protein (Figure 11D).

Thus, the transgenic expression of *Lin28* in thymic epithelia reduced the amounts of all Let-7 isomiRs characteristically detected in these cells.

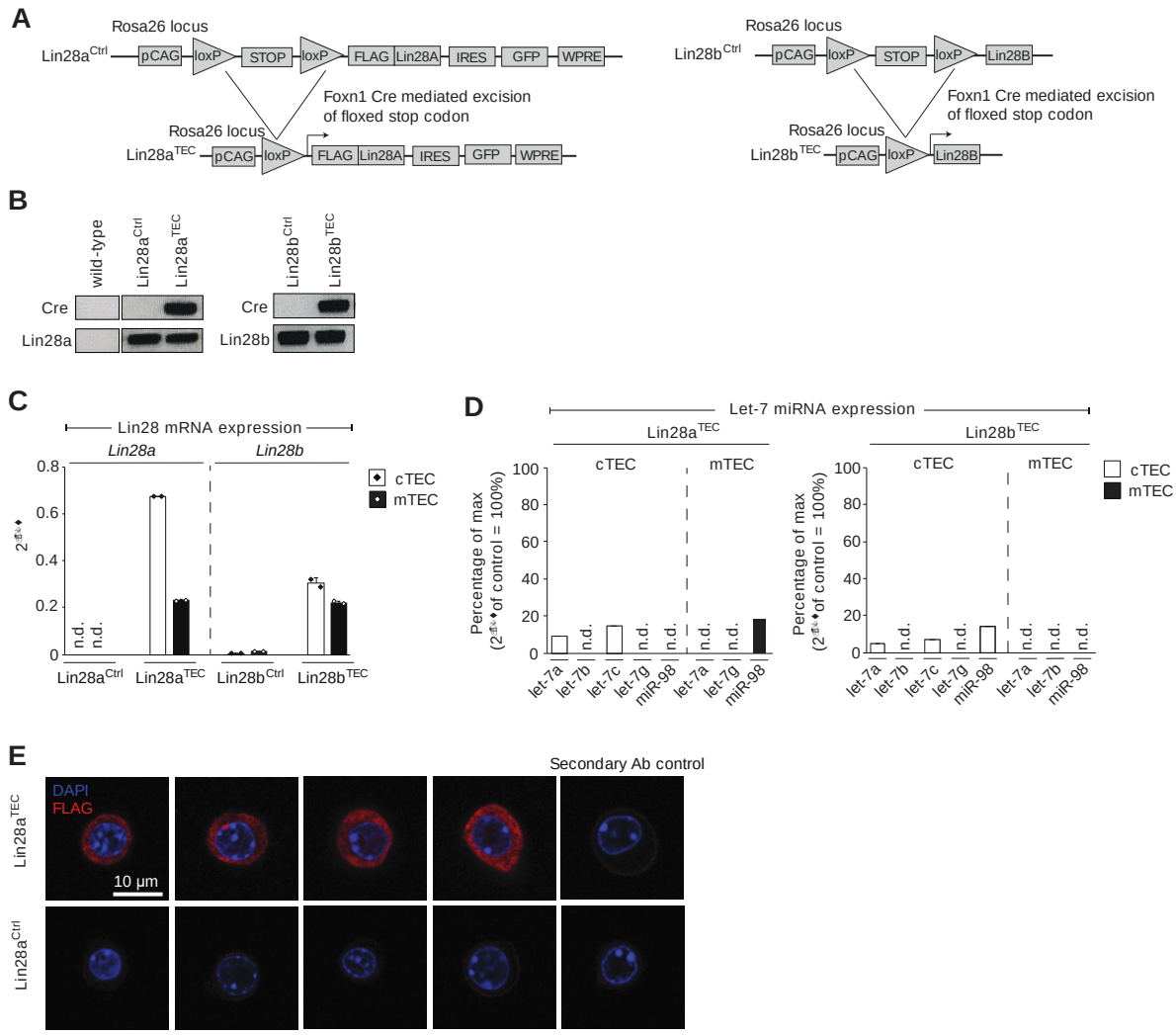

Figure 11: Transgenic *Lin28a* and *Lin28b* expression inhibits Let-7 maturation

(**A**) Schematic illustration of *Lin28* transgenic constructs. (**B**) Agarose gel electrophoresis results of PCR genotyping for *Cre*, *Lin28a* and *Lin28b* tg from genomic DNA derived from biopsies of wild-type, Lin28a^{Ctrl}, Lin28a^{TEC}, Lin28b^{Ctrl} and Lin28b^{TEC} mice. (**C**) Expression of *Lin28a* and *Lin28b* in sorted cTEC and mTEC of Lin28a^{TEC}, Lin28b^{TEC} and control mice at 2 weeks of age. qPCR is normalized to *beta actin* expression. (**D**) Percentage of maximum (max) Let-7 expression in mutant TEC relative to control TEC ($2^{-\Delta Ct}$ of control cTEC and control mTEC set to 100%) in sorted TEC subsets of Lin28a^{TEC} (n = 5) and Lin28b^{TEC} (n = 3-4) female and male mice at 2 weeks of age. Let-7d, e, f, i and miR-202 were undetectable in cTEC and mTEC. qPCR normalized to u6 expression. (**E**) Immunofluorescence images displaying subcellular localization of transgenic Lin28A in TEC of Lin28a^{TEC} and Lin28a^{Ctrl} mixed sex mice (n = 3) at 5-6 weeks of age. Images were taken with 63X magnification using Leica SP5 confocal microscope. Data is representative of two independent experiments.

4.3 TEC phenotype of young adult *Lin28* mutant animals

4.3.1 *Lin28a* and *Lin28b* tg differentially affect thymus and TEC cellularity

I next investigated the consequences of constitutive *Lin28* expression on thymus organ size and stromal organization in young adult animals (i.e. 4-7 week of age). In comparison to controls, total thymus cellularity was greatly reduced in Lin28a^{TEC} mice but increased in Lin28b^{TEC} animals (Lin28a^{TEC}: 0.82 ± 0.26 x 10^8 vs. Lin28a^{ctrl}: 2.34 ± 0.42 x 10^8; Lin28b^{TEC}: 3.2 ± 0.83 x 10^8 vs. Lin28b^{ctrl}: 2.51 ± 0.61 x 10^8; Figure 12A, 12B). The thymus of Lin28a^{TEC} and Lin28b^{TEC} mice displayed a normal segregation into individual cortical (CK8$^+$CK14$^-$) and medullary (CK8$^-$CK14$^+$) compartments with distinct junctions separating the two (Figure 12C).

TEC are positively identified by their expression of the cell surface markers MHCII and EpCAM and their lack of expression of the hematopoietic marker CD45 (CD45$^-$ MHCII$^+$ EpCAM$^+$). The frequency of TEC was unaltered while TEC cellularity correlated with total thymus cellularity in all mutant mouse strains (Figure 12D, 12E). To determine the epistatic relationship between *Lin28a* and *Lin28b* transgenes, I crossed Lin28a^{TEC} and Lin28b^{TEC} mice to generate Lin28axb^{TEC} animals. Both total and TEC absolute numbers were reduced in these triple-transgenic animals comparable to that observed for Lin28a^{TEC} mice and thus revealing a dominant effect of *Lin28a* over *Lin28b* (Figure 12D, 12E). To test whether the dominant effect of *Lin28a* was due to a down-modulation of *Lin28b* expression in Lin28axb^{TEC} mice, I analyzed the expression of *Lin28a* and *Lin28b* in these animals. Both, *Lin28a* and *Lin28b* were over-expressed in cTEC and mTEC of Lin28axb^{TEC} mice when compared to control cells of the same phenotype, hence excluding a negative effect of *Lin28a* on the expression of *Lin28b* (Figure 12F).

I then analysed the impact of transgenic *Lin28* expression on the differentiation and maintenance of individual, flow cytometry defined TEC subsets. cTEC are classified by their expression of Ly51 and lack of reactivity to the lectin Ulex Europaeus Agglutinin 1 (UEA-1)

(Ly51^{+}UEA1^{-}) while mTEC bind to UEA-1 and are Ly51 negative (Ly51^{-}UEA1^{+}). I found that the cTEC:mTEC ratio was increased in Lin28a^{TEC} and Lin28axb^{TEC} mice in comparison to age-matched controls (Figure 12G, 12H). In contrast, Lin28b^{TEC} mice showed a cTEC:mTEC ratio that was unchanged compared to control, albeit the cellularity of both subpopulations had increased as a result of a larger thymus size (Figure 12H, Figure 12I).

I then undertook a detailed analysis of cTEC and mTEC differentiation. To this end, cTEC and mTEC were further subdivided according to their expression of MHCII and Sca-1. In young adult mice cTEC progress from immature cTEC (designated cTEC^{lo} and defined as MHCII^{lo} Sca-1^{pos}) to mature cTEC (designated cTEC^{hi} and defined as MHCII^{hi} Sca-1^{lo}) while mTEC differentiate from an immature mTEC (designated mTEC^{lo}; defined as MHCII^{lo} Sca-1^{hi}) stage to mature mTEC (designated mTEC^{hi} and defined as MHCII^{hi} Sca-1^{int}) before becoming terminally mature mTEC (tm mTEC and defined as MHCII^{lo} Sca-1^{lo}). The frequency of immature cTEC^{lo} was 4-5 fold lower while the relative and absolute cellularity of mature cTEC^{hi} was increased in Lin28a^{TEC} and Lin28axb^{TEC} mice when compared to controls (Figure 12G, 12J, 12K). In contrast, maturational progression from an immature to a mature cTEC phenotype appeared to be unaffected in Lin28b^{TEC} mice (Figure 12G, 12J, 12K). Changes in mTEC differentiation consequent to the constitutive *Lin28* expression were uniform for all transgenic mice in that the frequency of immature mTEC^{lo} was reduced whereas tm mTEC were more abundant (Figure 12G, 12J, 12K). Concurrently, relative numbers of phenotypically mature mTEC^{hi} had also increased, although statistical significance was only observed for mice that expressed the *Lin28a* transgene either alone or together with *Lin28b* transgene (Figure 12G, 12J, 12K).

Thus, cTEC and mTEC numbers and subset composition were differentially affected in a Let-7 isomiR-independent fashion by the transgenic expression of *Lin28a* and *Lin28b*.

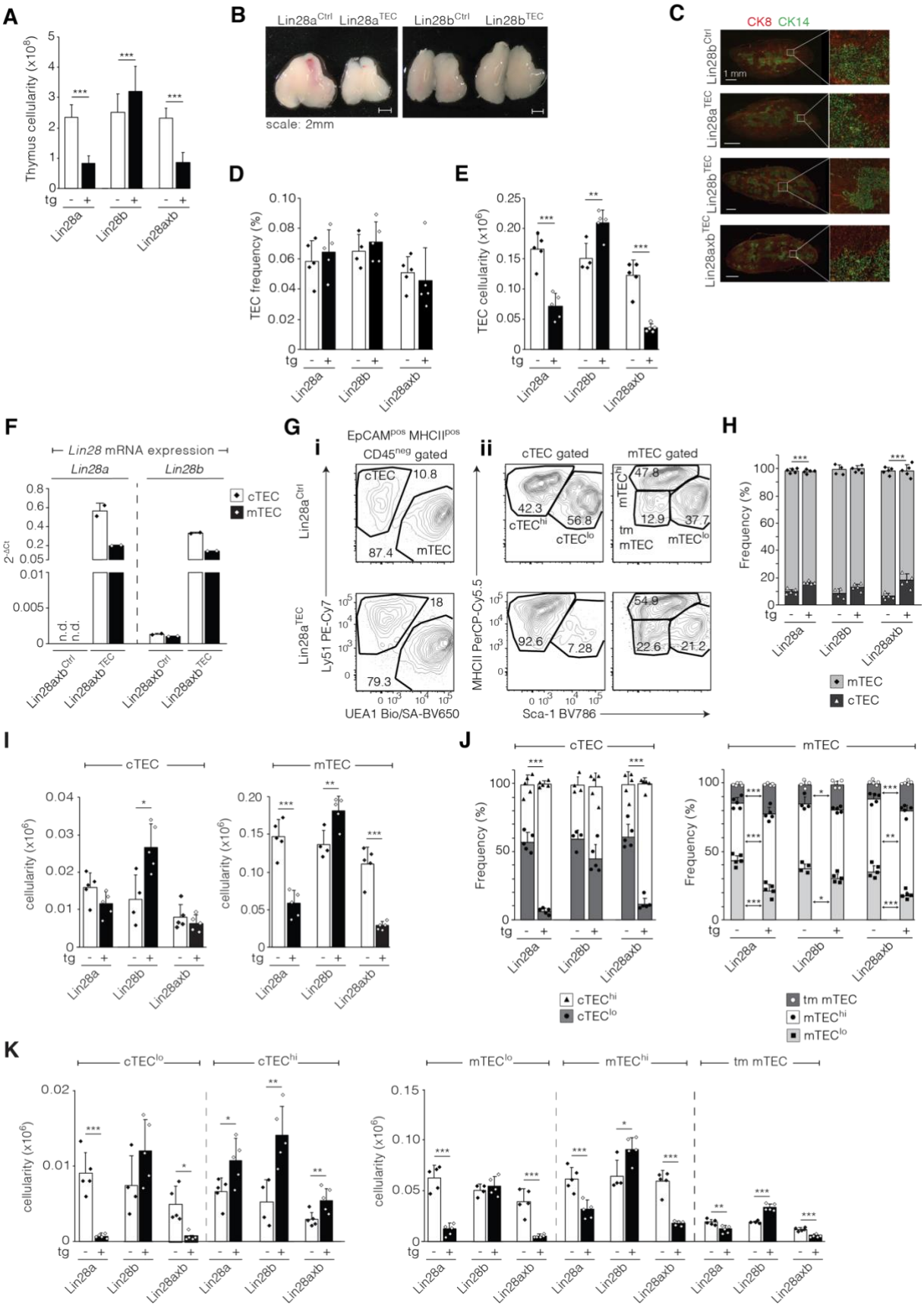
A
Thymus cellularity (x10^6)
tg
Lin28a
Lin28b
Lin28axb
B
Lin28a^Ctrl Lin28a^TEC Lin28b^Ctrl Lin28b^TEC
scale: 2mm
C
CK8 CK14
Lin28b^Ctrl
Lin28a^TEC
Lin28b^TEC
Lin28axb^TEC
1 mm
D
TEC frequency (%)
E
TEC cellularity (x10^6)
F
Lin28 mRNA expression
Lin28a
Lin28b
cTEC
mTEC
2^-ΔCt
n.d.
Lin28axb^Ctrl
Lin28axb^TEC
G
i
EpCAM^pos MHCII^pos
CD45^neg gated
cTEC
mTEC
10.8
87.4
Lin28a^Ctrl
Lin28a^TEC
Ly51 PE-Cy7
18
79.3
UEA1 Bio/SA-BV650
ii
cTEC gated
mTEC gated
42.3
cTEC^hi
56.8
cTEC^lo
47.8
mTEC^hi
12.9
tm mTEC
37.7
mTEC^lo
MHCII PerCP-Cy5.5
92.6
7.28
54.9
22.6
21.2
Sca-1 BV786
H
Frequency (%)
mTEC
cTEC
I
cTEC
mTEC
cellularity (x10^6)
J
cTEC
mTEC
Frequency (%)
cTEC^hi
cTEC^lo
tm mTEC
mTEC^hi
mTEC^lo
K
cTEC^lo
cTEC^hi
mTEC^lo
mTEC^hi
tm mTEC
cellularity (x10^6)

Figure 12: *Lin28a* and *Lin28b* tg differentially affect thymus and TEC cellularity

(**A**) Thymus cellularity of female mice, at 4-7 weeks of age. Data are pooled from multiple experiments, analyzing $Lin28a^{Ctrl}$ (i.e. Lin28a-) (*n* = 26), $Lin28a^{TEC}$ (i.e. Lin28a+) (*n* = 33), $Lin28b^{Ctrl}$ (i.e. Lin28b-) (*n* = 21), $Lin28b^{TEC}$ (Lin28b+) (*n* = 24), $Lin28axb^{Ctrl}$ (i.e. Lin28axb-) (*n* = 17) and $Lin28axb^{TEC}$ (Lin28axb+) (*n* = 8) animals. (**B**) Representative images of thymi from 5 week old $Lin28a^{TEC}$ and $Lin28a^{Ctrl}$ female mice and 14 week old $Lin28b^{Ctrl}$ and $Lin28b^{TEC}$ female animals. Data is taken from my Master Thesis. (**C**) Representative immunofluorescence images of thymic sections from 4-6 week control, $Lin28a^{TEC}$, $Lin28b^{TEC}$ and $Lin28axb^{TEC}$ female mice (*n* = 3) at 4-6 weeks of age. Antibodies specific for cytokeratin 8 (CK8) were used for the detection of cTEC and cytokeratin 14 (CK14) for the identification of mTEC. Data is representative of two independent experiments. Images were taken with 10X magnification using Zeiss Axio Imager Z2 scanning microscope. (**D**) Relative and (**E**) absolute TEC numbers. (**F**) Expression of *Lin28a* and *Lin28b* in sorted cTEC and mTEC of $Lin28axb^{TEC}$ and control mice at 2 weeks of age. qPCR is normalized to *beta actin* expression. (**G**) Representative flow cytometry plots detailing cTEC and mTEC composition based on Ly51 expression and reactivity for UEA-1 (**i**) and cTEC and mTEC subpopulations based on MHCII and Sca-1 expression (**ii**). (**H**) cTEC:mTEC ratio. (**I**) cTEC and mTEC absolute numbers. (**J**) Frequencies of $cTEC^{lo}$, $cTEC^{hi}$ and $mTEC^{lo}$, $mTEC^{hi}$, terminally mature (i.e. tm) mTEC within cTEC and mTEC, respectively. (**K**) Absolute number of $cTEC^{hi}$, $cTEC^{lo}$ and $mTEC^{lo}$, $mTEC^{hi}$, tm mTEC. For experiments (**D**) – (**E**) and (**G**) – (**K**) female mice, at 4 weeks of age were used. Data are representative of at least three independent experiments. * $p < .05$, ** $p < .01$, *** $p < .005$ (paired student's *t*-test).

4.3.2 Ectopic expression of *Lin28a* tg increases TEC proliferation and apoptosis

Lin28a is known to increase cell proliferation and reduce cell survival [100, 122]. Hence, I next assessed whether the *Lin28a* tg induced changes in the TEC compartment were due to alterations in TEC proliferation or apoptosis. Using BrdU pulse/chase experiments I found that $cTEC^{hi}$ of $Lin28a^{TEC}$ mice displayed an increased frequency of proliferating (BrdU positive) cells ($Lin28a^{TEC}$: 27.3 ± 5.6 % vs. $Lin28a^{Ctrl}$: 15.2 ± 3.3 %) while $cTEC^{lo}$ and all mTEC subpopulations showed comparable BrdU incorporation to control (Figure 13A, 13B).

In contrast, $cTEC^{lo}$ and mTEC were more prone to apoptosis, as they contained increased frequencies of cells with cleaved, activated caspase-3 identifying committed apoptotic cells (Figure 13C, 13D). To investigate whether these differences were the result of an increased availability of Caspase-3 in *Lin28a* mutant cells, I next stained for total Caspase-3 (i.e. cleaved plus non-cleaved Caspase-3). *Lin28a* mutant and control TEC showed similar expression of total Caspase-3 as determined by geometric mean fluorescence intensity (gMFI), indicating that the survival defect seen in these cells was due to an increased ratio of activated caspase-3/total caspase-3.

No differences in TEC proliferation and apoptosis were found in $Lin28b^{TEC}$ animals (Figure 13B, 13D, 13E). Hence, these results suggest that the increased $cTEC^{hi}$ cellularity in $Lin28a^{TEC}$ was due to their increased proliferative capacity while the reduction in $cTEC^{lo}$ and mTEC absolute numbers was a result of augmented cell death.

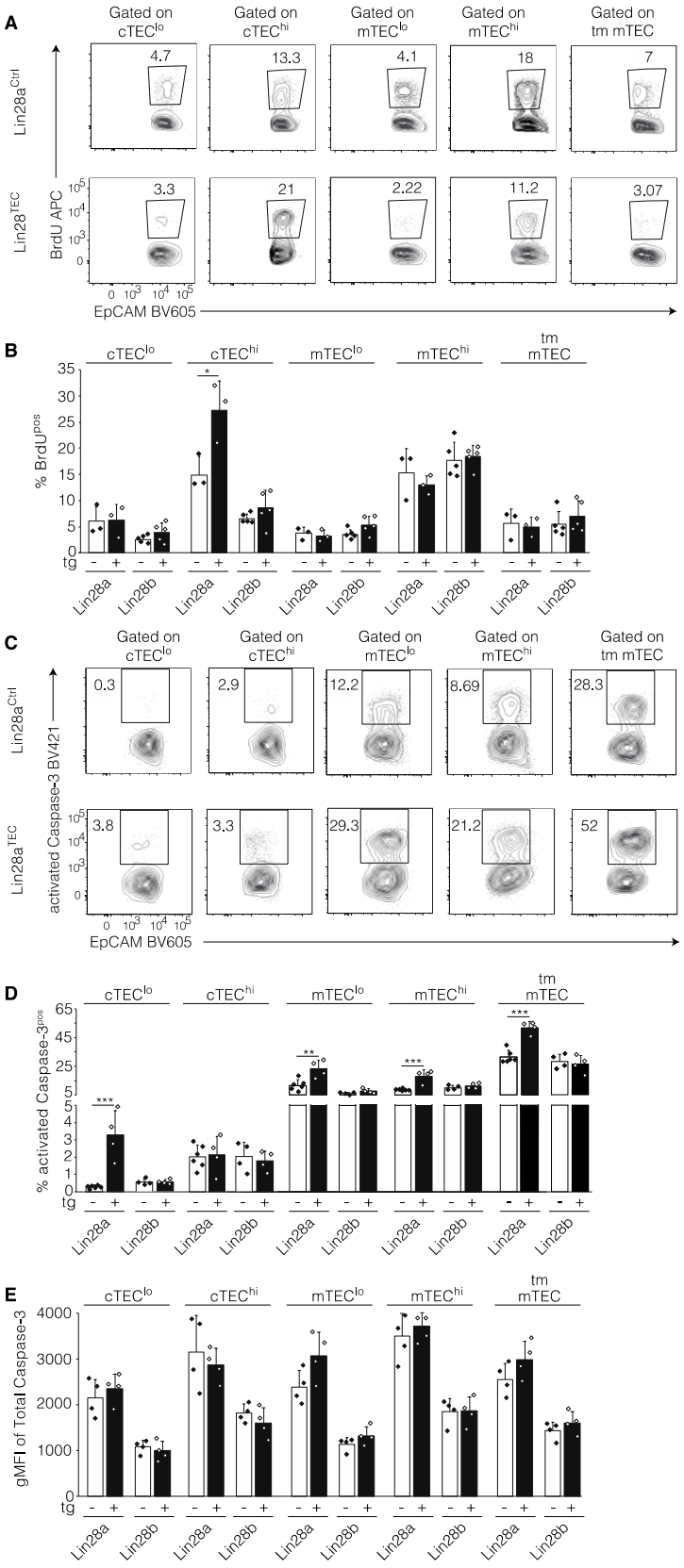
A
Gated on cTEC^lo
Gated on cTEC^hi
Gated on mTEC^lo
Gated on mTEC^hi
Gated on tm mTEC
Lin28a^Ctrl
Lin28^TEC
BrdU APC
EpCAM BV605
4.7
13.3
4.1
18
7
3.3
21
2.22
11.2
3.07
B
cTEC^lo
cTEC^hi
mTEC^lo
mTEC^hi
tm mTEC
% BrdU^pos
tg
Lin28a
Lin28b
C
Gated on cTEC^lo
Gated on cTEC^hi
Gated on mTEC^lo
Gated on mTEC^hi
Gated on tm mTEC
Lin28a^Ctrl
Lin28a^TEC
activated Caspase-3 BV421
EpCAM BV605
0.3
2.9
12.2
8.69
28.3
3.8
3.3
29.3
21.2
52
D
cTEC^lo
cTEC^hi
mTEC^lo
mTEC^hi
tm mTEC
% activated Caspase-3^pos
tg
Lin28a
Lin28b
E
cTEC^lo
cTEC^hi
mTEC^lo
mTEC^hi
tm mTEC
gMFI of Total Caspase-3
tg
Lin28a
Lin28b

Figure 13: Ectopic expression of *Lin28a* tg increases TEC proliferation and apoptosis
(**A**) Representative gating strategy and (**B**) quantitative analysis of BrdU positive TEC subsets 24 hours after BrdU administration. (**C**) Representative gating strategy and (**D**) relative numbers of activated Caspase-3 positive $cTEC^{lo}$, $cTEC^{hi}$ and $mTEC^{lo}$, $mTEC^{hi}$, tm mTEC. (**E**) Geometric mean fluorescence intensity (gMFI) of Total Caspase-3. Data is representative of three independent experiments analyzing $Lin28a^{TEC}$, $Lin28b^{TEC}$ and control mice at 4 weeks of age. * $p < .05$, ** $p < .01$, *** $p < .005$ (paired student's *t*-test).

4.4 Thymocyte development in young adult *Lin28* transgenic mice

4.4.1 Thymus settling is differentially affected by *Lin28a* and *Lin28b*

As thymocyte cellularity and thus thymic size linearly correlate to the number of early thymic progenitors (ETP) [123], we I next investigated the quantity of T cell progenitors in a microenvironment containing *Lin28a* and/or *Lin28b* over-expressing epithelia. Defined as NK cell, B cell, erythroid and myeloid lineage negative (Lin^-) and $CD117(ckit)^+CD44^+CD25^-$ cells, ETP were significantly reduced in mice expressing *Lin28a* tg whereas $Lin28b^{TEC}$ mice displayed an increase in ETP cellularity when compared to control (Figure 14A, 14B).

Thymus settling is orchestrated by a set of well-defined chemokines expressed in TEC, namely CC-chemokine ligand 21 (*Ccl21*), *Ccl19*, *Ccl25* and CXC-motif-chemokine 12 (*Cxcl12*) [52]. Moreover, the survival and proliferation of the most immature thymocytes are controlled by Interleukin-7 (*Il-7*) and stem cell factor (*Scf*) [54, 55, 57, 58]. Investigating the transcript numbers of these chemokines using qPCR, I found that in TEC of $Lin28a^{TEC}$ mice the expression of *Ccl21* was reduced by 3-fold, *Ccl19* levels decreased while the expression of *Ccl25* and *Cxcl12* increased when compared to control TEC (Figure 14C). The expression of factors that promote the survival and proliferation of these early thymic immigrants, namely *Il-7* and *Scf*, were significantly increased in TEC that express *Lin28a* transgene (Figure 14D).

In *Lin28b* tg TEC, the expression of *Ccl21* was slightly reduced, *Ccl19* and *Cxcl12* levels unchanged whereas the number of *Ccl25* transcripts was significantly increased compared to

TEC of Lin28b^{TEC} mice (Figure 14C). Moreover, the expression of *Il-7* was reduced while *Scf* transcript numbers increased upon *Lin28b* transgenic expression (Figure 14D).

As TEC numbers are severely reduced in *Lin28a* mutant mice, this data suggests that the lower expression of *Ccl21* and *Ccl19* in these cells may have caused a drop in ETP attraction and subsequent thymic hypoplasia. The increased expression of *Il-7* and *Scf* in *Lin28a* tg mice indicates that the survival of these early thymic immigrants is unaltered in these animals. In *Lin28b* mutant mice however, increased TEC numbers, producing more *Ccl25* and regular amounts of *Cxcl12* and *Ccl19* may compensate the slight reduction in *Ccl21* and cause increased ETP attraction and subsequent enlargement of the thymus. In Lin28b^{TEC} mice, the increased numbers of TEC expressing more *Scf* might balance the reduced expression of *Il-7* and induce regular maintenance of ETP.

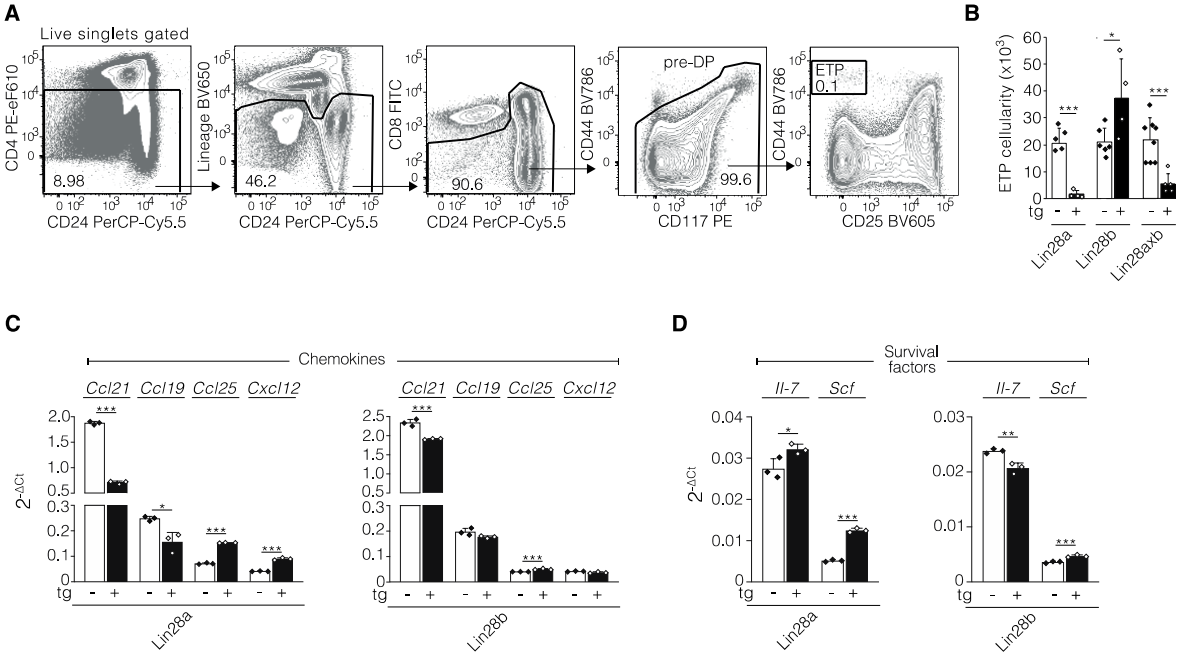

Figure 14: Thymus settling is differentially regulated by *Lin28a* and *Lin28b*

(**A**) Gating strategy for ETP thymocytes: live singlets, defined by FSC and SSC parameters and DAPI exclusion, were successively depleted of CD4^{pos}, Lineage^{pos}, CD8^{pos}CD24^{lo} and CD44^{pos} CD117^{neg} cells. (**B**) ETP cellularity. Data is representative of at least two independent experiments analyzing Lin28a^{TEC}, Lin28b^{TEC}, Lin28axb^{TEC} and control female mice at 4-7 weeks of age. (**C**) Expression of chemokines important for ETP attraction in sorted TEC. (**D**) Expression of survival factors for ETP in TEC. Data is representative of at least two independent experiments analyzing Lin28a^{TEC}, Lin28b^{TEC} and control female mice at 6-7 weeks of age. qPCR normalized to *bACT* expression. * $p < .05$, ** $p < .01$, *** $p < .005$ (paired student's *t*-test).

4.4.2 Initial stages of thymocyte maturation are unaffected in *Lin28* mutant mice

I next investigated whether the changes in the epithelial compartment of young adult Lin28a^{TEC}, Lin28b^{TEC} and Lin28axb^{TEC} mice affected thymocyte differentiation. Thymus size is determined by the numbers of CD4^{+}CD8^{+} double positive (DP) thymocytes that make up approximately 80% of the thymic cell mass in the steady state. DP cells originate from CD4^{-} CD8^{-} double negative (DN) cells that undergo a proliferative burst after successful rearrangement of their TCRβ chain (beta selection checkpoint). Early thymocyte differentiation proceeded normally in all three mutant strains demonstrated by comparable proportions of pre-DP maturational subsets both before (DN1 [CD44^{+}CD25^{-}], DN2 [CD44^{+} CD25^{+}], DN3a [CD44^{-} CD25^{+} CD71^{-}]) and after the TCR beta selection checkpoint (DN3b [CD44^{-}CD25^{lo} CD71^{+}], DN4 [CD44^{-} CD25^{-} CD71^{+}], CD8 ISP [CD4^{-} CD8^{+} CD71^{+} immature single positive]; Figure 15A, 15B). Hence, a developmental block in thymocyte differentiation (Lin28a^{TEC} and Lin28axb^{TEC}) or accelerated transitions (Lin28b^{TEC}) at the pre-DP stage could be ruled out as potential mechanisms for the observed differences in thymic organ size.

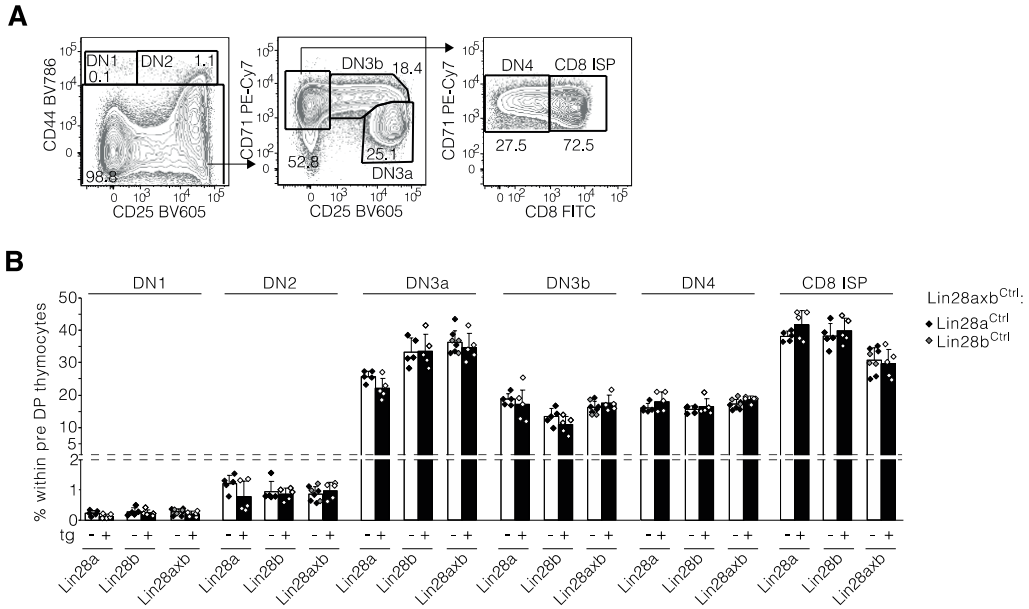

Figure 15: Initial stages of thymocyte maturation are unaffected in *Lin28* mutant mice
(**A**) Representative gating of preDP thymocytes. (**B**) Quantitative analysis of developmental stages within pre-DP thymocytes in Lin28a^{TEC}, Lin28b^{TEC} and Lin28axb^{TEC} animals. Female mice at 4-6 weeks of age were used, Cre^{neg} controls for Lin28axb^{TEC} consisted of single transgenic Lin28a^{Ctrl} and Lin28b^{Ctrl} animals. Data are representative of at least two independent experiments. * $p < .05$, ** $p < .01$, *** $p < .005$ (paired student's *t*-test).

4.4.3 Thymocyte positive selection is compromised in Lin28a^{TEC} and Lin28axb^{TEC} mice

Next, I analyzed whether subsequent thymocyte developmental stages were affected in *Lin28* mutant animals. Thymocyte maturation after the CD8 ISP stage involves the upregulation of CD4 and the productive rearrangement of the TCRα chain to express a TCRα/ TCRβ complex on the surface. DP thymocytes that generated a TCR with intermediate avidity to MHC:peptide complexes receive a survival signal and continue their maturation [63]. This process, known as positive selection, rescues thymocytes from undergoing programmed cell death and initiates differentiation into the CD4 or CD8 lineage [4, 61]. However, only a small fraction of DP cells will encounter a signal with intermediate avidity and continue with their development. DP cells expressing MHC II restricted TCR down-regulate CD8 surface expression to become CD4 single positive (SP) while MHC I binding by TCR promotes CD4 down-modulation and subsequent maturation into CD8 SP [124]. The frequencies of CD4 and CD8 SP thymocytes was decreased whereas that of DP cells increased in mice where *Lin28a* was constitutively expressed in TEC (Figure 16A). However, the DP gate displayed in Figure 16A also contains SP committed thymocytes that are "masked" as DP due to their complex maturational progression. Hence, I applied a more sophisticated gating strategy to reveal those SP committed thymocytes hiding behind a DP mask and to calculate the frequencies of DP and SP thymocytes in mutant and control animals (Figure 16B). Indeed, the relative numbers of CD4 and CD8 SP were reduced and that of DP cells increased in mice that express *Lin28a* transgene (Figure 16C).

I next analysed the efficacy of positive thymocyte selection in all three *Lin28* transgenic mouse lines. DP thymocytes that have received a positive selection signal are marked by the surface expression of the early activation marker CD69 [125]. The frequencies of TCR^{pos} DP thymocytes that have increased their TCR surface amounts and express CD69 were comparable in all animals. (Figure 16D). However, up-regulation of CD69 and TCR surface expression occur gradually, hence it is challenging to define clear boundaries to separate non-selected DP from those having received positive selection signals. Thymocytes also down-regulate the expression of the two co-receptors CD4 and CD8 upon positive selection (dulling) [67]. Hence, I utilized co-receptor dulling as an additional criterion to unequivocally identify positively selected cells. To compare for background levels, boundaries for DP^{dull} gating were set first on pre-selection $CD69^{neg}$ thymocytes and, as expected, the frequencies of cells residing within the DP^{dull} gate did not differ between mutant and control animals (Figure 16E). However, I detected a significant decrease of DP^{dull} cells within the $CD69^{pos}$ population in animals harbouring the *Lin28a* transgene suggestive of fewer DP undergoing positive selection (Figure 16E). As an independent means to rule out putative biases in defining DP^{dull} gates, I calculated the reduction of co-receptor gMFI in total $CD69^{pos}$ thymocytes in relation to the gMFI of their $CD69^{neg}$ counterparts. Compared to controls, $CD69^{pos}$ cells from $Lin28a^{TEC}$ and $Lin28axb^{TEC}$, but not $Lin28b^{TEC}$ mice had higher co-receptor gMFIs (Figure 16F), thus corroborating a *Lin28a* tg cTEC insufficiency in mediating positive selection. Consequently, phenotypically mature (i.e. TCR^{+}) SP thymocytes were also decreased in $Lin28a^{TEC}$ and $Lin28axb^{TEC}$ mice (Figure 16C).

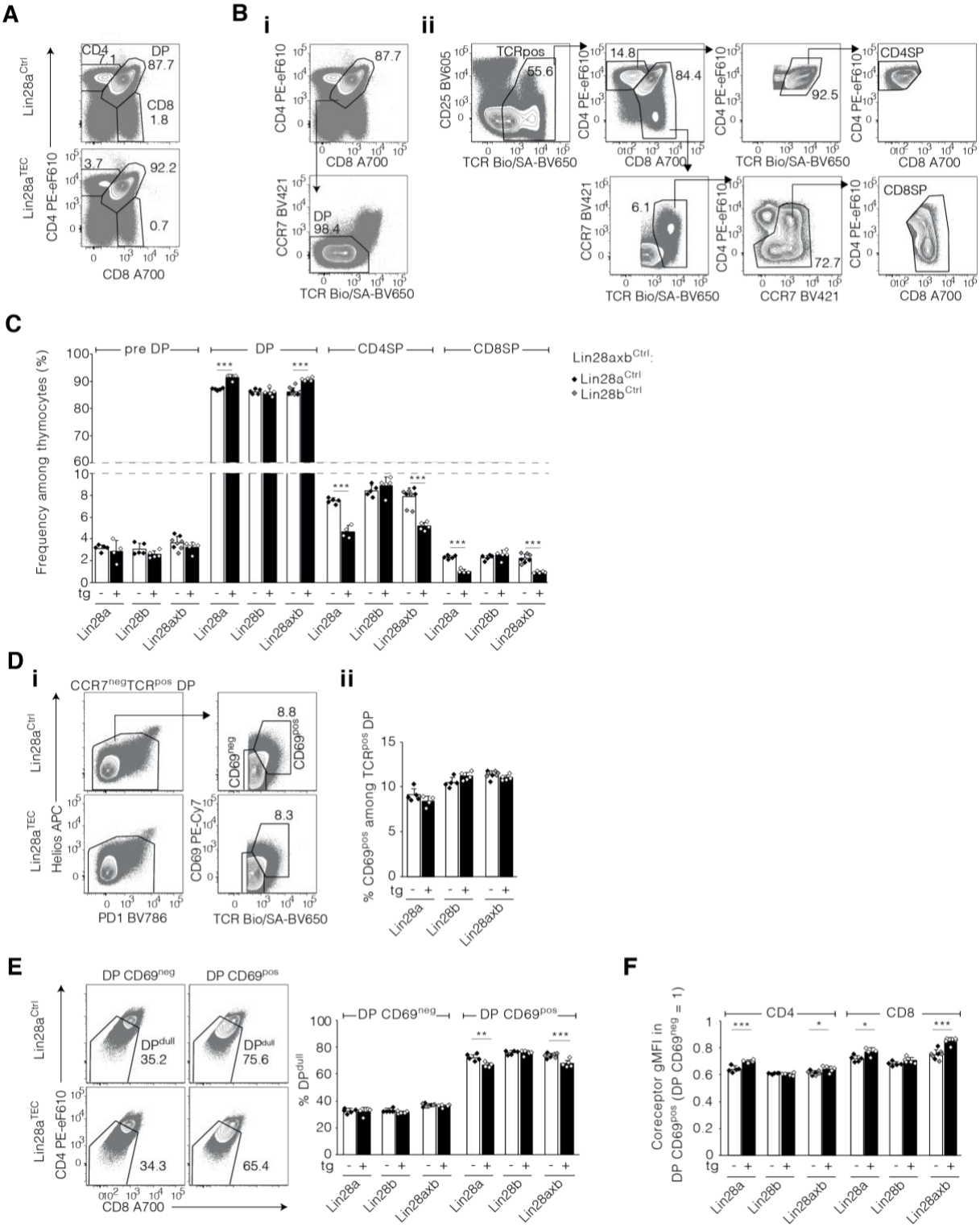

Figure 16: Thymocyte positive selection is compromised in Lin28a^{TEC} and Lin28axb^{TEC} animals
(**A**) Representative plots displaying frequencies of DP, CD4 and CD8SP in Lin28a^{TEC} and control animals. (**B$_i$**) Representative gating strategy for DP thymocytes: DP cells were identified as CD4^{pos}CD8^{pos} and were depleted of CCR7^{pos}TCR^{hi} (=medullary) cells. (**B$_{ii}$**) Gating strategy for TCR^{pos} thymocytes and SP cells: TCR^{neg} cells were excluded from live singlets and CD4SP cells were gated for high TCR expression. CD8SP were identified as TCR^{hi} cells depleted of CCR7^{neg} (=cortical) CD4^{pos} (i.e. DP) thymocytes.

Initial gates used for defining the CD4 and CD8 lineage were pasted back into the SP subsets to illustrate the cells' location. (**C**) Quantitative analysis of preDP, DP, CD4 and CD8SP within thymocytes in mutant Lin28a^{TEC}, Lin28b^{TEC}, Lin28axb^{TEC} and control animals. (**D$_i$**) Representative gating strategy for TCR^{pos} DP thymocytes before and after positive selection: DP cells were gated for TCR expression and depleted of CCR7^{pos} (=medullary) Helios^{pos}PD1^{pos} (=negatively selected) cells. Pre-positive selection DP were identified as CD69^{neg}TCR^{pos} while post-positive selection DP gated as CD69^{pos}TCR^{hi} cells. (**D$_{ii}$**) Quantitative analysis of TCR^{pos} DP thymocytes before (CD69^{neg}) and after (CD69^{pos}) positive selection. (**E**) Identification of co-receptor dulling in TCR^{pos} DP thymocytes before (DP CD69^{neg}) and after (DP CD69^{pos}) positive selection. (**F**) Geometric mean fluorescence intensity (gMFI) of co-receptors CD4 and CD8 in CCR7^{neg} (=cortical) TCR^{pos} DP thymocytes expressing CD69 compared to CD69^{neg} cells (arbitrarily set as 1). Female mice at 4-6 weeks of age were used, Cre^{neg} controls for Lin28axb^{TEC} consisted of single transgenic Lin28a^{Ctrl} and Lin28b^{Ctrl} animals. Data are representative of at least two independent experiments. * $p < .05$, ** $p < .01$, *** $p < .005$ (paired student's *t*-test).

4.4.4 Late stages of SP thymocyte maturation are altered by *Lin28a* tg

Next, I studied the maturational progression within SP thymocytes. The differentiation of CD4 SP thymocytes can be split into three developmental stages using the differential cell surface expression of CCR7, CD24 and CD69 [70]. The earliest CD4 SP thymocytes (designated SM) are CD24 positive, reside in the cortex and are CCR7 negative. Upon up-regulation of CCR7 they gain the capacity to migrate into the medulla [59] where they display increased CD69 expression and gain the competence to proliferate (designated M1) before down-regulating CD69 and CD24 to become fully mature cells (designated M2) that are equipped to produce cytokines and are ready to exit the thymus. However, CD4 SP thymocytes can also develop into regulatory T-cells. This developmental pathway requires TCR avidities which are at the border between positive and negative selection and is marked by the expression of the transcription factor forkhead box P3 (FoxP3) [126]. CD8 SP differentiate in the medulla where they first adopt a CD69^{+}CD24^{+} (M1) phenotype before down-modulating the surface expression of these markers to become M2 cells, competent to emigrate. Analyzing the frequency of these thymocyte subsets in *Lin28* mutant mice I found that the frequency of SM

in the CD4 lineage was increased while the relative numbers of M2 in CD4SP and CD8SP was decreased in Lin28a^{TEC} and Lin28axb^{TEC} animals (Figure 17A, 17B). Furthermore, frequencies of Foxp3^{+} T$_{reg}$ within CD4SP were reduced by 30 - 50% in mice where *Lin28a* was constitutively expressed (Figure 17C). Taken together, the enforced expression of *Lin28a* in TEC compromised the cells' capacity to terminally differentiate thymocytes and provide signals for high avidity interactions necessary for T$_{reg}$ generation.

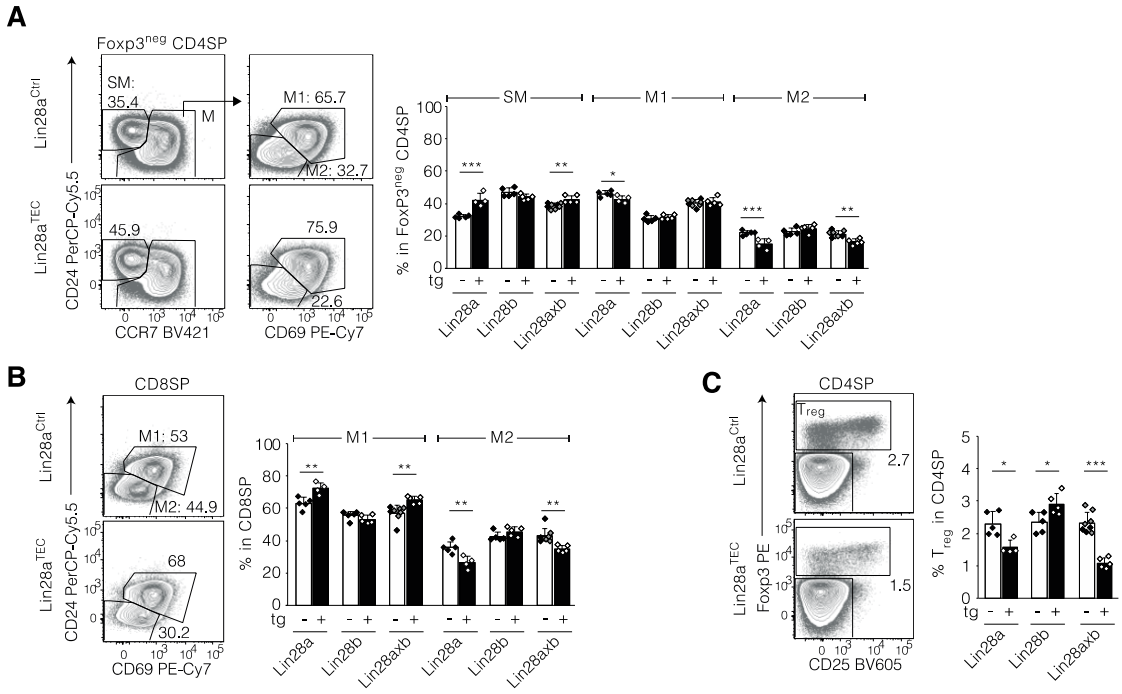

Figure 17: Late stages of SP thymocyte maturation are altered by *Lin28a* tg

(**A**) Representative plots and quantitative analysis of CCR7^{neg} (=cortical) semi-mature (SM) and CCR7^{pos} (=medullary) mature (M, divided into M1 and M2 according to CD69 and CD24 expression) subsets in Foxp3^{neg} (=excluding T$_{reg}$) CD4SP. (**B**) Representative plots and quantification of CD8SP M1 and M2 populations. (**C**) Frequencies of Foxp3^{pos} T$_{reg}$ in CD4SP. Female mice at 4-6 weeks of age were used, Cre^{neg} controls for Lin28axb^{TEC} consisted of single transgenic Lin28a^{Ctrl} and Lin28b^{Ctrl} animals. Data are representative of at least two independent experiments. * $p < .05$, ** $p < .01$, *** $p < .005$ (paired student's *t*-test).

4.4.5 *Lin28a* tg cTEC are limited in their capacity to induce thymocyte negative selection

As the frequency of mature SP thymocytes is also influenced by the extent of negative selection, I quantified negatively selected thymocytes. Thymocytes undergoing negative selection in the cortex are marked by high co-expression of Helios and PD-1 among CCR7^{-} Foxp3^{-} TCR^{+} DP and CD4SP cells (wave 1 negative selection). In the medulla, negatively selected cells are identified by the expression of Helios within the CCR7^{+} FoxP3^{-} CD4SP cells (wave 2 negative selection) [72].

Lin28a^{TEC} and Lin28axb^{TEC} displayed a 40-50% reduction in the frequency of negatively selected cortical thymocytes when compared to Lin28b^{TEC} or control mice (Figure 18A). In contrast, negative selection of medullary thymocytes was unaffected in all *Lin28* transgenic animals (Figure 18B). Taken together, these data demonstrate that enforced Lin28A expression in TEC dominantly interferes with cortical positive and negative selection, reduces the number of thymic T$_{reg}$ and affects developmental progression of SP in the medulla to a mature phenotype.

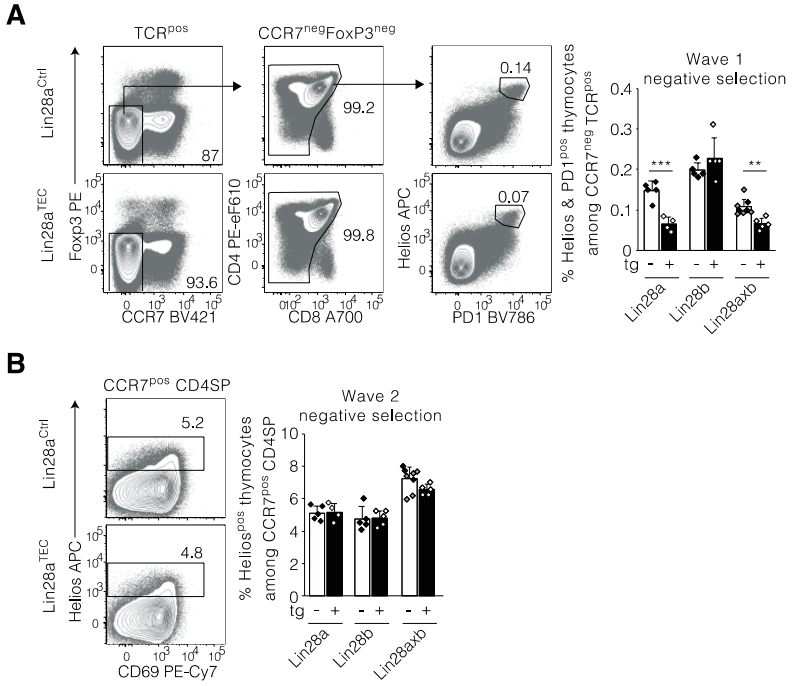

Figure 18: *Lin28a* tg cTEC are limited in their capacity to induce thymocyte negative selection
(**A**) Gating strategy and quantification of negatively selected $CCR7^{neg}$ (=cortical), $FoxP3^{neg}$ (=excluding T_{reg}) CD4 lineage thymocytes expressing Helios and $PD\text{-}1^{pos}$ (wave 1 negative selection). (**B**) Gating strategy and relative numbers of medullary $Helios^{pos}$ CD4SP undergoing negative selection (wave 2 negative selection). Female mice at 4-6 weeks of age were used, Cre^{neg} controls for $Lin28axb^{TEC}$ consisted of single transgenic $Lin28a^{Ctrl}$ and $Lin28b^{Ctrl}$ animals. Data are representative of at least two independent experiments. * $p < .05$, ** $p < .01$, *** $p < .005$ (paired student's *t*-test).

4.5 Thymus phenotype of juvenile Lin28a^{TEC} animals

4.5.1 Juvenile Lin28a^{TEC} mice have a regular cTEC but altered mTEC subset composition

Because of the interesting phenotype imposed by *Lin28a* tg, I analysed in the next experiments Lin28a^{TEC} animals. I hypothesized that the defects in T cell maturation in young adult Lin28a^{TEC} animals were due to the changes in their TEC subset composition. Upon closer inspection, the phenotype of *Lin28a* tg cTEC resembled that of neonatal wild-type cTEC (Figure 19A) [127]. I therefore compared juvenile Lin28a^{TEC} mice to age matched controls and, contrary to young adult adults, 2 week old Lin28a^{TEC} mice displayed unchanged thymus cellularity (Figure 19B). Only after this time point I found a significant reduction in thymus size caused by *Lin28a* tg expression (Figure 19B). Thus, I decided to probe whether the changes in absolute TEC numbers, TEC subset composition, ETP attraction and thymocyte development are also apparent in juvenile Lin28a^{TEC} mice. Total TEC, cTEC and mTEC cellularities were comparable between mutant and control animals at juvenile age (Figure 19C, 19D, 19E, 19F). While the composition of cTEC was normal, I found small differences in mTEC subset composition with mTEC^{lo} being mildly under-represented in Lin28a^{TEC} mice at 2 weeks of age (Figure 19G, 19H). While the transcripts of *Ccl21*, *Ccl19* and *Cxcl12* were significantly reduced, transcript numbers of *Ccl25* are significantly higher in mTEC of juvenile Lin28a^{TEC} mice. Furthermore, the expression of *Il-7* expression was unchanged and the amount of *Scf* transcripts increased in Lin28a^{TEC} animals at 2 weeks of age (Figure 19I).

Thymus organ size correlated with an unchanged cTEC compartment in juvenile Lin28a^{TEC} mice. As the expression of chemokines and survival factors for ETP was similarly affected in juvenile *Lin28a* mutant mice as in young adult Lin28a^{TEC} animals, this data suggests that cTEC^{hi} and cTEC^{lo} differentially regulate thymic settling, explaining the changes in thymus size in young adult *Lin28a* mutant animals. In contrast to the cortex, 2 week old Lin28a^{TEC} mice

already display some of the changes found in the mTEC compartment of young adult mutant animals.

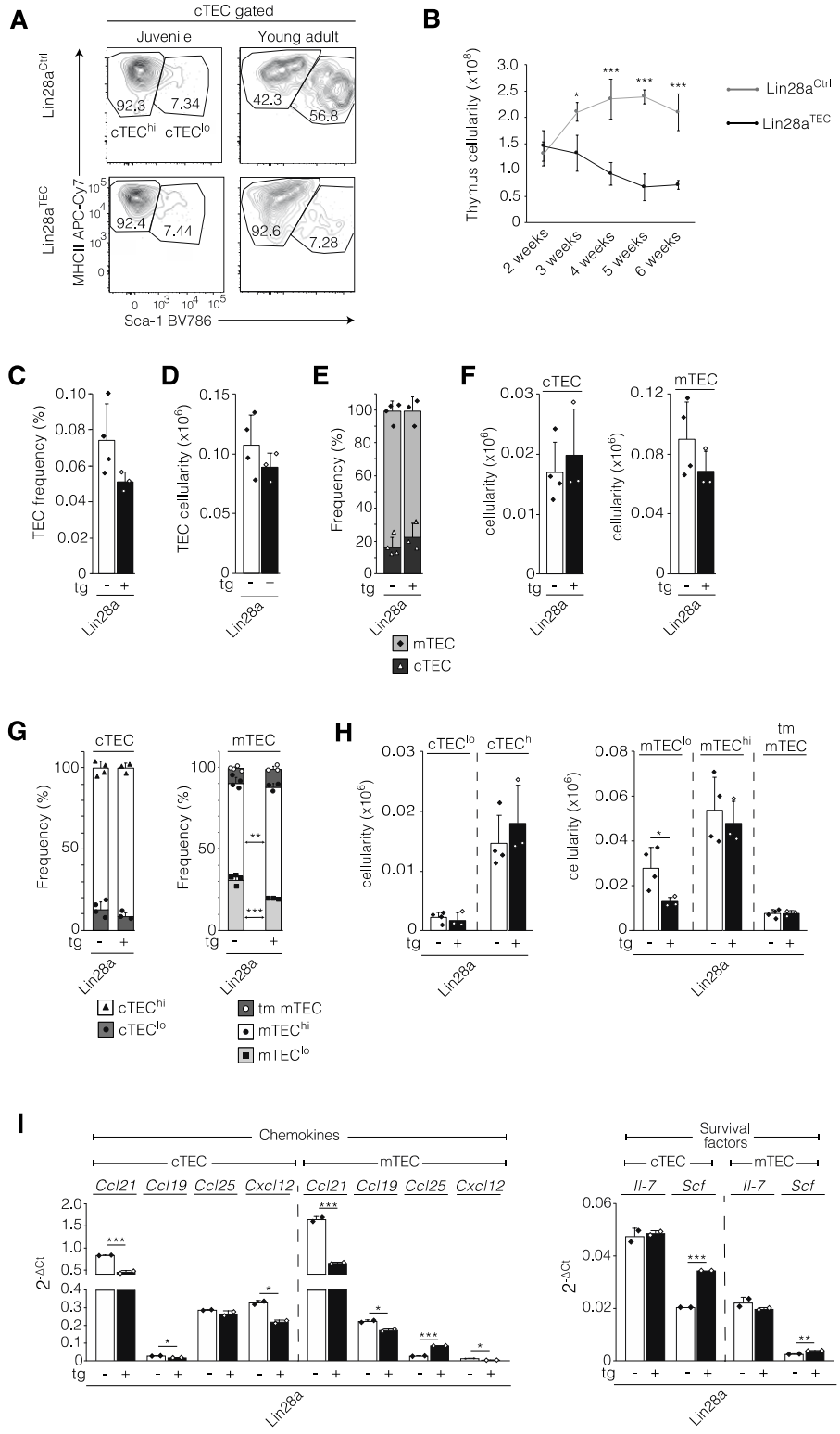

Figure 19: Juvenile Lin28a^{TEC} mice have regular cTEC but altered mTEC subset composition
(**A**) Representative Sca-1 and MHCII expression in cTEC of 2 week old (=juvenile) and 4 week old (=young adult) Lin28a^{TEC} and control female animals. Data are representative of at least two

independent experiments. (**B**) Thymus cellularity in Lin28a^{TEC} and controls between 2 and 6 weeks of age. Apart from 3-week time point (one experiment, $n = 3$, mixed sex mice), data are pooled from at least two independent experiments analyzing female and male mice ($n = 4 – 18$) at the indicated ages. (**C**) Relative and (**D**) absolute TEC numbers. (**E**) cTEC:mTEC ratio. (**F**) Absolute numbers of cTEC and mTEC. (**G**) Frequency and (**H**) absolute number of cTEC^{lo}, cTEC^{hi} and mTEC^{lo}, mTEC^{hi}, tm mTEC. (**I**) Expression of chemokines important for ETP attraction and survival factors for ETP in sorted cTEC and mTEC. For experiments (**C** – **I**), data are representative of at least two independent experiments analyzing *Lin28a* mutant and control female mice at 2 weeks of age. * $p < .05$, ** $p < .01$, *** $p < .005$ (paired student's *t*-test).

4.5.2 Cortical selection proceeds normally while medullary thymocyte maturation is compromised in juvenile Lin28a^{TEC} animals

Next, I investigated thymopoiesis in juvenile mice. Early thymocyte development was unaltered as the frequencies of pre-DP thymocyte subpopulations prior to and post TCR beta selection were comparable between mutant Lin28a^{TEC} and control littermates (Figure 20A). The relative numbers of CD4 and CD8 SP thymocyte were unchanged suggesting that thymocyte positive and negative selection are unaffected by ectopic *Lin28a* expression early in life (Figure 20B). The percentage of DP^{dull} and the gMFI of CD4 and CD8 co-receptors within the CD69^{pos} population in Lin28a^{TEC} mice were similar to those of control, confirming that positive selection of thymocytes proceeded normally (Figure 20C, 20D, 20E). In addition, I found no changes in the frequencies of thymocytes undergoing negative selection in the cortex as well as in the medulla (Figure 20F, 20G). However, late stages in the maturation of SP thymocytes were affected as I detected fewer M2 cells in both CD4 and CD8 lineages (Figure 20H, 20I). Furthermore, the percentage of regulatory thymocytes was reduced in Lin28a^{TEC} mice (Lin28a^{TEC}: 2.2 $\pm$ 0.1 % vs. Lin28a^{Ctrl}: 3.1 $\pm$ 0.5 %; Figure 20J). Hence, while Lin28a^{TEC} showed normal thymocyte positive and negative selection in juvenile mice, the ectopic expression of *Lin28a* caused a reduction of mature SP and FoxP3^{+} regulatory thymocytes.

Together, these results show that thymus cellularity, cTEC subset composition, as well as thymocyte positive and cortical negative selection are unaffected in 2 week old Lin28a^{TEC} animals. At this time point the cTEC compartment is mainly composed of cTEC^{hi}, indicating that cTEC^{hi} and cTEC^{lo} have distinct roles in controlling thymus seeding and regulating thymocyte positive and negative selection. However, transgenic *Lin28a* expression in TEC of juvenile mice affects the composition of the mTEC compartment, correlating with the alterations in medullary thymocyte development found in these mice.

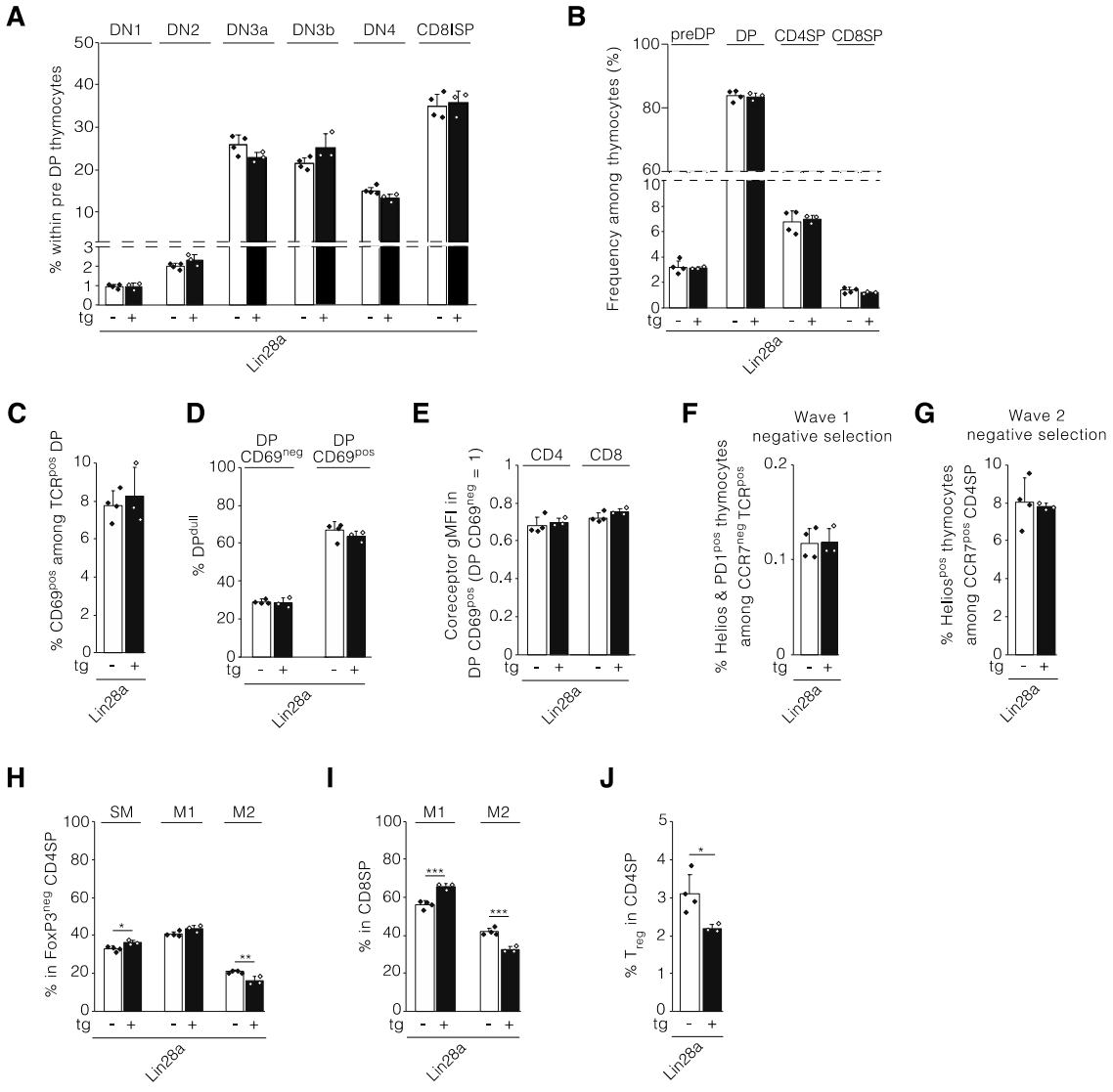

Figure 20: Cortical selection proceeds normally while medullary thymocyte maturation is compromised in juvenile Lin28a^{TEC} animals

(**A**) Frequencies of developmental stages within pre-DP thymocytes in mutant Lin28a^{TEC} and control

mice. (**B**) Relative numbers of preDP, DP, CD4 and CD8SP within thymocytes. (**C**) Frequencies of TCR^{pos} DP after ($CD69^{pos}$) positive selection. (**D**) Quantitative analysis of co-receptor dulling of $CD69^{neg}$ and $CD69^{pos}$ within TCR^{pos} DP thymocytes. (**E**) gMFI of CD4 and CD8 co-receptors in $CCR7^{neg}$ TCR^{pos} DP thymocytes expressing CD69 compared to $CD69^{neg}$ cells (arbitrarily set as 1). (**F**) Quantitative analysis of cortical $CCR7^{neg}$ (=cortical) CD4 lineage thymocytes expressing Helios and PD1 (wave 1 negative selection). (**G**) Frequency of medullary $Helios^{pos}$ CD4SP undergoing negative selection (wave 2 negative selection). (**H**) Relative numbers of SM, M1 and M2 in $FoxP3^{neg}$ (=exclude T_{reg}) CD4SP. (**I**) Quantification of M1 and M2 thymocytes in CD8SP. (**J**) Frequency of $FoxP3^{pos}$ T_{reg} in CD4SP. Data are representative of at least two independent experiments analyzing *Lin28a* mutant and control female mice at 2 weeks of age. * $p < .05$, ** $p < .01$, *** $p < .005$ (paired student's *t*-test).

4.6 cTEC^{lo} and cTEC^{hi} possess distinct positive selection potentials

To identify mechanisms that account for the observed defects in thymocyte selection by *Lin28a* transgenesis in young adult mice, I next analysed the TEC compartment of *Lin28a* mutant animals in more detail. While juvenile mutant mice had unchanged frequency of cTEC that express the inhibitory programmed death-ligand 1 (PD-L1), a cell surface molecule known to inhibit TCR-mediated positive selection of CD4+ thymocytes [128], young adult Lin28a^{TEC} mice displayed an increased frequency of PD-L1 positive cTEC when compared to age matched controls (Juvenile: Lin28a^{TEC}: 90.9 ± 2.2 % vs. Lin28a^{Ctrl}: 82.2 ± 5.8 %; Young adult: Lin28a^{TEC}: 77.5 ± 4.6 % vs. Lin28a^{Ctrl}: 31 ± 5.2 %, Figure 21A). Blocking PD-L1 in wild type fetal thymic organ cultures (FTOC) increased the generation of CD4 SP thymocytes (anti-PD-L1: 12.5 ± 1.5 vs. isotype: 10.2 ± 1.6 vs. untreated: 11 ± 0.8; Figure 21B). Because PD-L1 is differentially expressed between cTEC^{hi} and cTEC^{lo} (53.3 ± 5.6 % vs. 9.3 ± 2.8 %; Figure 21C) I next probed wild-type cTEC^{lo} and cTEC^{hi} separately for their capacity to mediate positive selection. To this end, I performed reaggregate thymic organ culture (RTOC) experiments and cultured CD69^{neg} DP thymocytes for 48h with either cTEC^{lo} and cTEC^{hi} and analysed the upregulation of CD69 (Figure 21D, 21E). I could demonstrate that cTEC^{lo} were more effective in positive selection of thymocytes (as identified CD69^{pos}, CD4CD8^{dull}) when compared to cTEC^{hi} (15 ± 1.3% vs. 10 ± 0.6%; Figure 21F).

Hence, reduced positive selection in young adult Lin28a^{TEC} can in part be explained by the over-representation of cTEC expressing high amounts of inhibitory PD-L1.

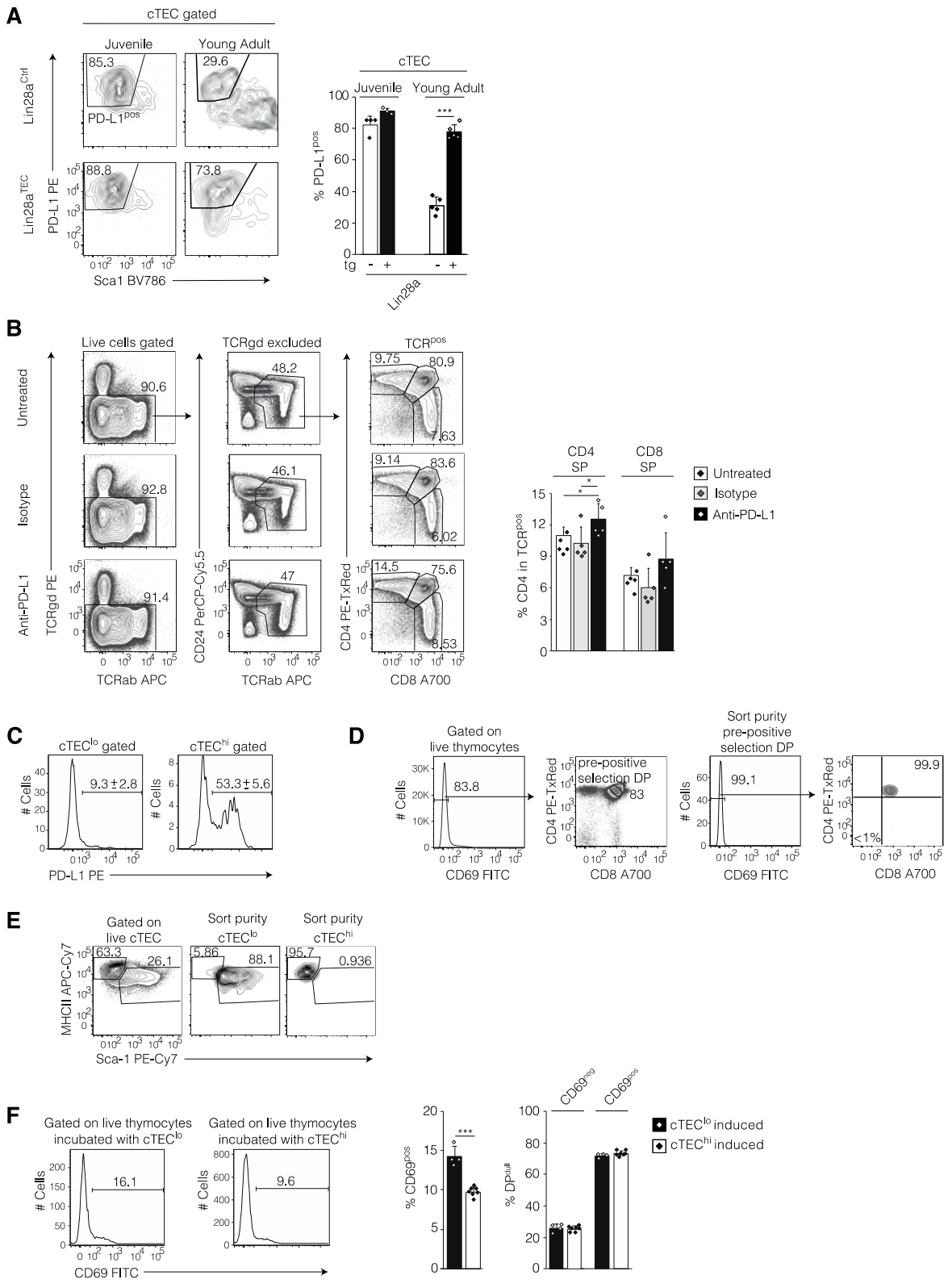

Figure 21: cTEC^{lo} and cTEC^{hi} possess distinct selection potentials

(**A**) Representative contour plots detailing PD-L1 expression in cTEC and quantitative analysis of PD-L1^{pos} cTEC. Data is representative of at least two independent experiments analyzing Lin28a^{TEC} and control mice at 2 (=juvenile mice) and 4 (=young adult) weeks of age. (**B**) Gating strategy and frequencies of CD4SP and CD8SP within TCR^{pos} thymocytes in fetal thymic organ cultures (FTOC).

Thymic lobes for FTOC were isolated from wild-type animals at embryonic day 14.5 (E14.5) and cultured in medium only, in the presence of isotype control or PD-L1 blocking antibody for 8 days. Data is representative of three independent experiments. (**C**) Representative flow cytometry histograms detailing PD-L1 expression in $cTEC^{hi}$ and cTEClo of 4 week old $Lin28a^{Ctrl}$ mice. (**D**) Flow cytometry sorting strategy and sort purity of $CD69^{neg}$ DP thymocytes (i.e. pre-positive selection DP). (**E**) Gating strategy and purity of isolated $cTEC^{hi}$ and $cTEC^{lo}$. (**F**) Relative numbers of thymocytes that received a positive selection signal from $cTEC^{hi}$ or $cTEC^{lo}$ based on CD69 upregulation and co-receptor dulling after 48 hours of culture. $CD69^{neg}$ thymocytes were sorted and reaggregated with either $cTEC^{lo}$ or $cTEC^{hi}$ for 48 hours (n = 4-8). (**D**) – (**F**) Cells were sorted from mixed sex wild-type animals at 1-2 weeks of age. Data is representative of two independent experiments analyzing reaggregate thymic organ cultures (RTOC). * $p < .05$, ** $p < .01$, *** $p < .005$ (paired student's t-test).

4.7 Transcriptomic analyses of cTEC^{lo} and cTEC^{hi} from juvenile and young adult Lin28a^{TEC} mice

4.7.1 *Lin28a* over-expression changes the TEC subtype composition at juvenile and adult age

I performed RNA-seq to identify in a non-supervised fashion the transcriptomic changes that relate to the numerical, phenotypic and functional changes of cTEC^{lo} and cTEC^{hi} in juvenile and young adult Lin28a^{TEC} mice. I first performed a principal component analysis (PCA) to assess the variability of the samples. I found that the cTEC^{lo} and cTEC^{hi} samples from each mouse genotype and each time point clustered together in the PCA diagram (Figure 22A). As expected, the *Lin28a* transgenic samples showed higher expression of *Lin28a* compared to control samples of the same phenotype and age (Figure 22B).

Because *Lin28a* over-expression lead to a near complete loss of cTEC^{lo} in young adult animals (Figure 12J), I analysed the effect of *Lin28a* tg on the abundance of transcriptomically specified TEC subtypes that were identified within flow cytometric defined cTEC at the single cell level [47]. For clarifications, hereafter I refer to cytometrically defined TEC as subsets and transcriptomically identified TEC as clusters.

To infer the composition of cTEC^{lo} and cTEC^{hi} from juvenile and young adult Lin28a^{TEC} animals I deconvoluted our bulk RNA sequencing data by using the marker genes for clusters identified recently [47]. This analysis revealed that cTEC^{lo} of 2 week old Lin28a^{TEC} mice had an increased signature of mature cTEC and proliferating TEC and showed a reduced signal from intertypical TEC than control (Figure 22C). At 7 weeks of age, intertypical TEC dominated the cTEC^{lo} that express *Lin28a* tg (Figure 22C). Intertypical TEC are a TEC cluster which are part of cytometrically defined cTEC as well as mTEC and are believed to be derived from a cTEC like progenitor (i.e. expressing β5t) that have the potential to develop into the mTEC lineage. The proportion of intertypical TEC increases over time, supporting the notion

that their contribution to the mTEC lineage increases with age [47]. Hence this result suggests, that early in life *Lin28a* tg expression increases the pool of proliferating and mature cTEC while at adult age blocks the further maturation of intertypical TEC into mTEC, leading to their over-representation within the cytometrically defined $cTEC^{lo}$ compartment. This result is also in line with our data from young adult mice showing that the relative and absolute mTEC numbers are reduced upon *Lin28a* ectopic expression (Figure 12H, 12I).

Within the $cTEC^{hi}$ subset of 2 week old $Lin28a^{TEC}$, I found an over-representation of the perinatal cTEC cluster (Figure 22C). Perinatal cTEC are a TEC cluster which are part of cytometrically identified cTEC that are most abundant in young mice and are thought to represent progenitor cells early in life. At 7 weeks of age *Lin28a* over-expression lead to a strong mature cTEC signature and a reduced intertypical signal (Figure 22C). Together, this result implies that *Lin28a* tg increases the cTEC progenitor pool at juvenile age and later in life inhibits the generation of intertypical TEC originating from the $cTEC^{hi}$ subset.

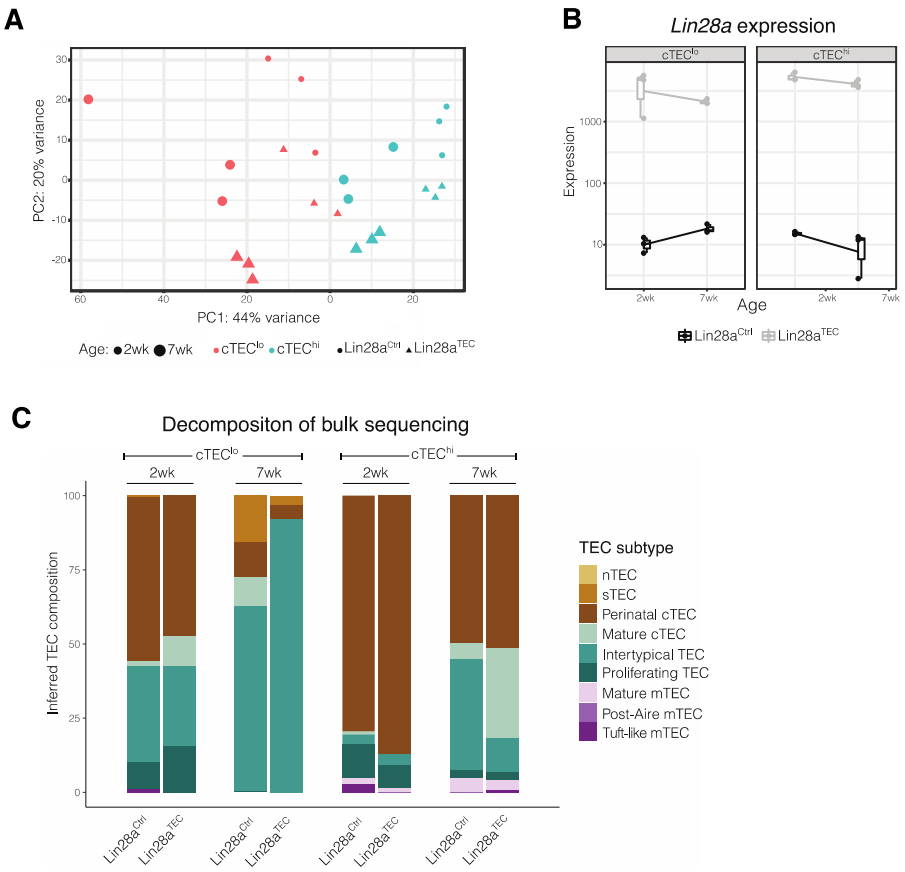

Figure 22: *Lin28a* over-expression changes the TEC subtype composition at juvenile and adult age
(**A**) Principal component analysis (PCA) of samples from RNA sequencing of cTEC^{lo} and cTEC^{hi} of 2 and 7 week old Lin28a^{TEC} and Lin28a^{Ctrl} animals. PC1 separates cTEC^{lo} from cTEC^{hi} and PC2 corresponds to the Lin28a^{Ctrl} / Lin28a^{TEC} axis. (**B**) Quality control of *Lin28a* expression in control and *Lin28a* tg samples. (**C**) Estimated composition of each data type based on the subsets defined in [47]. The deconvolution was performed using CIBERSORT with a custom gene expression generated from the data set in [47].

4.7.2 The impact of *Lin28a* tg on the transcriptome of cTEC increases with age

I next analyzed the differentially expressed genes in cTEC^{lo} and cTEC^{hi} of 2 week and 7 week old Lin28a^{TEC}. At 2 weeks of age, ectopic *Lin28a* expression caused 355 genes to be differentially expressed in cTEC^{lo} whereas 2437 genes were differentially regulated in *Lin28a* tg cTEC^{hi} (Figure 23A). In 7 week old Lin28a^{TEC} animals, 1896 differentially expressed genes were found in cTEC^{lo} while 4096 genes were differentially regulated in cTEC^{hi} (Figure 23A). Hence, this data suggests that *Lin28a* tg has a bigger effect on the transcriptome of cTEC^{hi} than cTEC^{lo} and that the impact of *Lin28a* over-expression on the gene expression profile of cTEC

increases with age. This result also correlates with our previous findings showing that the *Lin28a* tg causes more profound changes in TEC development and function as the mouse ages.

A Gene Set Enrichment (GSE) analysis of the differentially regulated genes in 2 week old *Lin28a* tg cTEC^{lo} showed a down-regulation of pathways related to the immune system, while there were no pathways that trended to be over-expressed in the mutant cells when compared to control (Figure 23B). In 2 week old *Lin28a* tg cTEC^{hi}, I found that immune system and cell cycle pathways were down-regulated while collagen biosynthesis and extracellular matrix organization pathways trended to be over-expressed compared to control (Figure 23B). 7 week old cTEC^{lo} of Lin28a^{TEC} mice did not display any significant changes in reactome pathway enrichment compared to control (Figure 23B). cTEC^{hi} of 7 week old Lin28a^{TEC} showed reduced immune and GPCR signaling whereas MAP kinase activation and IL-17 signaling were enriched when compared to control (Figure 23B).

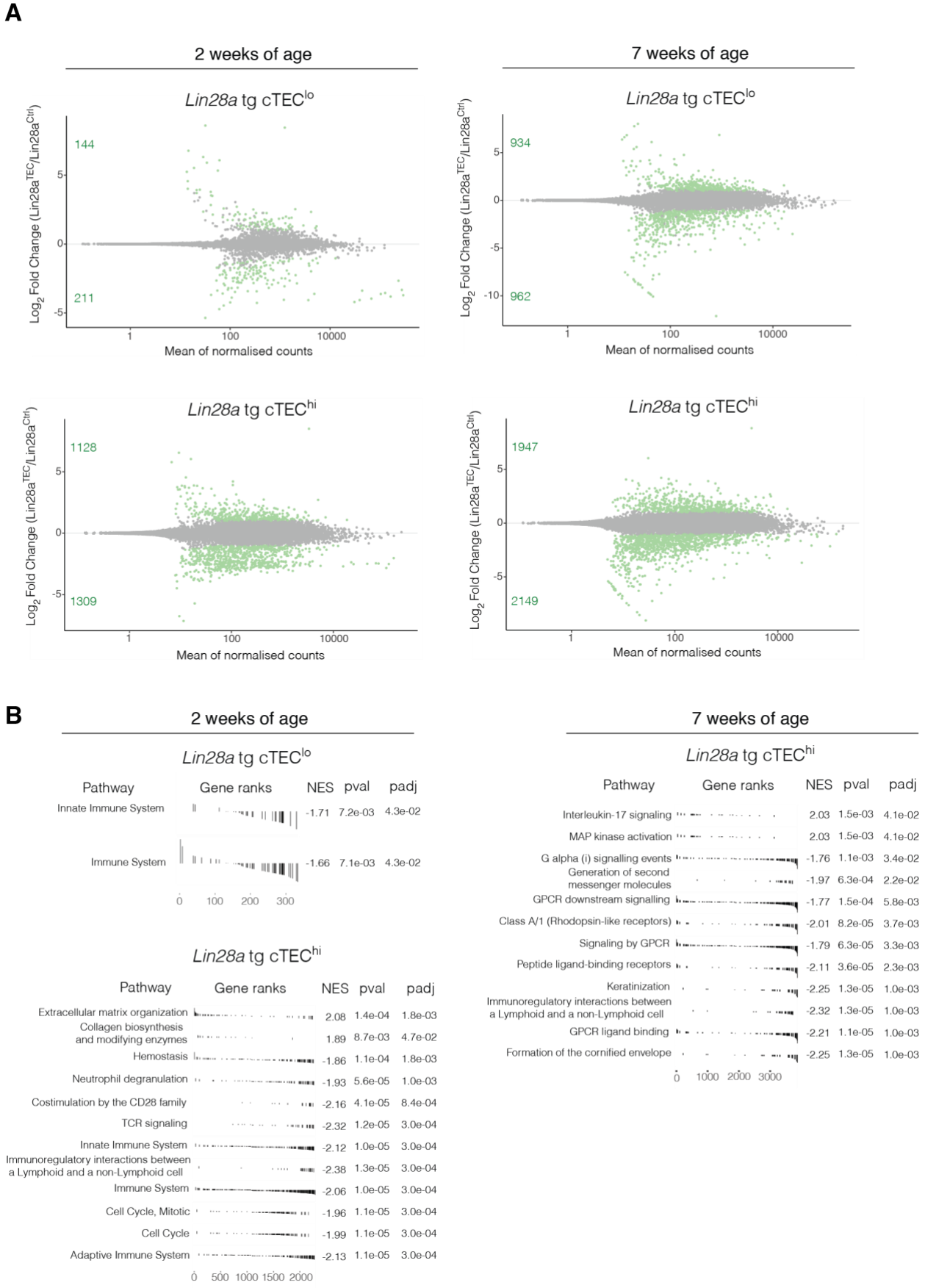

Figure 23: The impact of *Lin28a* tg on the transcriptome of cTEC increases with age

(**A**) MA-plot displaying the average expression (x-axis) versus the fold-change (log_2)

of genes in 2 and 7 week old *Lin28a* tg cTEC^{lo} and cTEC^{hi} versus control. Differentially expressed (DE) genes are shown in green. The number of DE genes (up/down) are shown along the left-side of the axis in green. (**B**) Gene set enrichment analysis for 2 and 7 week old *Lin28a* tg cTEC^{lo} and cTEC^{hi}. The differentially regulated genes in each pathway are represented by bars in rank order from 0 (most upregulated) to 300, 2000 or 3000 (most downregulated). The height of the bar signifies the amount of the gene that is up or down regulated. The normalized enrichment score (NES) visualizes if there are more up or downregulated genes in the pathway. A positive NES value indicates that the pathway is more enriched in the up regulated genes while a negative NES value shows that the pathway is more enriched in the down regulated genes.

4.7.3 Epithelial to mesenchymal transition is increased in cTEC that express *Lin28a* tg at 7 weeks of age

I next mapped the differentially expressed genes in 2 and 7 week old *Lin28a* mutant cTEC to Reactome pathways. 2 week old *Lin28a* tg cTEC^{lo} showed a significant increase in pathways dealing with the tricarboxylic acid cycle (TCA), respiratory electron transport chain and complex I biogenesis while cTEC^{hi} of 2 week old Lin28a^{TEC} displayed enhanced extracellular matrix organization, cell cycle and epithelial to mesenchymal transition (Figure 24A). In 7 week old Lin28a^{TEC} mice, I found that both cTEC^{lo} and cTEC^{hi} displayed an up-regulation in pathways related to extracellular matrix organization, kras signaling up and epithelial to mesenchymal transition (EMT) (Figure 24B). The latter pathway was previously described to contribute to thymic involution by reducing absolute TEC numbers, in line with our observations that adult Lin28a^{TEC} mice show reduced thymic size and absolute TEC numbers (Figure 12A, 12I) [129, 130, 131]. Hence, this result suggests that the up-regulation of EMT in cTEC by *Lin28a* tg contributes to the loss of TEC and subsequent thymic shrinkage in these mice.

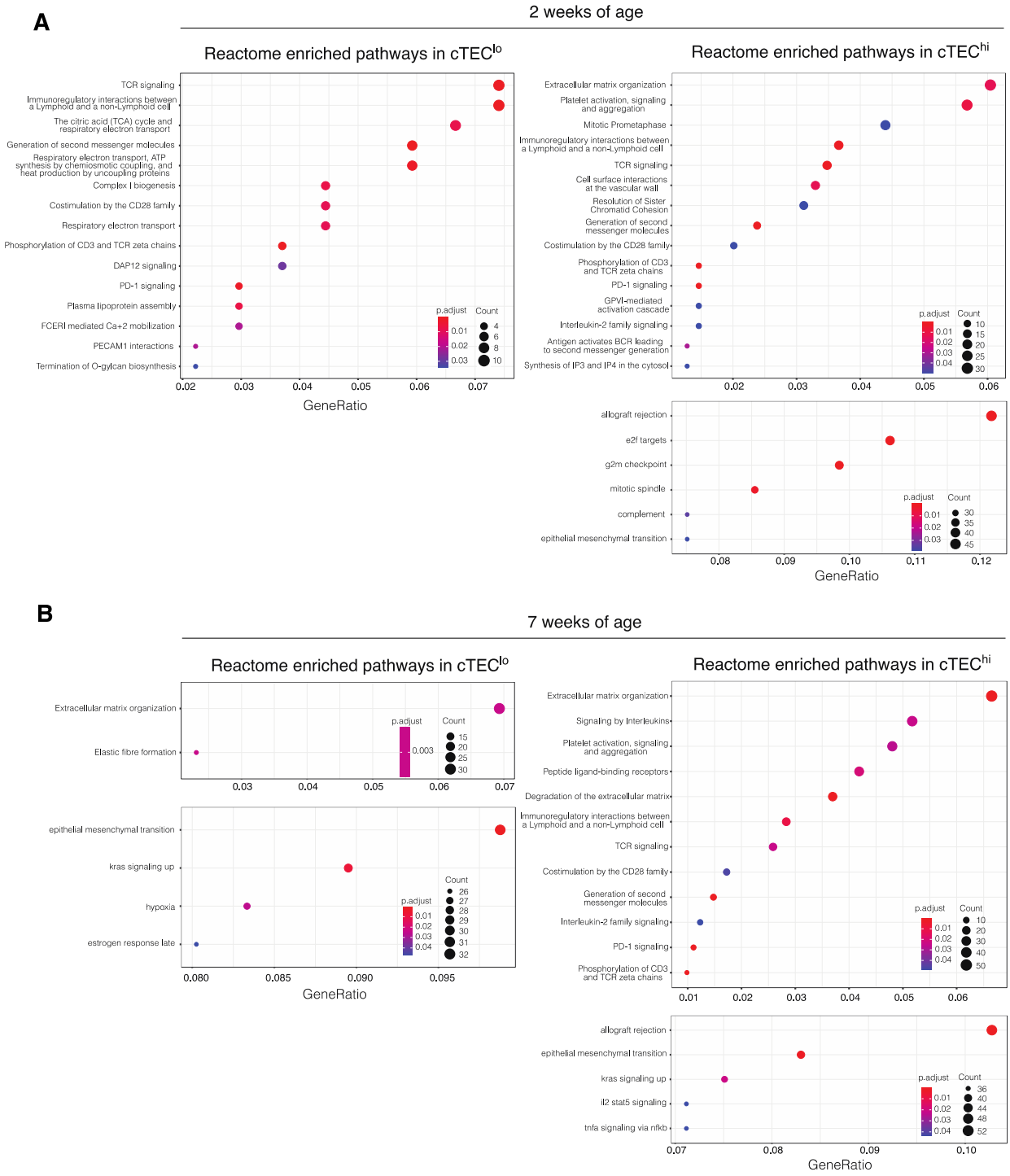

Figure 24: Epithelial to mesenchymal transition is increased in cTEC that express *Lin28a* tg at 7 weeks of age

(**A**) Dot plots displaying Molecular Signatures Database (Hallmark) enriched pathways in 2 week old *Lin28a* tg cTEC^{lo} and cTEC^{hi}. (**B**) Dot plots displaying Molecular Signatures Database (Hallmark) enriched pathways in 7 week old *Lin28a* tg cTEC^{lo} and cTEC^{hi}. The x-axis shows the gene ratio (differentially expressed genes in a certain pathway over total differentially expressed genes). The size of the dot corresponds to the number of differentially expressed genes in that pathway. The color of the dot is the adjusted p-value for that differentially expressed gene.

4.7.4 WNT signaling is down-regulated in *Lin28a* tg cTEC from 2 to 7 weeks of age

Considering that juvenile Lin28a^{TEC} mice showed normal cTEC subset composition while young adult *Lin28a* mutant mice displayed an increased cTEC^{hi}/cTEC^{lo} ratio, I next analyzed which transcriptomic changes occur in cTEC^{lo} and cTEC^{hi} from 2 weeks to 7 weeks of age. With age, control cTEC^{lo} increased genes related to extracellular matrix organization, metabolism of lipids and proteins, post-translational protein modification and WNT signaling. In contrast, *Lin28a* tg cTEC^{lo} increased the expression of transcripts associated with intracellular and G alpha signaling, immune system and hemostasis with age (Figure 25A). In control cTEC^{hi}, the expression of genes involved in GPCR ligand binding, ion channel transport and signaling by WNT were enhanced while transcripts related to RNA metabolism, cellular stress and antigen processing were increased in *Lin28a* tg cTEC^{hi} from 2 to 7 weeks of age (Figure 25B). As both cTEC subsets from control animals showed an increase in WNT signaling with age, this result suggests that this signaling pathway is important for the maintenance and maturation of cTEC. This hypothesis is also in line with earlier reports showing that inhibition of WNT signaling in post-natal mice leads to the loss of TEC progenitors and thymic atrophy [132]. Also, decreased WNT signaling in TEC has been described to drive EMT in these cells [133, 134]. Hence the reduced signaling by WNT in *Lin28a* tg cTEC correlated with the up-regulation of EMT associated genes in these cells. Together, this result implies that *Lin28a* tg reduces WNT signaling in TEC from juvenile to adult age which induces the up-regulation of EMT and subsequent depletion of TEC progenitors in the post-natal mouse and thymus hypoplasia.

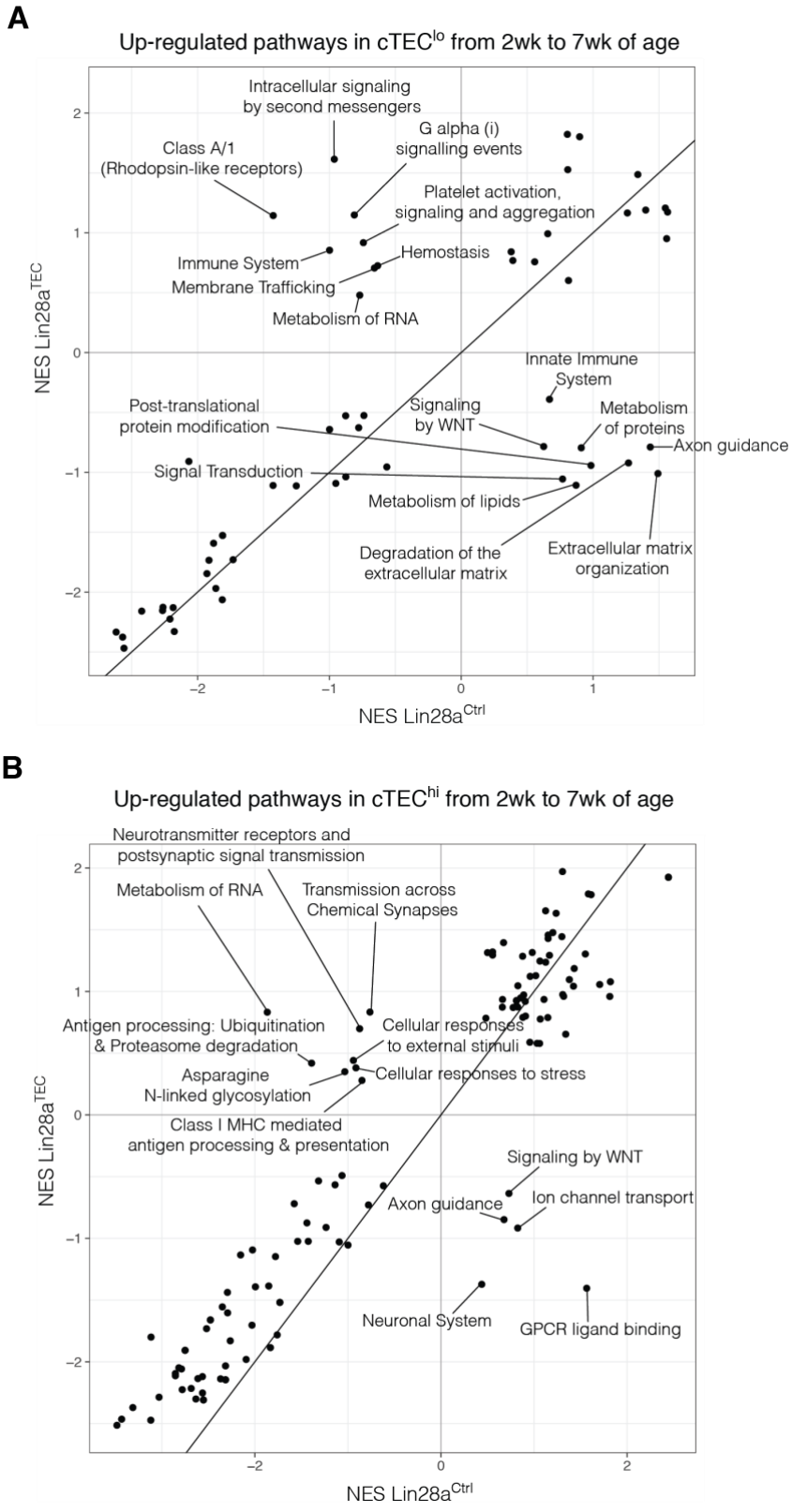

Figure 25: WNT signaling is down-regulated in *Lin28a* tg cTEC from 2 to 7 weeks of age

(**A**) Pathway enrichment comparison between Lin28a^{Ctrl} and Lin28a^{TEC} cTEC^{lo} from 2 to 7 week old mice. Pathways increased in control cTEC^{lo} are shown in the lower right box while pathways enriched in *Lin28a* tg cTEC^{lo} are displayed in the upper left box. (**B**) Pathway enrichment comparison between Lin28a^{Ctrl} and Lin28a^{TEC} cTEC^{hi} from 2 to 7 week old mice. Pathways increased in control cTEC^{hi} are

shown in the lower right box while pathways enriched in *Lin28a* tg cTEC^{hi} are displayed in the upper left box. NES = Normalized estimation score; a positive value visualizes that the DE genes are skewed towards up-regulation while a negative value indicates that the DE transcripts are skewed towards down-regulation.

4.8 Molecular consequences of *Lin28a* ectopic expression in TEC

4.8.1 *Lin28a* tg re-programs metabolism of cTEC^{hi} from oxidative phosphorylation to glycolysis

I next explored metabolic pathways allowing *Lin28a* tg cTEC^{hi} to maintain high proliferative rates [135, 136, 137, 138]. Cell division is an energetically challenging process that requires the synthesis of proteins, lipids and nucleic acids. Highly proliferating cells such as cancer, cells often reprogram their metabolism from oxidative phosphorylation (OxPhos) to increased glycolysis to produce metabolites for the synthesis of macromolecules in the pentose phosphate and L-serine biosynthesis pathway [137, 138]. In order to investigate whether *Lin28a* tg cTEC^{hi} also rewire their metabolism to support their high proliferative rates I employed the technique single-cell energetic metabolism by profiling translation inhibition (SCENITH), a method that is designed to reveal metabolic profiles of single cells by measuring protein translation rates using flow cytometry [139].

I quantified protein synthesis with puromycin which, as a mimic of tyrosyl-tRNA, is incorporated into the growing polypeptide chain and detected with a puromycin specific antibody [140]. To reveal the dependency on different metabolic pathways, the cells are treated with various metabolic inhibitors. The more a cell depends on a particular pathway, the more it will down-regulate its protein synthesis activity upon blockade of that metabolic pathway. Glycolysis is hereby inhibited using the non-metabolizable glucose analog 2-Deoxyglucose (2-DG). Oligomycin, a complex V inhibitor of the mitochondrial electron transport chain, is added to block ATP production via OxPhos and fatty acid and amino acid metabolism. To inhibit glycolysis, OxPhos as well as fatty acid and amino acid metabolism, 2-DG, oligomycin and Carbonyl cyanide-p-trifluoromethoxyphenylhydrazone (FCCP), an ionophore that disrupts the mitochondrial membrane potential, are used (Figure 26A).

In the absence of inhibitors, puromycin incorporation is similar between control and *Lin28a* tg cTEC^{hi}, suggesting a comparable metabolic activity of mutant and control cells in the steady-state case (Figure 26B). Blocking glycolysis by adding 2-DG enhanced protein translation cTEC^{hi} from control animals, hence implying increased energy metabolism. In contrast, cTEC^{hi} of *Lin28a* mutant mice significantly reduced their puromycin incorporation in response to 2-DG treatment, suggestive of reduced metabolism (Figure 26B). This result implies that cTEC^{hi} of control mice are able to rewire their metabolic prolife from glycolysis to OxPhos via fatty acid and/or amino acid metabolism upon 2-DG treatment while *Lin28a* tg cTEC^{hi} are unable to switch their metabolism and hence depend on glycolysis. Treating the cells with oligomycin and all inhibitors (2-DG, oligomycin and FCCP) had a similar effect in control and mutant cTEC^{hi}, suggesting a comparable OxPhos and fatty acid or amino acid activity (Figure 26B).

To understand why *Lin28a* tg cTEC^{hi} are unable to switch to OxPhos upon 2-DG treatment, I next analysed the number of mitochondria in these cells using MitoTracker dye, a probe that contains a reactive chloromethyl moiety which forms covalent bonds with thiol groups in the mitochondria and thus permanently labels mitochondria. I found that the number of mitochondria was significantly reduced upon *Lin28a* over-expression in cTEC^{hi} (Figure 26C). Hence, the reduced number of mitochondria in *Lin28a* tg cTEC^{hi} correlated with the inability of these cells to rewire from glucose metabolism to OxPhos.

To further dissect the molecular mechanisms of the observed changes in energy metabolism, I then performed proteomic analyses. Two of the key enzymes that are involved in fatty acid metabolism, namely Acyl-CoA dehydrogenase (Acadm) and 3-Ketoacyl CoA thiolase (Acaa2), were significantly reduced by *Lin28a* in cTEC (Figure 26D). In addition, Aldolase B (Aldob) and Aldolase C (Aldoc), enzymes that are involved in glucose metabolism, were increased in mutant cTEC when compared to control (Figure 26D). These changes in

protein expression of metabolic enzymes were not observed in *Lin28b* mutant cTEC, suggesting a Let-7 independent effect of *Lin28a* on energy metabolism of TEC.

As enhanced glucose dependency requires increased glucose uptake, I measured the expression of glucose transporter 4 (Glut4), a protein that is known to be positively regulated by *Lin28a* [98]. *Lin28a* was shown to enhance Glut4 translation in muscle cells via increasing the expression of genes in the Insulin-PI3K-mTOR pathway namely Insulin-like growth factor 1 (Igf1r), Insulin receptor (Insr) and Insulin receptor substrate 2 (Irs2). Indeed, protein expression of Glut4 was significantly higher in mutant cTEC^{hi} when compared to control (Figure 26E). I then tested the expression of *Igf1r*, *Insr* and *Irs2* via qPCR in *Lin28a* tg cTEC^{hi} and found that all three genes were significantly up-regulated in the mutant cells when compared to control (Figure 26F).

Together, our results suggest that *Lin28a* tg cTEC^{hi} depend more on glycolysis due to reduced fatty acid oxidation and decreased mitochondrial number and meet this dependency on glucose metabolism by increasing the expression of glycolytic enzymes and glucose transporters.

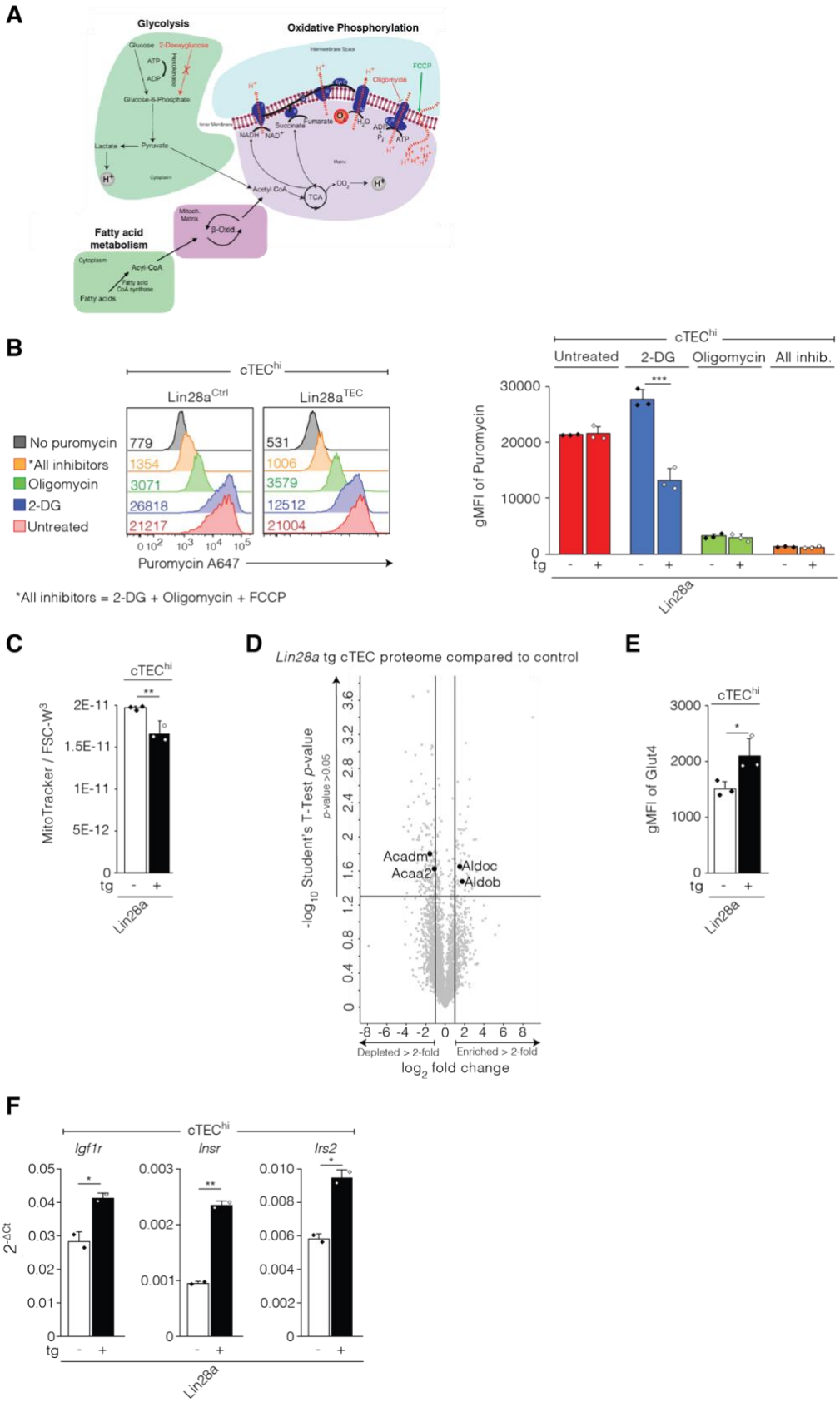

Figure 26: *Lin28a* tg re-programs metabolism of cTEC^{hi} from oxidative phosphorylation to glycolysis

(**A**) Overview of the different metabolic pathways that can be measured via SCENITH and their metabolic inhibition. (**B**) Representative histograms and metabolic profile of cTEC^{hi} after SCENITH

analysis. Data representative of one experiment analyzing new-born Lin28a^{TEC} and control mice. (**C**) Quantitative analysis of MitoTracker in cTEC^{hi} using median fluorescence intensity of Mitotracker divided by FSC-W^3. Data is representative of three independent experiments analyzing mutant and control female animals at 4-5 weeks of age. (**D**) Volcano plot displaying fold change and statistical significance of all detected proteins between control and mutant cTEC from 4-5 week old female mice. Enzymes of glycolysis and fatty acid metabolism that are significantly enriched or depleted by *Lin28a* tg are annotated. (**E**) Quantification of Glut4 expression in transgenic and control cTEC^{hi} using Glut4 geometric median fluorescence intensity (gMFI). Data representative of two independent experiment analyzing Lin28a^{TEC} and control female mice at 4-5 weeks of age. (**F**) Expression of *Igf1r*, *Insr* and *Irs2* in cTEC^{hi}. Data is representative of two independent experiments analyzing Lin28a^{TEC} and Lin28a^{Ctrl} female mice at 2 weeks of age. qPCR normalized to *Gapdh* expression. * $p < .05$, ** $p < .01$, *** $p < .005$ (paired student's *t*-test).

4.8.2 Ectopic *Lin28a* increases the activation of MAPK in cTEC^{lo} and mTEC

Lin28a over-expression increased TEC apoptosis, as indicated by increased cleaved Caspase-3 detection (see Figure 13D). To identify mechanisms and pathways that account for the observed change in TEC survival by *Lin28a* tg, I compared the gene expression profile of total cTEC from young adult mutant mice to cells from Lin28a^{Ctrl} animals. The reason for combining cTEC^{hi} and cTEC^{lo} for this study was that I aimed for a more in-depth analysis of the transcriptomic changes imposed by *Lin28a* tg.

This analysis revealed an up-regulation of transcripts involved in mitogen activated kinases (MAPK) signaling in *Lin28a* tg cTEC (Figure 27A). MAPK are Ser/Thr kinases that convert a variety of extracellular stimuli, such as radiation, cellular stress, growth factors, into a wide range of cellular responses [141]. In mammals, there are more than a dozen MAPK enzymes that coordinately regulate cell proliferation, differentiation, motility, and survival [142, 143, 144]. The best known are the conventional MAPK, which include the extracellular signal-regulated kinases 1 and 2 (ERK1/2), c-Jun amino-terminal kinases (JNK) 1 to 3, p38 (α, β, γ, and δ), and ERK5 families. A more refined analysis revealed that increased MAPK activity mapped to JNK signaling (Figure 27B). As JNK signaling is involved in apoptosis, its up-regulation in *Lin28a* tg TEC correlated with the observed increase of cell death (Figure 13D).

Hence, I probed the activation of MAPK signaling in TEC of Lin28a^{TEC} animals by measuring the phosphorylation state of TAK1 which is the central hub of the MAPK pathway [145].

The percentage of phosphor-TAK1 positive cTEC^{lo} and mTEC was increased in Lin28a^{TEC} mice while the frequency of activated TAK1 positive cTEC^{hi} was similar between mutant and control animals (Figure 27C, 27D). Furthermore, cTEC^{lo} and mTEC expressing *Lin28a* transgene showed increased phosphorylation of TAK1 when compared to control TEC (Figure 27E). In contrast, TAK1 phosphorylation was comparable between experimental and control mice when analysed for cTEC^{hi} (Figure 27D, 27E). Hence, this result shows that *Lin28a* tg increases the activation of MAPK in cTEC^{lo} and mTEC as measured by TAK1 activation. Furthermore, this data corroborates the increased apoptosis observed in these cells in Lin28a^{TEC} animals (see Figure 13D). Taken together, this data implies that *Lin28a* mediates activation of MAPK signaling and thus increased cell death in cTEC^{lo} and mTEC.

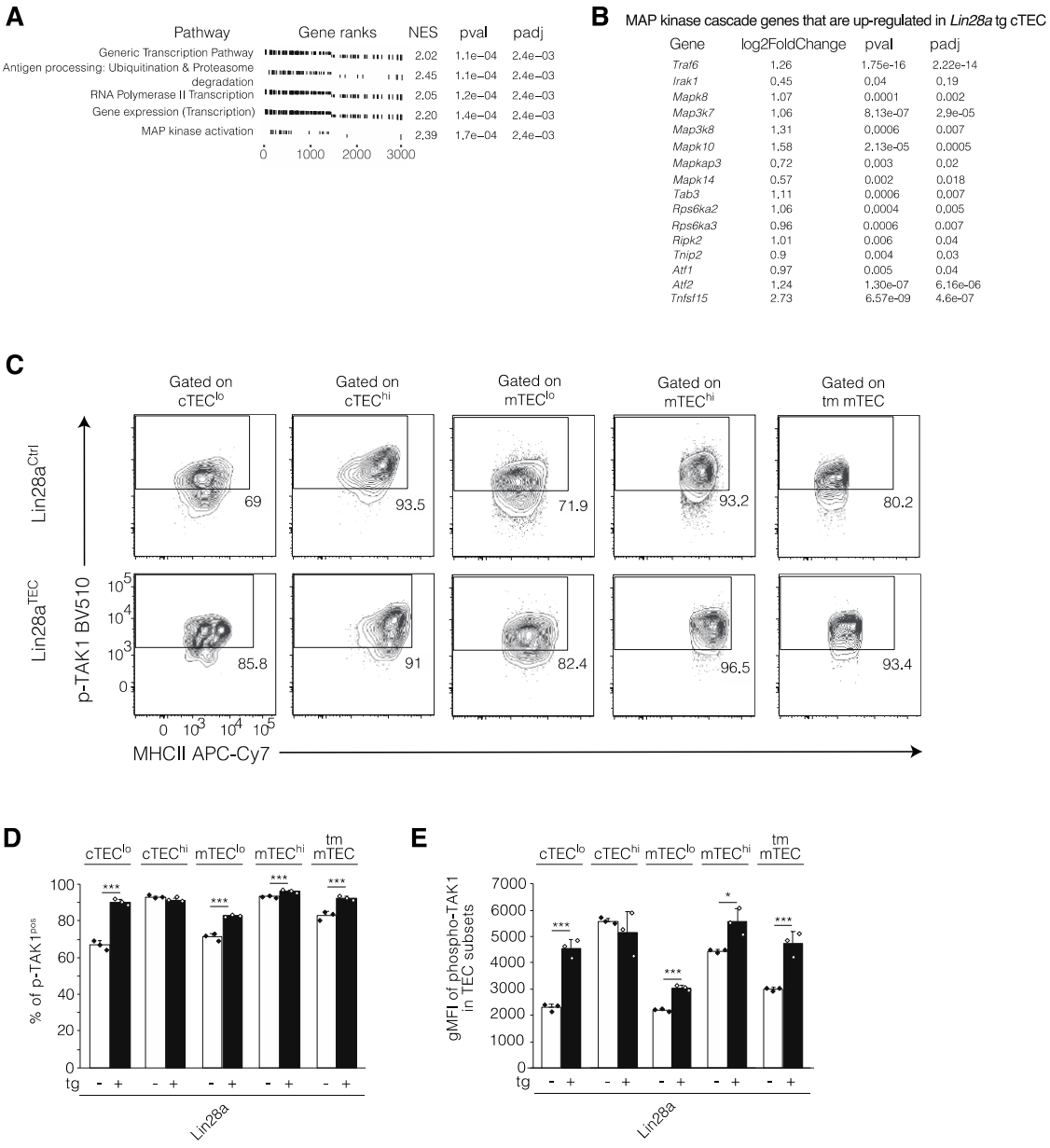

Figure 27: Ectopic *Lin28a* increases the activation of MAPK in cTEC^{lo} and mTEC

(**A**) Reactome pathways enriched in *Lin28a* tg cTEC. The differentially regulated genes in each pathway are represented by bars in rank order from 0 (most up-regulated) to 3000 (most down-regulated). The height of the bar signifies the amount of the gene that is up- or down-regulated. The normalized estimation score (NES) visualizes if there are more up- (i.e. positive NES value) or down-regulated (i.e. negative NES value) genes in the pathway. (**B**) List of the MAPK cascade genes that are up-regulated by *Lin28a* in cTEC and their respective log2fold change compared to control cTEC. (**C**) Representative plots of phosphorylated TAK1 (Thr184/187) (p-TAK1) positive cTEC^{lo}, cTEC^{hi} and mTEC^{lo}, mTEC^{hi}, tm mTEC. (**D**) Frequency of p-TAK1 positive TEC subset. (**E**) Quantification of TAK1 activation in p-TAK1^{pos} TEC subsets using p-TAK1 gMFI. Data representative of two independent experiment analyzing Lin28a^{TEC} and Lin28a^{Ctrl} female mice at 4 weeks of age. * $p < .05$, ** $p < .01$, *** $p < .005$ (paired student's *t*-test).

4.8.3 *Lin28a* tg TEC show higher *Foxo3a* expression and increased activation of JNK

Interleukin-1 receptor type 1 (IL-1R1), Toll-like receptor (TLR) 2 and 4 as well as tumor necrosis factor-receptor 1 (TNF-R1) are placed upstream of TAK1 and hence might induce the signaling cascade [146]. I analyzed the expression levels of these receptors in *Lin28a* mutant cTEC using our bulk transcriptomic data. While *Tlr2, Tlr4* and *Il-1r1* were expressed at very low copy numbers, *Tnfrsf1a*, the gene encoding TNF-R1, was highly expressed in cTEC of Lin28a^{TEC} mice (Figure 28A). Moreover, TNF-α is known to induce apoptosis through TNF-R1, suggesting that *Lin28a* tg TEC are experiencing TNF-R1 signaling and subsequent MAPK activation, leading to increased cell death [147]. Supporting this assumption, I found a strong increase of a TNF-α inducible gene, namely *Tnfsf15* (encoding vascular endothelial growth inhibitor; VEGI) in *Lin28a* tg cTEC (Figure 28B) [148].

TNF-R1 induces cell death via its cytoplasmic death domain in a variety of cells [149]. Although it was demonstrated that the death-inducing capability of TNF is masked by concomitant activation of NF-kB and its pro-survival effect, our data implies that in *Lin28a* tg TEC the pro-apoptotic effect of TNF-alpha dominates over NF-kB activation. Significant up-regulation of *Foxo3a* transcription, a molecule that is known to direct TNF-receptor signaling towards apoptosis through suppressing NF-kB activity, supports this assumption (Figure 28C) [150, 151]. As it was shown that FOXO3A promotes apoptosis through activation of JNK and suppression of NF-kB, I next tested whether JNK is activated in *Lin28a* mutant TEC. The percentage of phosphor-c-Jun positive TEC was increased in TEC of Lin28a^{TEC} mice (Figure 28D, 28E). Furthermore, TEC expressing *Lin28a* tg showed increased phosphorylation of c-

Jun when compared to control TEC (Figure 28F). Hence, our results imply that *Lin28a* tg mediates higher activation of MAPK and c-Jun signaling and thus increased cell death in TEC.

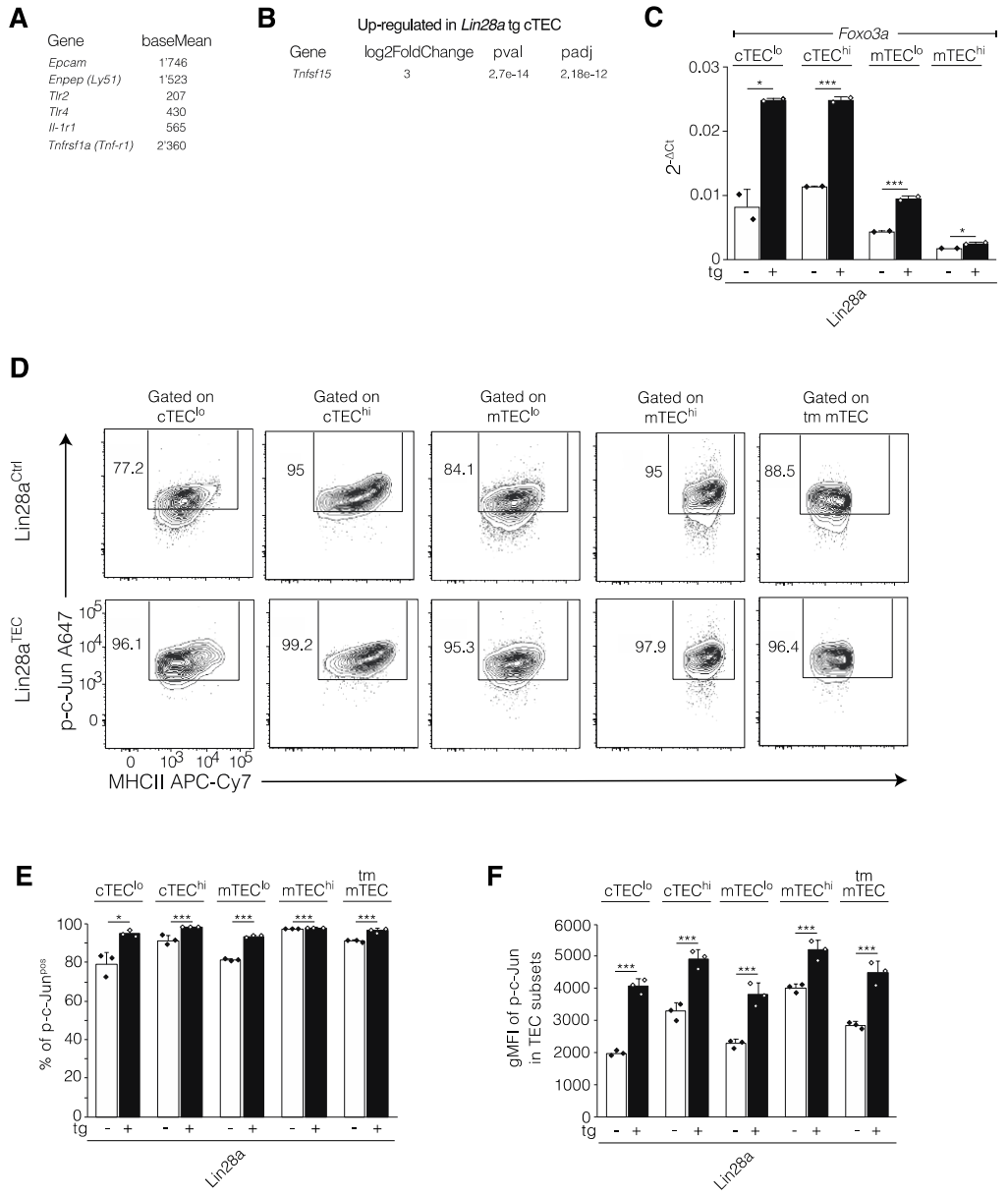

Figure 28: *Lin28a* tg TEC show higher *Foxo3a* expression and increased activation of JNK
(**A**) Expression levels of *Epcam*, *Enpep* (gene encoding Ly51), *Tlr2*, *Tlr4*, *Il-1r1* and *Tnfrsf1a* (encoding TNF-R1) in *Lin28a* tg cTEC using baseMean. The baseMean is the average of the normalized counts taken over all samples. (**B**) Log2FoldChange of *Tnfsf15* in *Lin28a* tg cTEC compared to control. (**C**) Expression of *Foxo3a* in cTEC^{lo}, cTEC^{hi}, mTEC^{lo} and mTEC^{hi}. Data is representative of two independent experiments analyzing Lin28a^{TEC} and Lin28a^{Ctrl} female mice at 4-7 weeks of age. qPCR normalized to *bACT* expression. (**D**) Representative plots of phosphorylated c-Jun (Ser63) (p-c-Jun) positive cTEC^{lo}, cTEC^{hi} and mTEC^{lo}, mTEC^{hi}, tm mTEC. (**E**) Frequency of p-c-Jun positive TEC subset. (**F**) Quantification of c-Jun activation in TEC subsets using p-c-Jun gMFI. Data representative of two independent experiment analyzing Lin28a^{TEC} and Lin28a^{Ctrl} female mice at 4-5 weeks of age. * $p < .05$, ** $p < .01$, *** $p < .005$ (paired student's *t*-test).

4.8.4 TNF-R1 expression is higher in *Lin28a* tg TEC and TNF-α increases TEC apoptosis upon NF-kB inhibition

To find out whether the heightened susceptibility of *Lin28a* tg TEC to cell death is driven by higher TNF-R1 expression, I next tested its surface expression in *Lin28a* mutant and control TEC. Indeed, TNF-R1 surface expression was significantly higher in *Lin28a* tg cTEC^{lo} and mTEC when compared to control cells of the same phenotype (Figure 29A). This data correlates with the increased apoptosis rates of these cells in Lin28a^{TEC} animals and indicates that cTEC^{lo} and mTEC expressing *Lin28a* tg experience higher TNF-alpha stimulation through increased TNF-R1 expression and that FOXO3A directs this signal in these cells towards apoptosis by inhibiting NF-kB activation.

To mechanistically prove this hypothesis, I incubated thymic lobes of new-born animals, in medium only, in the presence of TNF-α only or TNF-α and the NF-kB inhibitor, Ammonium pyrrolidineedithiocarbamate (APDC) and analyzed the percentage of activated Caspase-3 positive TEC. Indeed, the frequency of apoptotic TEC was significantly higher in the lobes treated with TNF-α plus APDC compared to non-treated or TNF-α only treated lobes (Figure 29B, 29C). This result supports our hypothesis and indicates that the enhanced susceptibility of *Lin28a* tg cTEC^{lo} and mTEC to apoptosis is driven by increased TNF-R1 signaling and that FOXO3A drives this signal towards apoptosis by inhibiting the activation of NF-kB in these cells.

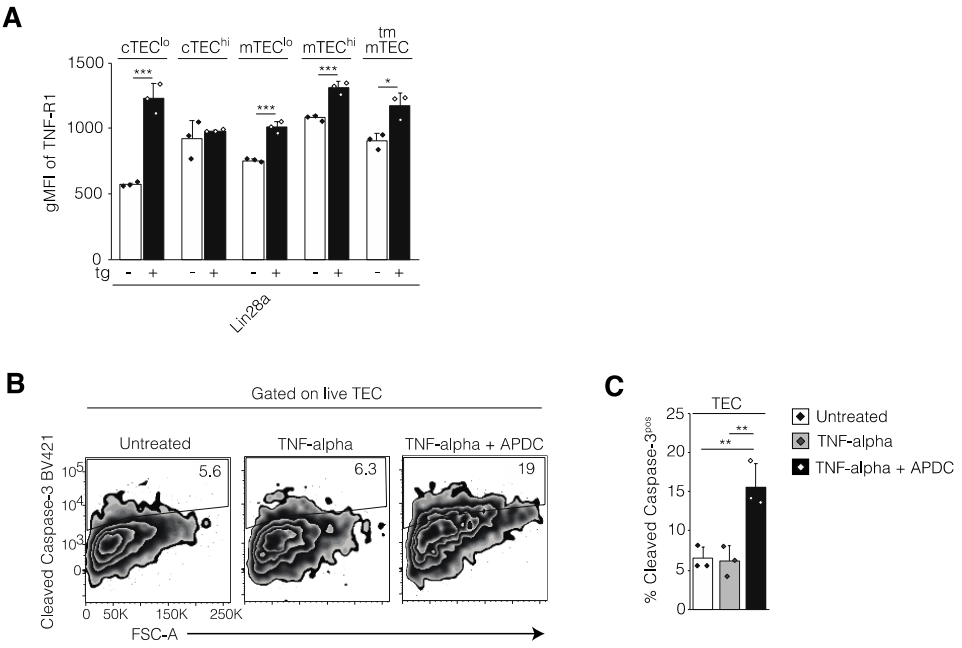

Figure 29: TNF-R1 expression is higher in *Lin28a* tg TEC and TNF-α increases TEC apoptosis upon NF-kB inhibition

(**A**) Quantification of TNF-R1 surface expression in TEC subsets using TNF-R1 gMFI. Data is representative of two independent experiment analyzing Lin28a^{TEC} and Lin28a^{Ctrl} female mice at 5 weeks of age. (**B**) Representative gating strategy and (**C**) quantitative analysis of cleaved Caspase-3 positive TEC in new-born thymic organ cultures (NTOC). Thymic lobes for NTOC were isolated from wild-type animals at 1 day of age, cut into half and cultured in medium only, in the presence of TNF-α or TNF-α plus Ammonium pyrrolidinedithiocarbamate (APDC) at 37° overnight. Data is representative of two independent experiments. * $p < .05$, ** $p < .01$, *** $p < .005$ (paired student's *t*-test).

5. Summary of findings

Whereas Lin28a^{TEC} mice display an hypocellular thymus, *Lin28b* transgenic expression causes hyperplasia of the thymus. In both mutant mouse models, the absolute number of ETP correlates with thymocyte numbers and thymic size. Size and composition of the TEC compartment is differentially affected as well, *Lin28a* tg mice displaying normal cTEC cellularity but 3-4 fold reduced mTEC numbers whereas *Lin28b* transgenesis causes a prominent increase in cTEC and a slight rise in mTEC cellularity. The transgenic expression of *Lin28* also impairs cTEC and mTEC subset compositions. The frequency and number of cTEC^{lo} is reduced by 4-5 fold in Lin28a^{TEC} mice while the cTEC^{hi}:cTEC^{lo} ratio is unchanged in Lin28b^{TEC} mice. The relative numbers of mTEC^{lo} and tm mTEC is reduced in both *Lin28a* and *Lin28b* mutant mice while the frequency of mTEC^{hi} is only increased in Lin28a^{TEC} animals. The underlying mechanisms that lead to these changes following a TEC-targeted transgenic expression of *Lin28a* are epistatic, as the phenotype of animals expressing concurrently *Lin28a* and *Lin28b* is comparable to that of Lin28a^{TEC} mice.

The reduced cellularity of cTEC^{lo} and mTEC in Lin28a^{TEC} mice correlates with an increased signal of activated Caspase-3, indicating decreased cell survival. The heightened susceptibility of cTEC^{lo} and mTEC to cell death is explained by increased MAPK signaling in these cells which is driven by TNF-R1 mediated signals. Under wild-type conditions, TNF-R1 activation leads to cell survival through suppression of JNK and caspase-3 activation by NF-κB. cTEC^{lo} and mTEC expressing *Lin28a* transgenically, however, demonstrate higher TNF-α stimulation secondary to increased TNF-R1 expression and *Foxo3a*, a transcription factor known to direct TNF-R1 signaling towards apoptosis via inhibiting NF-κB activation (Figure 30).

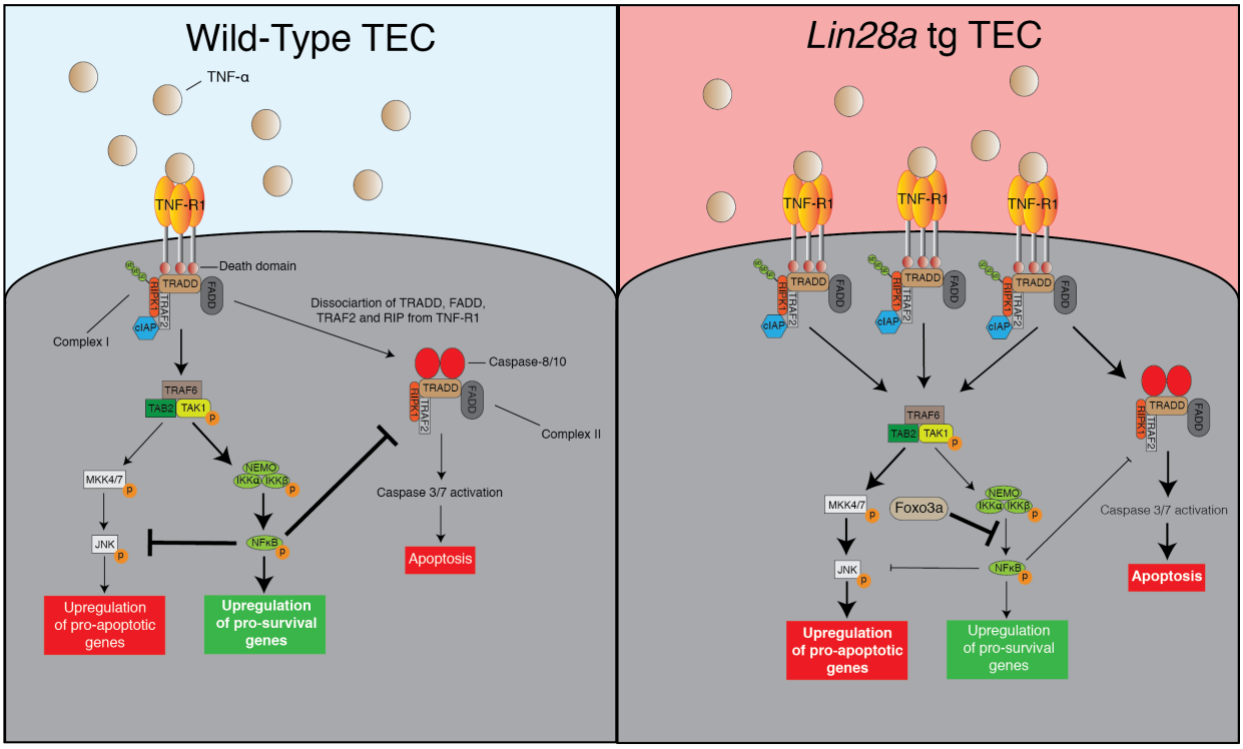

Figure 30: *Lin28a* tg TEC undergo TNF-R1 induced cell death

Upon TNF-α stimulation, TNF-R1 forms complex I, in which RIPK1 acquires a polyubiquitin chain. The formation of the TNF-R1 complex I leads to the phosphorylation of TAK1 which in turn activates JNK as well as NF-κB. In addition, complex I can also dissociate from TNF-R1, leading to the formation of complex II, which is composed of Caspase-8/10, TRADD, FADD, TRAF2 and RIPK1. The formation of complex II initiates the caspase cascade, which leads to apoptosis. In wild-type TEC, NF-κB signaling through TNF-R1 activation leads to cell survival through suppression of JNK and caspase activation by NF-κB. *Lin28a* tg TEC, however, experience higher TNF-α stimulation by increased TNF-R1 expression and Foxo3a, which directs this signal in these cells towards apoptosis by inhibiting NF-κB activation. Abbreviations: TNF: Tumor necrosis factor; TNF-R1: TNF-receptor type 1; TRADD: TNF-R1-associated death domain protein; FADD: Fas-associated protein with death domain; TRAF2: TNF-R-associated factor 2; RIPK1: Receptor-interacting serine/threonine-protein kinase 1; cIAP: Cellular inhibitor of apoptosis; TRAF6: TNF-R-associated factor 6; TAK1: Transforming growth factor-β-activated kinase 1; TAB2: TAK1-binding protein 2; MKK: Mitogen-activated protein kinase; NF-κB: Nuclear Factor-κB; JNK: c-Jun N-terminal kinases; NEMO: Nuclear factor-κB essential modulator; IKK: IκB kinase; Foxo3a: Forkhead-Box-Protein O3a.

The increased number of cTEC^{hi} in Lin28a^{TEC} mice is likely explained by the cells' higher proliferation. The ability of *Lin28a* tg cTEC^{hi} to proliferate more than control cells is metabolically supported by their higher glucose usage. Enhanced glycolysis in *Lin28a* tg cTEC^{hi} is hereby mediated through higher expression of glycolysis enzymes, namely Aldolase B and Aldolase C as well as increased insulin signaling, leading to more Glut4 surface

expression. However, the increased glucose usage of *Lin28a* tg cTEC^{hi} is most likely also a result of reduced mitochondrial numbers and decreased fatty acid oxidation in these cells (Figure 31).

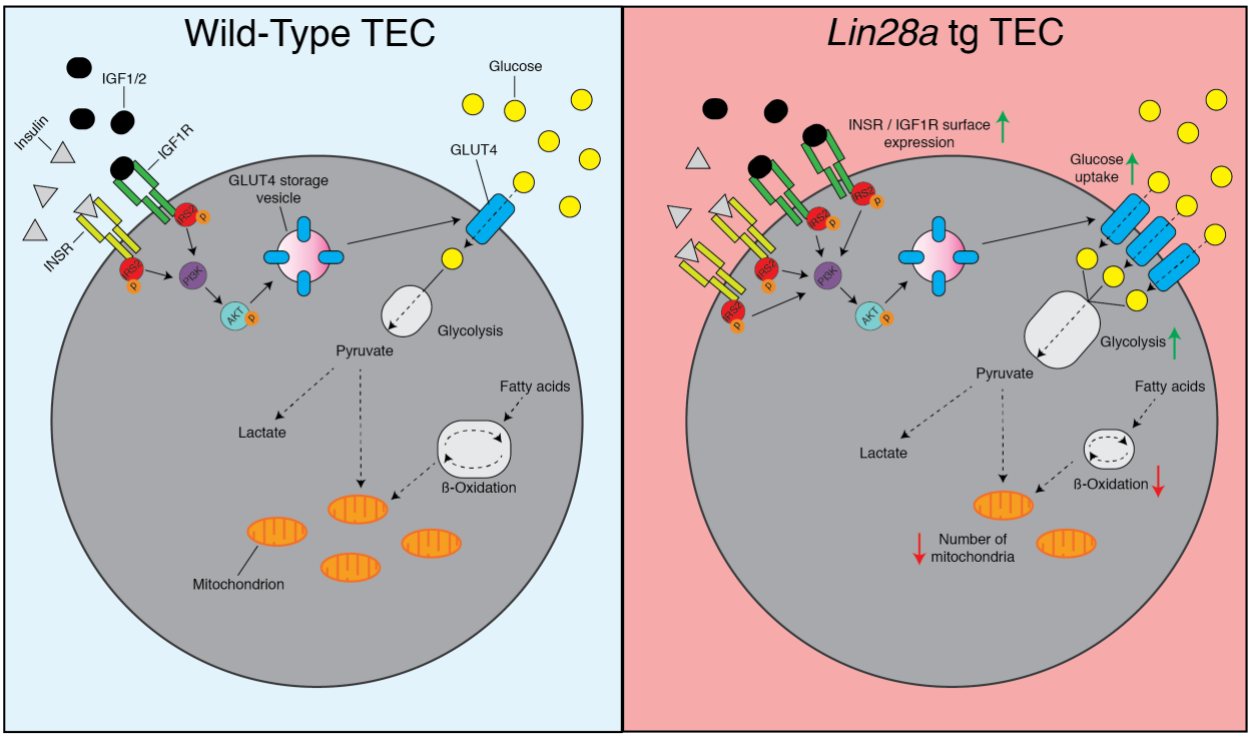

Figure 31: *Lin28a* over-expression in TEC leads to higher glucose usage through positive regulation of the Insulin-PI3K-mTOR pathway

Cells can generate adenosine triphosphate (ATP) through different metabolic pathways. One of the major energy metabolism pathways is glycolysis, which starts with the uptake of glucose through glucose transporters. Glucose uptake can be stimulated by insulin and IGF1/2 which activate the INSR and IGF1R, respectively. This then leads to the phosphorylation IRS2 which activates AKT through PI3K. Activated AKT induces the translocation of GLUT4 from vesicular compartments onto the plasma membrane of the cell, leading to increased glucose uptake. Once glucose is taken up, it is processed to pyruvate through a number of enzymes. In the presence of oxygen, pyruvate is being converted into Acetyl-coenzyme A (Acetyl-CoA) that enters the tricarboxylic acid (TCA) cycle and provides reducing intermediates NADH and FADH2 for the electron transport chain in the mitochondria. However, fatty acid ß-oxidation also generates Acetyl-CoA which fuels the TCA cycle and produces intermediates for the mitochondrial electron transport chain. Glucose usage is higher in TEC that express *Lin28a* tg due to their enhanced expression of glycolytic enzymes as well as increased GLUT4 surface density which is mediated by INSR/IGF1R signaling. Moreover, *Lin28a* tg TEC have decreased expression of enzymes involved in fatty acid ß-oxidation and reduced number of active mitochondria. Abbreviations: IGF: Insulin-like growth factor; IGF1R: Insulin-like growth factor 1 receptor; INSR: Insulin receptor; IRS2: Insulin receptor substrate 2; PI3K: Phosphoinositide 3-kinase; GLUT4: Glucose transporter 4.

The TEC subset changes identified in *Lin28a* tg animals correlate with alterations in thymocyte maturation, as these mice display reduced numbers of (i) positively selected thymocytes, (ii) negatively selected wave 1 cells, (ii) Foxp3 positive regulatory thymocytes and (iv) cytokine licensed CD69^{neg}, CD24^{lo} mature SP cells. Further detailed analyses provided convincing molecular mechanisms that account for these findings, for example the decrease in positive selection paralleled an increased frequency of PD-L1^{pos} cTEC^{hi}. This subpopulation of TEC is less effective in thymocyte positive selection due to their high PD-L1 cell surface expression and is found at a higher abundance in Lin28a^{TEC} animals (Figure 32).

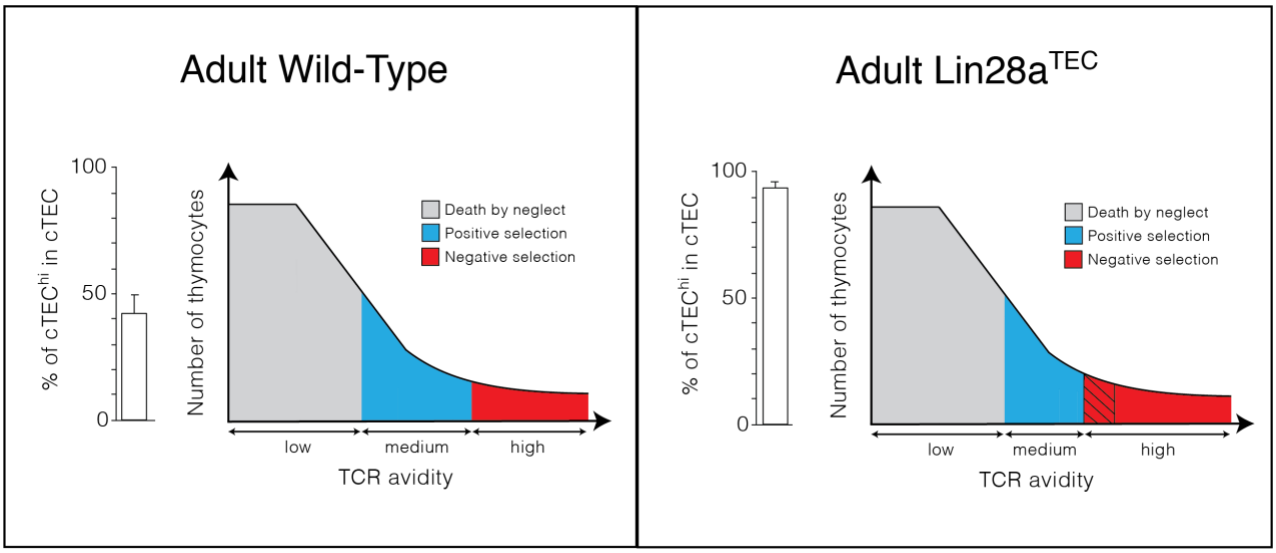

Figure 32: Adult Lin28a^{TEC} mice have increased frequency of cTEC^{hi} which are less effective in thymocyte positive selection

Thymocytes are tested for their TCR avidity to self-peptide/MHC-complexes expressed on cTEC. Most thymocytes die by neglect as they do not recognize self-peptide/MHC-complexes. Cells that have a TCR with medium avidity are positively selected and continue their development while thymocytes with high binding strengths are negatively selected and removed from the repertoire. In adult Lin28a^{TEC} mice, however, the existing cTEC are mainly of the cTEC^{hi} phenotype, i.e. cells that highly express MHCII on their surface. It is therefore probable that cTEC^{hi}, which have large amounts of the ligand for TCR plus PD-L1, set a signal threshold window where thymocytes with high TCR avidities are more efficiently removed (displayed as hatched pattern).

6. Discussion

Short, non-coding RNAs belonging to the miRNA family regulate organ development and function by targeting multiple components of regulatory networks controlling self-renewal and lineage determination [152]. The general importance of miRNAs for the maintenance of a regular composition and function of the thymic microenvironment has been unequivocally demonstrated using experimental conditions that ablated their Dicer-dependent progeny in TECs [83]. Furthermore, a number of individual miRNA, namely miR-181a, miR-449a and miR-155 have been shown to play an essential role in TEC biology [84, 85, 86]. Although these studies provided evidence for the importance of miRNAs for the development and function of thymic epithelia, the precise role of the majority of the up to 2000 individual mouse miRNAs in TEC biology remains largely unknown.

The dependence of TEC differentiation and function on the miRNA family Let-7 and on the epigenetic regulation by the RNA binding proteins Lin28A and Lin28B has been investigated in the presented experimental work. In general, overlapping biological effects have been attributed to *Lin28a* and *Lin28b* with both controlling the switch between pluripotency and cell differentiation. *Lin28a* over-expression leads to increased total body and organ sizes maintaining normal proportions [153]. Hence, the biological activity of sustained suppression of *Lin28a* controlled mRNA correlates with increased proliferation and consequently cell numbers [153]. When studying thymic organ size in the *Lin28* mutant mice, a hypocellular thymus is observed in *Lin28a* transgenic animals whereas *Lin28b* over-expression causes thymic hyperplasia. The thymic epithelial compartment is therefore to our knowledge the first example where *Lin28a* and *Lin28b* exert distinct roles in regulating organ size. Moreover, the underlying mechanisms that lead to these effects by *Lin28a* transgenesis are epistatic, as the phenotypes of Lin28axb^{TEC} animals is comparable to that of Lin28a^{TEC}

animals. Thus, our study reveals a previously unrecognized epistatic relationship between these RBPs in controlling thymus organ size. In addition, the different expression levels of *Lin28a* tg and *Lin28b* tg in TEC may also have an influence on thymic size regulation.

Studying the TEC compartment in *Lin28* mutant young adult mice, a decrease in overall TEC cellularity is observed in Lin28a^{TEC} animals while Lin28b^{TEC} mice show a significant increase in total TEC numbers, correlating with the changes in absolute thymus cellularity found in these mice and highlighting further the opposing effects of both RBPs. cTEC^{lo} and mTEC of Lin28a^{TEC} mice are more prone to apoptosis and have unchanged proliferative capacity, correlating with their reduced absolute numbers. This suggests that extensive TEC apoptosis in Lin28a^{TEC} mice contributes to the reduction in absolute TEC numbers in these mice. In addition to cell death, the decrease in overall TEC cellularity in *Lin28a* mutant mice could also be due to: (i) reduced numbers of TEC progenitors or (ii) increased EMT process. The first possibility is supported by our data showing that *Lin28a* tg expression reduces WNT signaling in TEC, a pathway shown to be involved in the maintenance of CK5^{+}CK8^{+} TEC progenitors in the post-natal mouse [132]. Others have reported that the WNT signaling pathway directly induces *Lin28a* up-regulation and subsequent Let-7 down-regulation [154]. Therefore, it is possible that there is a WNT/Lin28A negative feedback loop in which ectopic Lin28A inhibits WNT activity. Furthermore, decreased WNT signaling in TEC has been described to foster EMT, resulting in a reduction of total TEC numbers [133, 134]. Our data shows that *Lin28a* expression in cTEC correlates increased expression of genes related to EMT. The observed reduction of TEC cellularity consequent to targeted *Lin28a* expression may therefore be explained by increased EMT.

Over-expression of *Lin28b*, however, has no significant effect on TEC proliferation. This suggests that the increased number of TECs in Lin28b^{TEC} animals might be due to metabolic fitness achieved by enhanced mitochondrial function and glucose usage. In addition, increased TEC cellularity by *Lin28b* tg may also be mediated by a prolonged lifespan, a possibility that is in line with a recent finding showing that *Lin28b* promotes colon cancer development by increasing the expression of the pro-survival protein B-cell lymphoma 2 (BCL-2) and improving its protein stability [155].

As the TEC subset composition of Lin28b^{TEC} mice displays only minor differences compared to that of wild-type mice, I conclude that *Lin28b* tg has rather an effect on TEC metabolism and survival which contributes to the enlargement of the thymus and focused on the biological changes mediated by *Lin28a* tg.

Young adult *Lin28a* mutant mice display a regular segregation of the thymus into individual cortical and medullary compartments, parallel to a relative increased number of cTEC. The frequency of apoptotic TECs in Lin28a^{TEC} is increased among mTEC, indicating that the displayed change in the ratio of cortical to medullary TEC in favor of the cTEC is a combination of higher proliferation (cTEC) and cell death (mTEC). There are, however, also other possible explanations for this finding. cTEC and mTEC derive from a common bipotent progenitor present at high frequency in the embryonic and neonatal thymus [36, 37, 38]. The immediate progeny of these cells first attain a cTEC-like phenotype and subsequently diverge to the mTEC lineage [40, 41]. My results are therefore also comparable with a model where *Lin28a* over-expression mediates a maturational block of precursors adapting on a mTEC lineage tale, thus contributing to an overall decrease of mTECs. This explanation is also in line with the reduced signal of intertypical TEC in 7 week old *Lin28a* tg cTEC^{hi}, which are the predominant cTEC subset in these mice. Intertypical TEC are understood to be progenitor cells

abundant in the post-natal mouse, which derive from a $\beta5t^+$ precursor cell and that are able to differentiate into mTEC [47]. Further detailed investigations will, however, be necessary to phenotypic characterize intertypical TEC in order to quantify their numbers in Lin28a^{TEC} animals.

Young adult Lin28a^{TEC} animals show an increase in the frequency of cTEC^{hi}. According to transcriptomic analyses and in vivo transplantation assays cTEC^{lo} can differentiate into cTEC^{hi} in post-natal tissues [49, 127]. However, cTEC^{hi} are the first cTEC subset that arises during fetal development, while cTEC^{lo} only emerge one week after birth and steadily increase as the animal ages, suggesting that cTEC^{lo} differentiate from cTEC^{hi} in juvenile mice. Hence, the phenotypic transition between cTEC^{hi} and cTEC^{lo} is an age-dependent process. My results, however, imply that ectopic *Lin28a* expression locks cTEC in a cTEC^{hi} stage and blocks their transition into a cTEC^{lo} phenotype. This hypothesis is in line with our results from juvenile mice showing that the cTEC^{hi}:cTEC^{lo} ratio is unchanged in *Lin28a* mutant mice at this age. As it currently debated whether cTEC^{lo} also arise independently of cTEC^{hi} from a separate progenitor that is only present in the post-natal animal, it could also be that *Lin28a* tg (i) reduces the pool of these post-natal cTEC progenitors and/or (ii) impairs the maturation of cTEC^{lo} from post-natal progenitor cells. Future work will need to identify the exact progenitor:progeny relationships between the different TEC subsets during pre-natal and post-natal life. Moreover, *Lin28a* tg cTEC fail to up-regulate WNT signaling at 7 weeks of age, implying that this pathway, besides being involved in the maintenance of post-natal TEC progenitors, is also important for further cTEC differentiation. This is not surprising, as signaling through WNT was shown to promote cell differentiation in various tissues [160, 161, 162, 163]. In addition, WNT signaling needs to be precisely regulated to control normal TEC maturation [121, 132, 160]. While *Lin28a* tg cTEC^{hi} show no change in apoptosis *Lin28a*

tg cTEC^{lo} have increased cell death rates, suggesting that the increased rate of apoptosis in cTEC^{lo} might also be responsible for the reduction in the population size of cTEC^{lo}.

Within the mTEC compartment of young adult *Lin28a* mutant mice the frequency of mTEC^{lo} is reduced while that of terminally mature mTEC and mTEC^{hi} increased, implying that *Lin28a* tg also regulates mTEC maturation, specifically at the transition of mTEC^{hi} to terminally mature mTEC. *Foxo3a*, a molecule which is known to block signaling trough the NF-kB pathway is over-expressed in mTEC of Lin28a^{TEC} animals [150, 151]. As signaling via NF-kB regulates the maturation of mTEC this implies that the alterations in the mTEC subset composition of Lin28a^{TEC} animals may be caused by increased *Foxo3a* expression [162, 163]. Because NF-kB signaling also controls the size of the mTEC compartment [162, 163], this data implies that increased *Foxo3a* expression could also be responsible for the reduction in absolute mTEC numbers in *Lin28a* tg animals.

The main thymus size determining factor is the absolute number of DP thymocytes that derive from ETP. Hence, the attraction and/or survival of ETP play a crucial role in regulating thymic size. Whereas thymus cellularity is clearly distinct in Lin28a^{TEC} and Lin28b^{TEC} mice, the expression of chemokines important for ETP homing is similarly affected by both transgenes, implying Let-7 dependent mechanisms regulating chemokine expression. Hence, this data implies that the differences in thymic organ size are mainly driven by changes in the absolute number of TEC in Lin28a^{TEC} and Lin28b^{TEC} mice. Reduced thymic cellularity in *Lin28a* tg mice can be explained by a decrease in TEC numbers that express reduced amounts of the ETP attractant *Ccl21* and *Ccl19*. *Lin28b* tg animals show an increase in ETP and thymic cellularity despite *Ccl21* reduction in mTEC. My studies revealed that in *Lin28b* tg TEC the expression of ETP attractant *Cxcl12* is on a comparable level to that of control littermates and that of *Ccl25* increased. Hence, increased numbers of TEC producing normal amounts of

Cxcl12 and increased quantities of *Ccl25* might compensate the reduced *Cccl21* and *Ccl19* expression in TEC. These combined effects could lead to increased numbers of ETP correlating to the enlargement of the thymic organ in *Lin28b* tg mice. In addition, the contribution of other chemokines that are differentially regulated by *Lin28a* and *Lin28b* tg cannot be ruled out.

Transgenic expression of *Lin28a* compromises thymocyte positive selection as the frequency of CD4 and CD8SP thymocytes is reduced. The ability of the cTEC compartment to negatively select self-reactive thymocytes is also reduced by *Lin28a*. The defects in thymocyte positive selection correlate with an increased frequency of PD-L1 positive cTEC in young adult Lin28a^{TEC} animals. PD-L1:PD-1 interaction had already been shown to negatively affect positive selection of CD4 SP thymocytes via inhibition of extracellular signal regulated kinase (ERK) activation and blocking BCL-2 up-regulation, two downstream events of TCR signaling that are crucial to thymocyte positive selection [128]. Indeed, blocking PD-L1 in wild-type FTOC increases the generation of CD4 SP thymocytes, as described [128], CD8 lineage selection is however not affected using this experimental approach.

PD-L1 is mainly expressed in cTEC^{hi}. Although it was shown that Let-7a and -7c directly bind to *Pd-l1* mRNA and reduce its expression, I do not observe any change in the amounts of PD-L1 protein in Lin28a^{TEC} mice when compared to control [112]. However, the low amounts of mature Let-7a and -7c in control TEC might not be sufficient to reduce PD-L1 expression in TEC.

cTEC provide signals for early thymocyte development and restrict TCR specificities to self-MHC recognition. However, there have been so far no studies that investigated the function of different cTEC subsets which develop during thymus ontogeny. My studies have provided experimental evidence that cTEC^{hi} are more stringent in positive selection of

thymocytes when compared to cTEC^{lo}. Hence, the higher frequency of PD-L1^{hi} cTEC^{hi} in Lin28a^{TEC} mice explains, at least in part, the reduced capacity to positively select thymocytes. As positive selection is based on TCR avidity for self-MHC it is probable that cTEC^{hi}, which have large amounts of MHCII and PD-L1 on their surface, set a signal threshold window where thymocytes with higher TCR avidities are removed. As cTEC^{hi} are the predominant cTEC subset in juvenile animals, this implies that, early in life, thymic output contains fewer potentially auto-reactive T cell clones, a hypothesis that is also supported by Sharpe et al [128]. If not properly deleted, these cells have a competitive advantage against T cells with lower TCR avidity undergoing homeostatic expansion early in life [163] and lead to dysregulated immune responses such as autoimmunity and wasting disease [164]. Hence, my studies in a transgenic system provide novel insights into thymocyte maturation in wild-type animals.

Lin28a tg cTEC^{hi} increase their glucose metabolism and this dependence is met by higher surface expression of the insulin sensitive Glut4, corroborating that insulin is involved in regulating glucose uptake in TEC [165]. In addition, TEC that express *Lin28a* tg show increased expression of *Insr*, *Igf1r* and *Irs2* which are involved in the Insulin-PI3K-mTOR pathway and that are mechanistically linked to higher Glut4 expression [98, 166]. Hence, these studies provide novel insights into TEC energy metabolism on a single cell level.

The increased usage of glucose in *Lin28a* over-expressing muscle cells was described by Zhu et al. [98] as being driven through Let-7-mediated repression of several components of the Insulin-PI3K-mTOR pathway. However, in addition to these Let-7 dependent results, I uncover some novel changes in metabolism, that are only observed in Lin28a^{TEC} mice but not in Lin28b^{TEC} animals, hence suggesting Let-7 independent mechanisms. Enzymes involved in the breakdown of glucose, namely Aldolase B and Aldolase C are increased on protein level in *Lin28a* mutant TEC. The aldolase family members take part in the breakdown of glucose and

catalyze the reversible conversion of fructose-1,6-biphosphate to glyceraldehydes-3-phosphate (G3P) and dihydroxyacetone [166]. The increased expression of these enzymes correlates with our documented enhanced glucose dependency and Glut4 expression, thus further corroborating that *Lin28a* over-expression causes increased glucose usage.

The number of mitochondria is reduced in *Lin28a* tg TEC, indicative of altered mitochondrial biogenesis in TEC. This is in contrast to a previous report showing that *Lin28a* over-expression increases the amount of mitochondria in cardiomyocytes [167]. However, different methodological approaches were taken to measure the number of mitochondria. While I used MitoTracker dye, a probe that chemically labels mitochondria, Wang et al. performed electron microscopy studies to determine the number of mitochondria. In addition, I worked with primary cells whereas Wang et al. studies were performed in cell lines.

The reduced number of mitochondria correlates with a decrease in the expression of enzymes involved in fatty acid β-oxidation, a process that takes place in the mitochondrial matrix. Specifically, Acyl-CoA dehydrogenase and 3-Ketoacyl-CoA thiolase, are significantly depleted by *Lin28a* tg. Acyl-CoA dehydrogenase catalyzes the initial step of each cycle of fatty acid β-oxidation in the mitochondria of cells by oxidizing acyl-CoA thioesters, forming the corresponding enoyl-CoA. On the other hand, 3-Ketoacyl-CoA thiolase is involved in the last step of mitochondrial β-oxidation and catalyzes the thiolytic cleavage of 3-Ketoacyl-CoA into an Acetyl-CoA and a Fatty acyl-CoA shortened by two carbon atoms [168].

Thus, our results indicate that *Lin28a* tg cTEC^{hi} depend more on glycolysis because of reduced fatty acid β-oxidation and impaired mitochondrial biogenesis and meet their dependency on glucose metabolism by increasing the expression of glycolytic enzymes. Furthermore, this data corroborates studies performed in cancer cells, which showed that these highly proliferating cells fuel their metabolic needs by increasing glycolysis and reducing oxidative phosphorylation, a phenomenon known as the Warburg effect [169]. Several papers

even suggested that the Warburg effect is a common characteristic of cells with high proliferation rates. Hence, our data implies that ectopic expression of *Lin28a* in TEC facilitates the Warburg effect to promote TEC proliferation, in line with a previous finding [170]. The authors of this study showed that this effect was mediated by increased expression of pyruvate dehydrogenase kinase 1 (PDK1) by *Lin28a*. PDK1 is a molecule that suppresses the activity of pyruvate dehydrogenase (PDH), an enzyme that catalyzes the conversion of pyruvate to acetyl-CoA, thereby increases the influx of glycolysis derived acetyl-CoA into the TCA cycle.

MAPK signaling defined by transcriptomics and TAK1 phosphorylation is significantly increased in TEC expressing *Lin28a* tg, a pathway known to trigger apoptosis in a variety of cells [142]. Furthermore, our transcriptomic data indicates that the activation of TAK1 has been mediated by TNF-alpha through TNF-R1. Indeed, I find increased expression of TNF-R1 on cTEC^{lo} and mTEC of Lin28a^{TEC} mice, correlating increased cell death with TNF-R1 induced MAPK signaling. However, I do not observe a significant difference in the expression of TNF-R1 in *Lin28a* tg cTEC^{hi}. This subset could be less susceptible to changes mediated by ectopic *Lin28a* which eventually lead to differential TNF-R1 expression. This line of thought is supported by our bulk transcriptomics data showing a significant increase in estrogen signaling in 7 week old *Lin28a* tg cTEC^{lo}, but not in cTEC^{hi}. Estrogen is a sex hormone which is primarily responsible for the development of the reproductive system and physical characteristics of females and, of interest to this thesis, is known to increase TNF-R1 expression [172, 173]. Hence, it may be that cTEC^{lo} and mTEC in Lin28a^{TEC} mice are experiencing enhanced estrogen stimulation which result in increased TNF-R1 surface expression.

The death inducing competence of TNF is normally balanced by simultaneous activation of NF-kB and its pro-survival effect [173]. However, our data suggests that in *Lin28a* tg TEC the pro-apoptotic effect of TNF-alpha overrules NF-kB activation. Supporting this hypothesis, *Foxo3a*, a transcription factor that is known to direct TNF-receptor signaling towards apoptosis through suppression of NF-kB activity and activation of c-Jun N-terminal kinases activation (JNK) is significantly over-expressed in TEC that express *Lin28a* tg [150]. In line with this data, I find that the activation of JNK is increased in TEC of Lin28a^{TEC} animals. Hence, our results imply that *Lin28a* tg cTEC^{lo} and mTEC experience higher TNF-alpha stimulation through increased TNF-R1 expression and that *Foxo3a* diverts this signal in these cells towards apoptosis by inhibiting NF-kB activation and increasing JNK phosphorylation.

Testing this hypothesis, I could confirm that TNF-alpha plus NF-kB inhibition significantly increased TEC apoptosis. Collectively, our data imply that the enhanced cell death rates of *Lin28a* tg cTEC^{lo} and mTEC is driven by increased TNF-R1 signaling and down-stream NF-kB inhibition by *Foxo3a*.

This thesis reveals a previous unknown epistatic relationship between Lin28A and Lin28B in regulating thymus size and TEC function. Further experiments analyzing the direct targets of both RBPs will be required to disentangle the exact molecular events that result in these opposing results.

Our data implies that the increased TEC compartment in Lin28b^{TEC} animals relates to metabolic fitness and prolonged lifespan. Hence, experiments dissecting pro- and anti-apoptotic pathways and further metabolic analyses of *Lin28b* tg TEC are required.

Changes in TEC subset composition and TEC numbers in Lin28a^{TEC} animals coincide with increased EMT and a defect in the up-regulation of WNT signaling in *Lin28a* tg TEC. As these two pathways are known to regulate TEC differentiation and TEC cellularity, it would be of interest to dissect WNT and EMT signaling in TEC that ectopically express *Lin28a* tg.

Because the composition of cytometrically-defined mTEC subpopulations is significantly changed by *Lin28a* tg in young adult mice, more refined omics on a single cell resolution related to public data sets is required.

The data shown in this thesis implies that ectopic *Lin28a* leads to enhanced glucose usage and reduced OxPhos by TEC. Hence, further characterization of glucose metabolism and mitochondrial biogenesis is needed to explore the mechanism behind these effects.

Our results suggest that cTEC^{lo} and mTEC in Lin28a^{TEC} mice are experiencing higher estrogen stimulation which result in increased TNF-R1 surface expression. It would therefore be of interest to elucidate the mechanistic link between estrogen signaling and TNF-R1 expression in *Lin28a* tg TEC.

The findings reported in this thesis make an important contribution in better understanding the role of *Lin28a* in thymus organogenesis, maintenance and function. Moreover, this study identifies mechanisms imposed by *Lin28a* in TEC biology. Collectively, our studies in a transgenic system provide novel insights into TEC metabolism, TEC apoptosis and thymocyte selection in wild-type animals and hence generate new knowledge that may be applied in therapeutic approaches that reverse thymic shrinkage and boost thymus function by metabolic supplementation.

7. REFERENCES

[1] C. Lavini, “The thymus from antiquity to the present day: The history of a mysterious gland,” in *Thymus Gland Pathology: Clinical, Diagnostic, and Therapeutic Features*, 2008.

[2] D. Liu and H. Ellis, “The mystery of the thymus gland,” *Clin. Anat.*, vol. 29, no. 6, 2016, doi: 10.1002/ca.22724.

[3] J. F. A. P. Miller, “IMMUNOLOGICAL FUNCTION OF THE THYMUS,” *Lancet*, vol. 278, no. 7205, 1961, doi: 10.1016/S0140-6736(61)90693-6.

[4] S. C. Jameson, K. A. Hogquist, and M. J. Bevan, “Positive selection of thymocytes,” *Annual Review of Immunology*, vol. 13. 1995, doi: 10.1146/annurev.iy.13.040195.000521.

[5] J. W. Kappler, N. Roehm, and P. Marrack, “T cell tolerance by clonal elimination in the thymus,” *Cell*, vol. 49, no. 2, 1987, doi: 10.1016/0092-8674(87)90568-X.

[6] M. S. Jordan *et al.*, “Thymic selection of CD4+CD25+ regulatory T cells induced by an agonist self-peptide,” *Nat. Immunol.*, vol. 2, no. 4, 2001, doi: 10.1038/86302.

[7] C. C. Blackburn and N. R. Manley, “Developing a new paradigm for thymus organogenesis,” *Nature Reviews Immunology*, vol. 4, no. 4. 2004, doi: 10.1038/nri1331.

[8] J. Han and J. C. Zúñiga-Pflücker, “A 2020 View of Thymus Stromal Cells in T Cell Development,” *J. Immunol.*, vol. 206, no. 2, 2021, doi: 10.4049/jimmunol.2000889.

[9] J. Gordon and N. R. Manley, “Mechanisms of thymus organogenesis and morphogenesis,” *Development*, vol. 138, no. 18. 2011, doi: 10.1242/dev.059998.

[10] H. von Boehmer, H. S. Teh, and P. Kisielow, “The thymus selects the useful, neglects the useless and destroys the harmful,” *Immunol. Today*, vol. 10, no. 2, 1989, doi: 10.1016/0167-5699(89)90307-1.

[11] G. Anderson, E. J. Jenkinson, N. C. Moore, and J. J. T. Owen, “MHC class II-positive epithelium and mesenchyme cells are both required for T-cell development in the thymus,” *Nature*, vol. 362, no. 6415, 1993, doi: 10.1038/362070a0.

[12] Y. Shi *et al.*, “LTβR controls thymic portal endothelial cells for haematopoietic progenitor cell homing and T-cell regeneration,” *Nat. Commun.*, vol. 7, 2016, doi: 10.1038/ncomms12369.

[13] E. Esashi, T. Sekiguchi, H. Ito, S. Koyasu, and A. Miyajima, “ Cutting Edge: A Possible Role for CD4 + Thymic Macrophages as Professional Scavengers of Apoptotic Thymocytes ,” *J. Immunol.*, vol. 171, no. 6, 2003, doi: 10.4049/jimmunol.171.6.2773.

[14] M. Sospedra, X. Ferrer-Francesch, O. Domínguez, M. Juan, M. Foz-Sala, and R. Pujol-Borrell, “Transcription of a broad range of self-antigens in human thymus suggests a role for central mechanisms in tolerance toward peripheral antigens.,” *J. Immunol.*, vol. 161, no. 11, 1998.

[15] L. Klein, B. Kyewski, P. M. Allen, and K. A. Hogquist, “Positive and negative selection of the T cell repertoire: What thymocytes see (and don’t see),” *Nature Reviews Immunology*, vol. 14, no. 6. 2014, doi: 10.1038/nri3667.

[16] J. Oh and J.-S. Shin, “The Role of Dendritic Cells in Central Tolerance,” *Immune Netw.*, vol. 15, no. 3, 2015, doi: 10.4110/in.2015.15.3.111.

[17] F. Frommer and A. Waisman, “B cells participate in thymic negative selection of murine auto-reactive CD4+ T cells,” *PLoS One*, vol. 5, no. 10, 2010, doi: 10.1371/journal.pone.0015372.

[18] J. Perera, L. Meng, F. Meng, and H. Huang, “Autoreactive thymic B cells are efficient antigen-presenting cells of cognate self-antigens for T cell negative selection,” *Proc. Natl. Acad. Sci. U. S. A.*, vol. 110, no. 42, 2013, doi: 10.1073/pnas.1313001110.

[19] J. Gordon, A. R. Bennett, C. C. Blackburn, and N. R. Manley, “Gcm2 and Foxn1 mark early parathyroid- and thymus-specific domains in the developing third pharyngeal pouch,” *Mech. Dev.*, vol. 103, no. 1–2, 2001, doi: 10.1016/S0925-4773(01)00333-1.

[20] J. Bukowska, M. Kopcewicz, K. Walendzik, and B. Gawronska-Kozak, “Foxn1 in skin development, homeostasis and wound healing,” *International Journal of Molecular Sciences*, vol. 19, no. 7. 2018, doi: 10.3390/ijms19071956.

[21] J. L. Brissette, J. Li, J. Kamimura, D. Lee, and G. P. Dotto, “The product of the mouse nude locus, whn, regulates the balance between epithelial cell growth and differentiation,” *Genes Dev.*, vol. 10, no. 17, 1996, doi: 10.1101/gad.10.17.2212.

[22] M. Itoi, N. Tsukamoto, H. Yoshida, and T. Amagai, “Mesenchymal cells are required for functional development of thymic epithelial cells,” *Int. Immunol.*, vol. 19, no. 8, 2007, doi: 10.1093/intimm/dxm060.

[23] K. Foster *et al.*, “Contribution of Neural Crest-Derived Cells in the Embryonic and Adult Thymus,” *J. Immunol.*, vol. 180, no. 5, 2008, doi: 10.4049/jimmunol.180.5.3183.

[24] K. M. Sitnik, K. Kotarsky, A. J. White, W. E. Jenkinson, G. Anderson, and W. W. Agace,

"Mesenchymal Cells Regulate Retinoic Acid Receptor-Dependent Cortical Thymic Epithelial Cell Homeostasis," *J. Immunol.*, vol. 188, no. 10, 2012, doi: 10.4049/jimmunol.1200358.
[25] F. M. V. Rossi *et al.*, "Recruitment of adult thymic progenitors is regulated by P-selectin and its ligand PSGL-1," *Nat. Immunol.*, vol. 6, no. 6, 2005, doi: 10.1038/ni1203.
[26] M. L. Scimone, I. Aifantis, I. Apostolou, H. Von Boehmer, and U. H. Von Andrian, "A multistep adhesion cascade for lymphoid progenitor cell homing to the thymus," *Proc. Natl. Acad. Sci. U. S. A.*, vol. 103, no. 18, 2006, doi: 10.1073/pnas.0602024103.
[27] J. L. Bryson *et al.*, "Cell-Autonomous Defects in Thymic Epithelial Cells Disrupt Endothelial-Perivascular Cell Interactions in the Mouse Thymus," *PLoS One*, vol. 8, no. 6, 2013, doi: 10.1371/journal.pone.0065196.
[28] J. J. Owen and M. A. Ritter, "Tissue interaction in the development of thymus lymphocytes.," *J. Exp. Med.*, vol. 129, no. 2, 1969, doi: 10.1084/jem.129.2.431.
[29] I. Douagi, I. Andre, J. C. Ferraz, and A. Cumano, "Characterization of T cell precursor activity in the murine fetal thymus: Evidence for an input of T cell precursors between days 12 and 14 of gestation," *Eur. J. Immunol.*, vol. 30, no. 8, 2000, doi: 10.1002/1521-4141(2000)30:8<2201::AID-IMMU2201>3.0.CO;2-2.
[30] W. Savino, D. A. Mendes-Da-Cruz, J. S. Silva, M. Dardenne, and V. Cotta-De-Almeida, "Intrathymic T-cell migration: A combinatorial interplay of extracellular matrix and chemokines?," *Trends in Immunology*, vol. 23, no. 6. 2002, doi: 10.1016/S1471-4906(02)02224-X.
[31] W. Savino, D. A. Mendes-da-Cruz, S. Smaniotto, E. Silva-Monteiro, and D. M. S. Villa-Verde, "Molecular mechanisms governing thymocyte migration: combined role of chemokines and extracellular matrix," *J. Leukoc. Biol.*, vol. 75, no. 6, 2004, doi: 10.1189/jlb.1003455.
[32] M. Ciofani and J. C. Zúñiga-Pflücker, "The thymus as an inductive site for T lymphopoiesis," *Annual Review of Cell and Developmental Biology*, vol. 23. 2007, doi: 10.1146/annurev.cellbio.23.090506.123547.
[33] M. Zhu and Y. X. Fu, "Coordinating Development of Medullary Thymic Epithelial Cells," *Immunity*, vol. 29, no. 3. 2008, doi: 10.1016/j.immuni.2008.09.001.
[34] J. Abramson and G. Anderson, "Thymic epithelial cells," *Annual Review of Immunology*, vol. 35. 2017, doi: 10.1146/annurev-immunol-051116-052320.
[35] N. Kadouri, S. Nevo, Y. Goldfarb, and J. Abramson, "Thymic epithelial cell heterogeneity: TEC by TEC," *Nature Reviews Immunology*, vol. 20, no. 4. 2020, doi: 10.1038/s41577-019-0238-0.
[36] C. Röpke, P. Van Soest, P. Paul Platenburg, and W. Van Ewijk, "A Common Stem Cell for Murine Cortical and Medullary Thymic Epithelial Cells?," *Dev. Immunol.*, vol. 4, no. 2, 1995, doi: 10.1155/1995/23168.
[37] D. B. Klug, C. Carter, E. Crouch, D. Roop, C. J. Conti, and E. R. Richie, "Interdependence of cortical thymic epithelial cell differentiation and T-lineage commitment," *Proc. Natl. Acad. Sci. U. S. A.*, vol. 95, no. 20, 1998, doi: 10.1073/pnas.95.20.11822.
[38] S. W. Rossi, W. E. Jenkinson, G. Anderson, and E. J. Jenkinson, "Clonal analysis reveals a common progenitor for thymic cortical and medullary epithelium," *Nature*, vol. 441, no. 7096, 2006, doi: 10.1038/nature04813.
[39] A. Apavaloaei *et al.*, "PSMB11 Orchestrates the Development of CD4 and CD8 Thymocytes via Regulation of Gene Expression in Cortical Thymic Epithelial Cells," *J. Immunol.*, vol. 202, no. 3, 2019, doi: 10.4049/jimmunol.1801288.
[40] I. Ohigashi *et al.*, "Adult Thymic Medullary Epithelium Is Maintained and Regenerated by Lineage-Restricted Cells Rather Than Bipotent Progenitors," *Cell Rep.*, vol. 13, no. 7, 2015, doi: 10.1016/j.celrep.2015.10.012.
[41] C. E. Mayer *et al.*, "Dynamic spatio-temporal contribution of single β5t+ cortical epithelial precursors to the thymus medulla," *Eur. J. Immunol.*, vol. 46, no. 4, 2016, doi: 10.1002/eji.201545995.
[42] G. E. Desanti *et al.*, "Developmentally Regulated Availability of RANKL and CD40 Ligand Reveals Distinct Mechanisms of Fetal and Adult Cross-Talk in the Thymus Medulla," *J. Immunol.*, vol. 189, no. 12, 2012, doi: 10.4049/jimmunol.1201815.
[43] T. Boehm, S. Scheu, K. Pfeffer, and C. C. Bleul, "Thymic medullary epithelial cell differentiation, thymocyte emigration, and the control of autoimmunity require lympho-epithelial cross talk via LTβR," *J. Exp. Med.*, vol. 198, no. 5, 2003, doi: 10.1084/jem.20030794.
[44] R. K. Chin *et al.*, "Lymphotoxin pathway directs thymic Aire expression," *Nat. Immunol.*, vol. 4, no. 11, 2003, doi: 10.1038/ni982.
[45] M. Yano *et al.*, "Aire controls the differentiation program of thymic epithelial cells in the medulla for the establishment of self-tolerance," *J. Exp. Med.*, vol. 205, no. 12, 2008, doi: 10.1084/jem.20080046.
[46] C. Bornstein *et al.*, "Single-cell mapping of the thymic stroma identifies IL-25-producing tuft epithelial cells," *Nature*, vol. 559, no. 7715. 2018, doi: 10.1038/s41586-018-0346-1.

[47] J. Baran-Gale *et al.*, “Ageing compromises mouse thymus function and remodels epithelial cell differentiation,” *Elife*, vol. 9, 2020, doi: 10.7554/ELIFE.56221.
[48] E. M. Kernfeld, R. M. J. Genga, K. Neherin, M. E. Magaletta, P. Xu, and R. Maehr, “A Single-Cell Transcriptomic Atlas of Thymus Organogenesis Resolves Cell Types and Developmental Maturation,” *Immunity*, vol. 48, no. 6, 2018, doi: 10.1016/j.immuni.2018.04.015.
[49] J. L. Bautista *et al.*, “Single-cell transcriptional profiling of human thymic stroma uncovers novel cellular heterogeneity in the thymic medulla,” *Nat. Commun.*, vol. 12, no. 1, 2021.
[50] T. C. Luis *et al.*, “Initial seeding of the embryonic thymus by immune-restricted lympho-myeloid progenitors,” *Nat. Immunol.*, vol. 17, no. 12, 2016, doi: 10.1038/ni.3576.
[51] Y. Takahama, “Journey through the thymus: Stromal guides for T-cell development and selection,” *Nature Reviews Immunology*, vol. 6, no. 2. 2006, doi: 10.1038/nri1781.
[52] L. Calderón and T. Boehm, “Three chemokine receptors cooperatively regulate homing of hematopoietic progenitors to the embryonic mouse thymus,” *Proc. Natl. Acad. Sci. U. S. A.*, vol. 108, no. 18, 2011, doi: 10.1073/pnas.1016428108.
[53] D. L. Foss, E. Donskoy, and I. Goldschneider, “The importation of hematogenous precursors by the thymus is a gated phenomenon in normal adult mice,” *J. Exp. Med.*, vol. 193, no. 3, 2001, doi: 10.1084/jem.193.3.365.
[54] H. R. Rodewald, K. Kretzschmar, W. Swat, and S. Takeda, “Intrathymically expressed c-kit ligand (stem cell factor) is a major factor driving expansion of very immature thymocytes in vivo,” *Immunity*, vol. 3, no. 3, 1995, doi: 10.1016/1074-7613(95)90116-7.
[55] S. Massa, G. Balciunaite, R. Ceredig, and A. G. Rolink, “Critical role for c-kit (CD117) in T cell lineage commitment and early thymocyte development in vitro,” *Eur. J. Immunol.*, vol. 36, no. 3, 2006, doi: 10.1002/eji.200535760.
[56] F. Radtke *et al.*, “Deficient T cell fate specification in mice with an induced inactivation of Notch1,” *Immunity*, vol. 10, no. 5, 1999, doi: 10.1016/S1074-7613(00)80054-0.
[57] U. Von Freeden-Jeffry, P. Vieira, L. A. Lucian, T. McNeil, S. E. G. Burdach, and R. Murray, “Lymphopenia in interleukin (IL)-7 gene-deleted mice identifies IL-7 as a nonredundant cytokine,” *J. Exp. Med.*, vol. 181, no. 4, 1995, doi: 10.1084/jem.181.4.1519.
[58] J. J. Peschon *et al.*, “Early Lymphocyte Expansion Is Severely Impaired in Interleukin 7 Receptor-deficient Mice,” *J. Exp. Med.*, vol. 180, no. 5, 1994, doi: 10.1084/jem.180.5.1955.
[59] T. Ueno *et al.*, “CCR7 signals are essential for cortex-medulla migration of developing thymocytes,” *J. Exp. Med.*, vol. 200, no. 4, 2004, doi: 10.1084/jem.20040643.
[60] J. Plotkin, S. E. Prockop, A. Lepique, and H. T. Petrie, “Critical Role for CXCR4 Signaling in Progenitor Localization and T Cell Differentiation in the Postnatal Thymus,” *J. Immunol.*, vol. 171, no. 9, 2003, doi: 10.4049/jimmunol.171.9.4521.
[61] C. Benz, K. Heinzel, and C. C. Bleul, “Homing of immature thymocytes to the subcapsular microenvironment within the thymus is not an absolute requirement for T cell development,” *Eur. J. Immunol.*, vol. 34, no. 12, 2004, doi: 10.1002/eji.200425248.
[62] L. A. Turka *et al.*, “Thymocyte expression of RAG-1 and RAG-2: Termination by T cell receptor cross-linking,” *Science (80-.).*, vol. 253, no. 5021, 1991, doi: 10.1126/science.1831564.
[63] E. C. Dudley, H. T. Petrie, L. M. Shah, M. J. Owen, and A. C. Hayday, “T cell receptor β chain gene rearrangement and selection during thymocyte development in adult mice,” *Immunity*, vol. 1, no. 2, 1994, doi: 10.1016/1074-7613(94)90102-3.
[64] P. Kisielow, H. S. Teh, H. Blüthmann, and H. Von Boehmer, “Positive selection of antigen-specific T cells in thymus by restricting MHC molecules,” *Nature*, vol. 335, no. 6192, 1988, doi: 10.1038/335730a0.
[65] M. Oh-Hora *et al.*, “Agonist-Selected T Cell Development Requires Strong T Cell Receptor Signaling and Store-Operated Calcium Entry,” *Immunity*, vol. 38, no. 5, 2013, doi: 10.1016/j.immuni.2013.02.008.
[66] S. Sakaguchi, T. Yamaguchi, T. Nomura, and M. Ono, “Regulatory T Cells and Immune Tolerance,” *Cell*, vol. 133, no. 5. 2008, doi: 10.1016/j.cell.2008.05.009.
[67] M. A. McGargill and K. A. Hogquist, “Antigen-induced coreceptor down-regulation on thymocytes is not a result of apoptosis.,” *J. Immunol.*, vol. 162, no. 3, 1999.
[68] T. Barthlott, H. Kohler, and K. Eichmann, “Asynchronous coreceptor downregulation after positive thymic selection: Prolonged maintenance of the double positive state in CD8 lineage differentiation due to sustained biosynthesis of the CD4 coreceptor,” *J. Exp. Med.*, vol. 185, no. 2, 1997, doi: 10.1084/jem.185.2.357.
[69] H. Suzuki, J. A. Punt, L. G. Granger, and A. Singer, “Asymmetric signaling requirements for thymocyte commitment to the CD4+ versus CD8+ T cell lineages: A new perspective on thymic commitment and selection,” *Immunity*, vol. 2, no. 4, 1995, doi: 10.1016/1074-7613(95)90149-3.
[70] Y. Xing, X. Wang, S. C. Jameson, and K. A. Hogquist, “Late stages of T cell maturation in the thymus

involve NF-κB and tonic type i interferon signaling," *Nat. Immunol.*, vol. 17, no. 5, 2016, doi: 10.1038/ni.3419.
[71] Y. Xing and K. A. Hogquist, "T-Cell tolerance: Central and peripheral," *Cold Spring Harb. Perspect. Biol.*, vol. 4, no. 6, 2012, doi: 10.1101/cshperspect.a006957.
[72] S. R. Daley, D. Y. Hu, and C. C. Goodnow, "Helios marks strongly autoreactive CD4+ T cells in two major waves of thymic deletion distinguished by induction of PD-1 or NF-κB," *J. Exp. Med.*, vol. 210, no. 2, 2013, doi: 10.1084/jem.20121458.
[73] M. Egerton, R. Scollay, and K. Shortman, "Kinetics of mature T-cell development in the thymus," *Proc. Natl. Acad. Sci. U. S. A.*, vol. 87, no. 7, 1990, doi: 10.1073/pnas.87.7.2579.
[74] R. Scollay and D. I. Godfrey, "Thymic emigration: conveyor belts or lucky dips?," *Immunol. Today*, vol. 16, no. 6, 1995, doi: 10.1016/0167-5699(95)80179-0.
[75] J. N. Lancaster, H. M. Thyagarajan, J. Srinivasan, Y. Li, Z. Hu, and L. I. R. Ehrlich, "Live-cell imaging reveals the relative contributions of antigen-presenting cell subsets to thymic central tolerance," *Nat. Commun.*, vol. 10, no. 1, 2019, doi: 10.1038/s41467-019-09727-4.
[76] S. Murata *et al.*, "Regulation of CD8+ T cell development by thymus-specific proteasomes," *Science (80-.).*, vol. 316, no. 5829, 2007, doi: 10.1126/science.1141915.
[77] T. Nakagawa *et al.*, "Cathepsin L: Critical role in Ii degradation and CD4 T cell selection in the thymus," *Science (80-.).*, vol. 280, no. 5362, 1998, doi: 10.1126/science.280.5362.450.
[78] J. Gommeaux *et al.*, "Thymus-specific serine protease regulates positive selection of a subset of CD4+ thymocytes," *Eur. J. Immunol.*, vol. 39, no. 4, 2009, doi: 10.1002/eji.200839175.
[79] L. Klein and B. Kyewski, "A central role for central tolerance," *Annu. Rev. Immunol.*, vol. 24, pp. 571–606, 2006.
[80] H. Takaba *et al.*, "Fezf2 Orchestrates a Thymic Program of Self-Antigen Expression for Immune Tolerance," *Cell*, vol. 163, no. 4, 2015, doi: 10.1016/j.cell.2015.10.013.
[81] D. Amsen, C. R. Calvo, B. A. Osborne, and A. M. Kruisbeek, "Costimulatory signals are required for induction of transcription factor Nur77 during negative selection of CD4+CD8+ thymocytes," *Proc. Natl. Acad. Sci. U. S. A.*, vol. 96, no. 2, 1999, doi: 10.1073/pnas.96.2.622.
[82] J. O'Brien, H. Hayder, Y. Zayed, and C. Peng, "Overview of microRNA biogenesis, mechanisms of actions, and circulation," *Frontiers in Endocrinology*, vol. 9, no. AUG. 2018, doi: 10.3389/fendo.2018.00402.
[83] S. Zuklys *et al.*, "MicroRNAs Control the Maintenance of Thymic Epithelia and Their Competence for T Lineage Commitment and Thymocyte Selection," *J. Immunol.*, vol. 189, no. 8, 2012, doi: 10.4049/jimmunol.1200783.
[84] D. Guo *et al.*, "MicroRNA-181a-5p enhances cell proliferation in medullary thymic epithelial cells via regulating TGF-β signaling," *Acta Biochim. Biophys. Sin. (Shanghai).*, vol. 48, no. 9, 2016, doi: 10.1093/abbs/gmw068.
[85] P. Chen *et al.*, "MicroRNA-449a modulates medullary thymic epithelial cell differentiation," *Sci. Rep.*, vol. 7, no. 1, 2017, doi: 10.1038/s41598-017-16162-2.
[86] J. Dong, L. M. Warner, L. L. Lin, M. C. Chen, R. M. O'Connell, and L. F. Lu, "miR-155 promotes T reg cell development by safeguarding medullary thymic epithelial cell maturation," *J. Exp. Med.*, vol. 218, no. 2, 2021, doi: 10.1084/jem.20192423.
[87] H. Lee, S. Han, C. S. Kwon, and D. Lee, "Biogenesis and regulation of the let-7 miRNAs and their functional implications," *Protein and Cell*, vol. 7, no. 2. 2016, doi: 10.1007/s13238-015-0212-y.
[88] F. Yu *et al.*, "let-7 Regulates Self Renewal and Tumorigenicity of Breast Cancer Cells," *Cell*, vol. 131, no. 6, 2007, doi: 10.1016/j.cell.2007.10.054.
[89] F. Biamonte *et al.*, "MicroRNA let-7g acts as tumor suppressor and predictive biomarker for chemoresistance in human epithelial ovarian cancer," *Sci. Rep.*, vol. 9, no. 1, 2019, doi: 10.1038/s41598-019-42221-x.
[90] R. J. A. Frost and E. N. Olson, "Control of glucose homeostasis and insulin sensitivity by the Let-7 family of microRNAs," *Proc. Natl. Acad. Sci. U. S. A.*, vol. 108, no. 52, 2011, doi: 10.1073/pnas.1118922109.
[91] J. Tsialikas and J. Romer-Seibert, "LIN28: Roles and regulation in development and beyond," *Dev.*, vol. 142, no. 14, 2015, doi: 10.1242/dev.117580.
[92] D. Ustianenko *et al.*, "LIN28 Selectively Modulates a Subclass of Let-7 MicroRNAs," *Mol. Cell*, vol. 71, no. 2, 2018, doi: 10.1016/j.molcel.2018.06.029.
[93] F. Mayr, A. Schütz, N. Döge, and U. Heinemann, "The Lin28 cold-shock domain remodels pre-let-7 microRNA," *Nucleic Acids Res.*, vol. 40, no. 15, 2012, doi: 10.1093/nar/gks355.
[94] F. Mayr and U. Heinemann, "Mechanisms of Lin28-mediated miRNA and mRNA regulation--a structural and functional perspective.," *International journal of molecular sciences*, vol. 14, no. 8. 2013, doi: 10.3390/ijms140816532.

[95] E. Piskounova *et al.*, “Lin28A and Lin28B inhibit let-7 MicroRNA biogenesis by distinct mechanisms,” *Cell*, vol. 147, no. 5, 2011, doi: 10.1016/j.cell.2011.10.039.
[96] A. Rybak *et al.*, “A feedback loop comprising lin-28 and let-7 controls pre-let-7 maturation during neural stem-cell commitment,” *Nat. Cell Biol.*, vol. 10, no. 8, 2008, doi: 10.1038/ncb1759.
[97] S. R. Viswanathan, G. Q. Daley, and R. I. Gregory, “Selective blockade of microRNA processing by Lin28,” *Science (80-.).*, vol. 320, no. 5872, 2008, doi: 10.1126/science.1154040.
[98] H. Zhu *et al.*, “The Lin28/let-7 axis regulates glucose metabolism,” *Cell*, vol. 147, no. 1, 2011, doi: 10.1016/j.cell.2011.08.033.
[99] A. Polesskaya, S. Cuvellier, I. Naguibneva, A. Duquet, E. G. Moss, and A. Harel-Bellan, “Lin-28 binds IGF-2 mRNA and participates in skeletal myogenesis by increasing translation efficiency,” *Genes Dev.*, vol. 21, no. 9, 2007, doi: 10.1101/gad.415007.
[100] N. Li *et al.*, “Lin-28 homologue A (LIN28A) promotes cell cycle progression via regulation of cyclin-dependent kinase 2 (CDK2), cyclin D1 (CCND1), and cell division cycle 25 homolog A (CDC25A) expression in cancer,” *J. Biol. Chem.*, vol. 287, no. 21, 2012, doi: 10.1074/jbc.M111.321158.
[101] X. U. Bingsen, K. Zhang, and Y. Huang, “Lin28 modulates cell growth and associates with a subset of cell cycle regulator mRNAs in mouse embryonic stem cells,” *RNA*, vol. 15, no. 3, 2009, doi: 10.1261/rna.1368009.
[102] X. Lin *et al.*, “RNA-binding protein LIN28B inhibits apoptosis through regulation of the AKT2/FOXO3A/BIM axis in ovarian cancer cells,” *Signal Transduct. Target. Ther.*, vol. 3, no. 1, 2018, doi: 10.1038/s41392-018-0026-5.
[103] H. Xiong *et al.*, “Oncogenic mechanisms of Lin28 in breast cancer: New functions and therapeutic opportunities,” *Oncotarget*, vol. 8, no. 15, 2017, doi: 10.18632/oncotarget.14891.
[104] J. Jin *et al.*, “Evidence that Lin28 stimulates translation by recruiting RNA helicase A to polysomes,” *Nucleic Acids Res.*, vol. 39, no. 9, 2011, doi: 10.1093/nar/gkq1350.
[105] J. F. De Vasconcellos *et al.*, “LIN28A expression reduces sickling of cultured human erythrocytes,” *PLoS One*, vol. 9, no. 9, 2014, doi: 10.1371/journal.pone.0106924.
[106] N. Shyh-Chang *et al.*, “XLin28 enhances tissue repair by reprogramming cellular metabolism,” *Cell*, vol. 155, no. 4, 2013, doi: 10.1016/j.cell.2013.09.059.
[107] M. Chang *et al.*, “ LIN 28A loss of function is associated with Parkinson’s disease pathogenesis ,” *EMBO J.*, vol. 38, no. 24, 2019, doi: 10.15252/embj.2018101196.
[108] C. Feng *et al.*, “Lin28 regulates HER2 and promotes malignancy through multiple mechanisms,” *Cell Cycle*, vol. 11, no. 13, 2012, doi: 10.4161/cc.20893.
[109] R. Hamano *et al.*, “High expression of Lin28 is associated with tumour aggressiveness and poor prognosis of patients in oesophagus cancer,” *Br. J. Cancer*, vol. 106, no. 8, 2012, doi: 10.1038/bjc.2012.90.
[110] C. E. King, M. Cuatrecasas, A. Castells, A. R. Sepulveda, J. S. Lee, and A. K. Rustgi, “LIN28B promotes colon cancer progression and metastasis,” *Cancer Res.*, vol. 71, no. 12, 2011, doi: 10.1158/0008-5472.CAN-10-4637.
[111] Y. Liu *et al.*, “Lin28 induces epithelial-to-mesenchymal transition and stemness via downregulation of let-7a in breast cancer cells,” *PLoS One*, vol. 8, no. 12, 2013, doi: 10.1371/journal.pone.0083083.
[112] Y. Chen *et al.*, “LIN28/let-7/PD-L1 pathway as a target for cancer immunotherapy,” *Cancer Immunol. Res.*, vol. 7, no. 3, 2019, doi: 10.1158/2326-6066.CIR-18-0331.
[113] Y. Zhang *et al.*, “ Lin28 enhances de novo fatty acid synthesis to promote cancer progression via SREBP -1 ,” *EMBO Rep.*, vol. 20, no. 10, 2019, doi: 10.15252/embr.201948115.
[114] L. Madisen *et al.*, “A toolbox of Cre-dependent optogenetic transgenic mice for light-induced activation and silencing,” *Nat. Neurosci.*, vol. 15, no. 5, 2012, doi: 10.1038/nn.3078.
[115] S. Tyanova and J. Cox, “Perseus: A bioinformatics platform for integrative analysis of proteomics data in cancer research,” in *Methods in Molecular Biology*, vol. 1711, 2018.
[116] A. Dobin *et al.*, “STAR: Ultrafast universal RNA-seq aligner,” *Bioinformatics*, vol. 29, no. 1, 2013, doi: 10.1093/bioinformatics/bts635.
[117] R. Patro, G. Duggal, M. I. Love, R. A. Irizarry, and C. Kingsford, “Salmon provides fast and bias-aware quantification of transcript expression,” *Nat. Methods*, vol. 14, no. 4, 2017, doi: 10.1038/nmeth.4197.
[118] M. I. Love, W. Huber, and S. Anders, “Moderated estimation of fold change and dispersion for RNA-seq data with DESeq2,” *Genome Biol.*, vol. 15, no. 12, 2014, doi: 10.1186/s13059-014-0550-8.
[119] A. M. Newman *et al.*, “Robust enumeration of cell subsets from tissue expression profiles,” *Nat. Methods*, vol. 12, no. 5, 2015, doi: 10.1038/nmeth.3337.
[120] G. Yu, L. G. Wang, Y. Han, and Q. Y. He, “ClusterProfiler: An R package for comparing biological themes among gene clusters,” *Omi. A J. Integr. Biol.*, vol. 16, no. 5, 2012, doi: 10.1089/omi.2011.0118.
[121] S. Zuklys *et al.*, “Stabilized β-Catenin in Thymic Epithelial Cells Blocks Thymus Development and Function,” *J. Immunol.*, vol. 182, no. 5, 2009, doi: 10.4049/jimmunol.0713723.

[122] Y. J. Hwang, G. Jung, W. Jeon, and K. Lee, “Lin28a ameliorates glucotoxicity-induced beta-cell dysfunction and apoptosis,” vol. 54, no. March, pp. 215–220, 2021.
[123] L. T. Jeker *et al.*, “Maintenance of a normal thymic microenvironment and T-cell homeostasis require Smad4-mediated signaling in thymic epithelial cells,” *Blood*, vol. 112, no. 9, 2008, doi: 10.1182/blood-2008-04-150532.
[124] R. N. Germain, “t-cell development and the CD4-CD8 lineage decision,” *Nature Reviews Immunology*, vol. 2, no. 5. 2002, doi: 10.1038/nri798.
[125] I. Yamashita, T. Nagata, T. Tada, and T. Nakayama, “CD69 cell surface expression identifies developing thymocytes which audition for T cell antigen receptor-mediated positive selection,” *Int. Immunol.*, vol. 5, no. 9, 1993, doi: 10.1093/intimm/5.9.1139.
[126] A. Y. Rudensky, “Regulatory T cells and Foxp3,” *Immunol. Rev.*, vol. 241, no. 1, 2011, doi: 10.1111/j.1600-065X.2011.01018.x.
[127] K. Wong *et al.*, “Multilineage potential and self-renewal define an epithelial progenitor cell population in the adult thymus,” *Cell Rep.*, vol. 8, no. 4, 2014, doi: 10.1016/j.celrep.2014.07.029.
[128] M. E. Keir, Y. E. Latchman, G. J. Freeman, and A. H. Sharpe, “Programmed Death-1 (PD-1):PD-Ligand 1 Interactions Inhibit TCR-Mediated Positive Selection of Thymocytes,” *J. Immunol.*, vol. 175, no. 11, 2005, doi: 10.4049/jimmunol.175.11.7372.
[129] H. Yang, Y.-H. Youm, and V. D. Dixit, “Inhibition of Thymic Adipogenesis by Caloric Restriction Is Coupled with Reduction in Age-Related Thymic Involution,” *J. Immunol.*, vol. 183, no. 5, 2009, doi: 10.4049/jimmunol.0900562.
[130] J. Tan, Y. Wang, N. Zhang, and X. Zhu, “Induction of epithelial to mesenchymal transition (EMT) and inhibition on adipogenesis: Two different sides of the same coin? Feasible roles and mechanisms of transforming growth factor β1 (TGF-β1) in age-related thymic involution,” *Cell Biol. Int.*, vol. 40, no. 8, 2016, doi: 10.1002/cbin.10625.
[131] Y. H. Youm *et al.*, “Deficient ghrelin receptor-mediated signaling compromises thymic stromal cell microenvironment by acceleratingthymic adiposity,” *J. Biol. Chem.*, vol. 284, no. 11, 2009, doi: 10.1074/jbc.M808302200.
[132] M. Osada, L. Jardine, R. Misir, T. Andl, S. E. Millar, and M. Pezzano, “DKK1 mediated inhibition of Wnt signaling in postnatal mice leads to loss of TEC progenitors and thymic degeneration,” *PLoS One*, vol. 5, no. 2, 2010, doi: 10.1371/journal.pone.0009062.
[133] G. Talaber *et al.*, “Wnt-4 protects thymic epithelial cells against dexamethasone-induced senescence,” *Rejuvenation Res.*, vol. 14, no. 3, 2011, doi: 10.1089/rej.2010.1110.
[134] K. Kvell *et al.*, “Wnt4 and LAP2alpha as pacemakers of thymic epithelial senescence,” *PLoS One*, vol. 5, no. 5, 2010, doi: 10.1371/journal.pone.0010701.
[135] C. K. Docherty, I. P. Salt, and J. R. Mercer, “Lin28A induces energetic switching to glycolytic metabolism in human embryonic kidney cells,” *Stem Cell Res. Ther.*, vol. 7, no. 1, 2016, doi: 10.1186/s13287-016-0323-2.
[136] N. Shyh-Chang and G. Q. Daley, “Lin28: Primal regulator of growth and metabolism in stem cells,” *Cell Stem Cell*, vol. 12, no. 4. 2013, doi: 10.1016/j.stem.2013.03.005.
[137] O. Warburg, F. Wind, and E. Negelein, “The metabolism of tumors in the body,” *J. Gen. Physiol.*, vol. 8, no. 6, 1927, doi: 10.1085/jgp.8.6.519.
[138] R. J. DeBerardinis, J. J. Lum, G. Hatzivassiliou, and C. B. Thompson, “The Biology of Cancer: Metabolic Reprogramming Fuels Cell Growth and Proliferation,” *Cell Metabolism*, vol. 7, no. 1. 2008, doi: 10.1016/j.cmet.2007.10.002.
[139] R. J. Argüello *et al.*, “SCENITH: A Flow Cytometry-Based Method to Functionally Profile Energy Metabolism with Single-Cell Resolution,” *Cell Metab.*, vol. 32, no. 6, 2020, doi: 10.1016/j.cmet.2020.11.007.
[140] R. Aviner, “The science of puromycin: From studies of ribosome function to applications in biotechnology,” *Computational and Structural Biotechnology Journal*, vol. 18. 2020, doi: 10.1016/j.csbj.2020.04.014.
[141] A. G. Turjanski, J. P. Vaqué, and J. S. Gutkind, “MAP kinases and the control of nuclear events,” *Oncogene*, vol. 26, no. 22. 2007, doi: 10.1038/sj.onc.1210415.
[142] T. Wada and J. M. Penninger, “Mitogen-activated protein kinases in apoptosis regulation,” *Oncogene*, vol. 23, no. 16 REV. ISS. 2. 2004, doi: 10.1038/sj.onc.1207556.
[143] E. Rodríguez-Carballo, B. Gámez, and F. Ventura, “p38 MAPK signaling in osteoblast differentiation,” *Frontiers in Cell and Developmental Biology*, vol. 4, no. MAY. 2016, doi: 10.3389/fcell.2016.00040.
[144] M. Cargnello and P. P. Roux, “Activation and Function of the MAPKs and Their Substrates, the MAPK-Activated Protein Kinases,” *Microbiol. Mol. Biol. Rev.*, vol. 75, no. 1, 2011, doi: 10.1128/mmbr.00031-10.
[145] S. R. Mihaly, J. Ninomiya-Tsuji, and S. Morioka, “TAK1 control of cell death,” *Cell Death and*

Differentiation, vol. 21, no. 11. 2014, doi: 10.1038/cdd.2014.123.
[146] Y. Hirata, M. Takahashi, T. Morishita, T. Noguchi, and A. Matsuzawa, "Post-translational modifications of the TAK1-TAB complex," *International Journal of Molecular Sciences*, vol. 18, no. 1. 2017, doi: 10.3390/ijms18010205.
[147] P. C. Rath and B. B. Aggarwal, "TNF-induced signaling in apoptosis," *Journal of Clinical Immunology*, vol. 19, no. 6. 1999, doi: 10.1023/A:1020546615229.
[148] Z. Zhang and L. Y. Li, "TNFSF15 modulates neovascularization and inflammation," *Cancer Microenviron.*, vol. 5, no. 3, 2012, doi: 10.1007/s12307-012-0117-8.
[149] M. S. Hayden and S. Ghosh, "Regulation of NF-κB by TNF family cytokines," *Seminars in Immunology*, vol. 26, no. 3. 2014, doi: 10.1016/j.smim.2014.05.004.
[150] H. Y. Lee *et al.*, "FOXO3a turns the tumor necrosis factor receptor signaling towards apoptosis through reciprocal regulation of c-Jun N-terminal kinase and NF-κB," *Arterioscler. Thromb. Vasc. Biol.*, vol. 28, no. 1, 2008, doi: 10.1161/ATVBAHA.107.153304.
[151] L. Lin, J. D. Hron, and S. L. Peng, "Regulation of NF-κB, Th activation, and autoinflammation by the forkhead transcription factor Foxo3a," *Immunity*, vol. 21, no. 2, 2004, doi: 10.1016/j.immuni.2004.06.016.
[152] K. N. Ivey and D. Srivastava, "microRNAs as developmental regulators," *Cold Spring Harb. Perspect. Biol.*, vol. 7, no. 7, 2015, doi: 10.1101/cshperspect.a008144.
[153] H. Zhu *et al.*, "Lin28a transgenic mice manifest size and puberty phenotypes identified in human genetic association studies," *Nat. Genet.*, vol. 42, no. 7, 2010, doi: 10.1038/ng.593.
[154] W. Y. Cai *et al.*, "The wnt-β-catenin pathway represses let-7 microrna expression through transactivation of Lin28 to augment breast cancer stem cell expansion," *J. Cell Sci.*, vol. 126, no. 13, 2013, doi: 10.1242/jcs.123810.
[155] L. Yuan and J. Tian, "LIN28B promotes the progression of colon cancer by increasing B-cell lymphoma 2 expression," *Biomed. Pharmacother.*, vol. 103, 2018, doi: 10.1016/j.biopha.2018.04.002.
[156] K. C. Davidson *et al.*, "Wnt/β-catenin signaling promotes differentiation, not self-renewal, of human embryonic stem cells and is repressed by Oct4," *Proc. Natl. Acad. Sci. U. S. A.*, vol. 109, no. 12, 2012, doi: 10.1073/pnas.1118777109.
[157] S. L. Paige, T. Osugi, O. K. Afanasiev, L. Pabon, H. Reinecke, and C. E. Murry, "Endogenous wnt/β-Catenin signaling is required for cardiac differentiation in human embryonic stem cells," *PLoS One*, vol. 5, no. 6, 2010, doi: 10.1371/journal.pone.0011134.
[158] N. C. Inestrosa and L. Varela-Nallar, "Wnt signalling in neuronal differentiation and development," *Cell Tissue Res.*, vol. 359, no. 1, 2015, doi: 10.1007/s00441-014-1996-4.
[159] X. Shen *et al.*, "Differentiation of mesenchymal stem cells into cardiomyocytes is regulated by miRNA-1-2 via WNT signaling pathway," *J. Biomed. Sci.*, vol. 24, no. 1, 2017, doi: 10.1186/s12929-017-0337-9.
[160] J. B. Swann, C. Happe, and T. Boehm, "Elevated levels of Wnt signaling disrupt thymus morphogenesis and function," *Sci. Rep.*, vol. 7, no. 1, 2017, doi: 10.1038/s41598-017-00842-0.
[161] L. Onder *et al.*, "Alternative NF-κB signaling regulates mTEC differentiation from podoplanin-expressing presursors in the cortico-medullary junction," *Eur. J. Immunol.*, vol. 45, no. 8, 2015, doi: 10.1002/eji.201545677.
[162] L. Burkly *et al.*, "Expression of relB is required for the development of thymic medulla and dendritic cells," *Nature*, vol. 373, no. 6514, 1995, doi: 10.1038/373531a0.
[163] A. Le Campion *et al.*, " IL-2 and IL-7 Determine the Homeostatic Balance between the Regulatory and Conventional CD4 + T Cell Compartments during Peripheral T Cell Reconstitution ," *J. Immunol.*, vol. 189, no. 7, 2012, doi: 10.4049/jimmunol.1103152.
[164] W. C. Kieper, J. T. Burghardt, and C. D. Surh, "A Role for TCR Affinity in Regulating Naive T Cell Homeostasis," *J. Immunol.*, vol. 172, no. 1, 2004, doi: 10.4049/jimmunol.172.1.40.
[165] L. M. Furtado, R. Somwar, G. Sweeney, W. Niu, and A. Klip, "Activation of the glucose transporter GLUT4 by insulin," *Biochemistry and Cell Biology*, vol. 80, no. 5. 2002, doi: 10.1139/o02-156.
[166] Y. C. Chang, Y. C. Yang, C. P. Tien, C. J. Yang, and M. Hsiao, "Roles of Aldolase Family Genes in Human Cancers and Diseases," *Trends in Endocrinology and Metabolism*, vol. 29, no. 8. 2018, doi: 10.1016/j.tem.2018.05.003.
[167] M. Zhang *et al.*, "Lin28a protects against hypoxia/reoxygenation induced cardiomyocytes apoptosis by alleviating mitochondrial dysfunction under high glucose/high fat conditions," *PLoS One*, vol. 9, no. 10, 2014, doi: 10.1371/journal.pone.0110580.
[168] Q. Qu, F. Zeng, X. Liu, Q. J. Wang, and F. Deng, "Fatty acid oxidation and carnitine palmitoyltransferase I: Emerging therapeutic targets in cancer," *Cell Death and Disease*, vol. 7, no. 5. 2016, doi: 10.1038/cddis.2016.132.
[169] M. G. V. Heiden, L. C. Cantley, and C. B. Thompson, "Understanding the warburg effect: The

metabolic requirements of cell proliferation," *Science*, vol. 324, no. 5930. 2009, doi: 10.1126/science.1160809.
[170] X. Ma *et al.*, "Lin28/let-7 axis regulates aerobic glycolysis and cancer progression via PDK1," *Nat. Commun.*, vol. 5, 2014, doi: 10.1038/ncomms6212.
[171] V. Zaldivar *et al.*, "Estradiol increases the expression of TNF-α and TNF receptor 1 in lactotropes," *Neuroendocrinology*, vol. 93, no. 2, 2011, doi: 10.1159/000323760.
[172] S. Deb *et al.*, "Estrogen regulates expression of tumor necrosis factor receptors in breast adipose fibroblasts," *J. Clin. Endocrinol. Metab.*, vol. 89, no. 8, 2004, doi: 10.1210/jc.2004-0127.
[173] H. Wajant, K. Pfizenmaier, and P. Scheurich, "Tumor necrosis factor signaling," *Cell Death and Differentiation*, vol. 10, no. 1. 2003, doi: 10.1038/sj.cdd.4401189.
[174] G. Anderson and E. J. Jenkinson, "Lymphostromal interactions in thymic development and function," *Nature Reviews Immunology*, vol. 1, no. 1. 2001, doi: 10.1038/35095500.
[175] B. Yi, G. A. Piazza, X. Su, and Y. Xi, "Micro RNA and cancer chemoprevention," *Cancer Prevention Research*, vol. 6, no. 5. 2013, doi: 10.1158/1940-6207.CAPR-13-0032.
[176] S. R. Viswanathan and G. Q. Daley, "Lin28: A MicroRNA Regulator with a Macro Role," *Cell*, vol. 140, no. 4. 2010, doi: 10.1016/j.cell.2010.02.007.
[177] J. E. Thornton and R. I. Gregory, "How does Lin28 let-7 control development and disease?," *Trends in Cell Biology*, vol. 22, no. 9. 2012, doi: 10.1016/j.tcb.2012.06.001.